78-8681

GUPTA, Om Prakash, 1951-
A STUDY OF THE SEQUENTIAL PROCESS IN THE REACTION $^{6}Li\ (^{3}He,\alpha)\ ^{5}Li\ (g.s.) \rightarrow \alpha + p.$

City University of New York,
Ph.D., 1977
Physics, nuclear

A STUDY OF THE SEQUENTIAL PROCESS IN THE REACTION $^{6}Li\ (^{3}He,\alpha)^{5}\ Li\ (g.s.) \rightarrow \alpha + p$

by

OM PRAKASH GUPTA

A dissertation submitted to the
Graduate Faculty in Physics in
partial fulfillment of the requirements
for the degree of Doctor of Philosophy,
The City University of New York

1977

This manuscript has been read and accepted for the Graduate Faculty in Physics in satisfaction of the dissertation requirement for the degree of Doctor of Philosophy.

1/19/78 date — Chairman of Examining Committee

1/9/78 date — Executive Officer

Professor Carl M. Shakin, Brooklyn College/CUNY

Professor C. Carroll Trail, Brooklyn College/CUNY

Professor Ambuj Mukerji, Lehman College/CUNY

Professor Lee Grodzins, Massachusetts Institute of Technology

Supervisory Committee

The City University of New York

Abstract

A STUDY OF THE SEQUENTIAL PROCESS
IN THE REACTION $^{6}Li\ (^{3}He,\alpha)\ ^{5}Li\ (g.s.) \rightarrow \alpha + p$

by

Om Prakash Gupta

Advisor: Professor A. H. Bond, Jr.

Formation of the ^{9}B 16.74 MeV state has been observed in the first step of the reaction $^{6}Li\ (^{3}He,\alpha)\ ^{5}Li\ (g.s.) \rightarrow p + \alpha$ by using an α-α coincidence technique. The resonance ^{3}He bombarding energy is measured as 1.58± .02 MeV and the width of the resonance is found to be 70± 20 KeV. Formation of the ^{9}B state leads to a 90° symmetry in the center of mass, in the measured angular distribution of the first emitted α particle. The mechanism of this reaction at off-resonance bombarding energies of 1.47 MeV and 1.69 MeV has been shown to be a direct reaction involving both a neutron transfer and a deuteron transfer in the first step.

The measured α - p angular correlation functions show a 180° - aperiodicity at ^{3}He bombarding energies of 1.47 MeV, 1.58 MeV, and 1.69 MeV which correspond to being below, on, and above the ^{9}B resonance. This aperiodicity means that the parity quantum number of the ^{5}Li (g.s.) is not well-defined. The aperiodicity is seen to reduce at resonance bombarding energy compared with the off-resonance bombarding energies. The shift in the minimum and the shape of the angular correlation function at the off-resonance bombarding energies can be explained using a direct reaction for the first step. The on-resonance angular correlation function does not possess the shape seen at other bombarding energies. The effect of ^{9}B resonance formation on the angular correlation functions is not very clear from this work.

ACKNOWLEDGMENTS

I would like to express my gratitude to Professor A. Bond and Professor P. M. S. Lesser, whose efforts made possible the completion of this work. I would also like to thank Mr. Ira Senzon of Brooklyn College Dynamitron Laboratory and Mr. Dan Riel of State University of New York, Stoneybrook for providing some technical help relating to this work.

TABLE OF CONTENTS

LIST OF TABLES

LIST OF FIGURES

CHAPTER I

INTRODUCTION

A nuclear reaction initiated by a ^3He nucleus usually has a very high Q value. Such a reaction may lead to more than two particles in the final state. This is particularly true when ^3He interacts with nuclei of $Z \lesssim 5$.

The reaction of ^3He with ^6Li leads to the formation of a proton and two α-particles in the final state, with Q value of 16.88 MeV.

A three-body final state in a $^6Li + ^3He$ reaction can occur in many different ways, but several experimental studies [1-6] on the ^6Li (^3He, $p\alpha\alpha$) reaction at a low bombarding energy indicate that it proceeds predominantly as follows:

$$^6Li + ^3He \rightarrow \alpha_1 + ^5Li \rightarrow p + \alpha_2 \quad or$$

$$^6Li + ^3He \rightarrow p + ^8Be \rightarrow \alpha_1 + \alpha_2$$

When a reaction proceeds by the formation of well-defined neclear states in the intermediate step, it is known as a Sequential Process.

Another process that may occur in the reaction $^6Li + ^3He$ is the Simultaneous Process, in which the three-body final state is created directly without going through an intermediate step.

The energetically possible intermediate states of ^8Be which are known to break up predominantly by α-decay, are the 0^+ ground state, the 2^+ first excited state at 2.9MeV,

ENERGY LEVELS OF ^{9}B

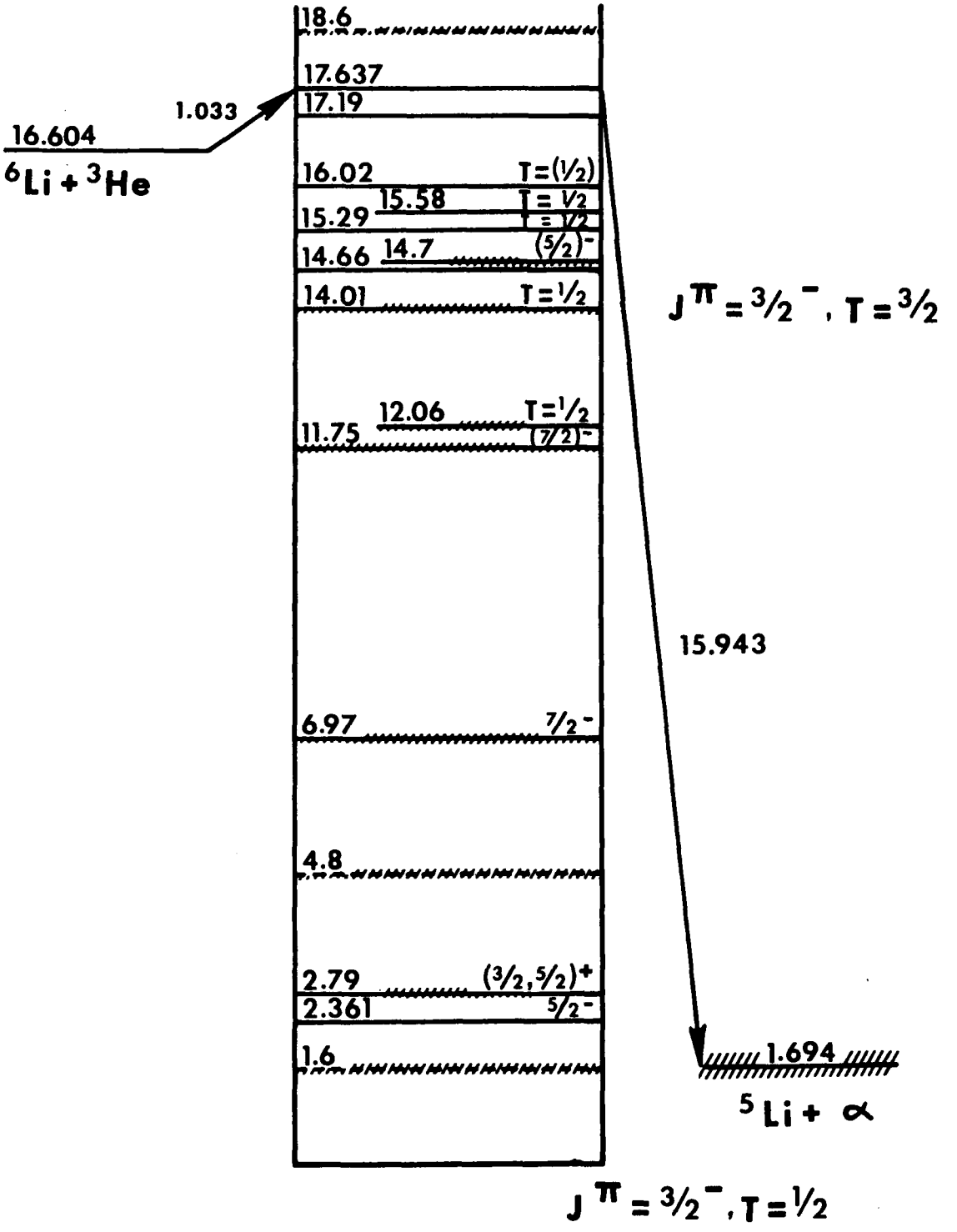

FIGURE 1

VELOCITY-VECTOR DIAGRAM SHOWING MEASUREMENT OF THE ASSYMETRY OF PROTON EMISSION IN THE REACTION $^{6}Li\ (^{3}He, \alpha)\ ^{5}Li\ g.s. \rightarrow p + \alpha$

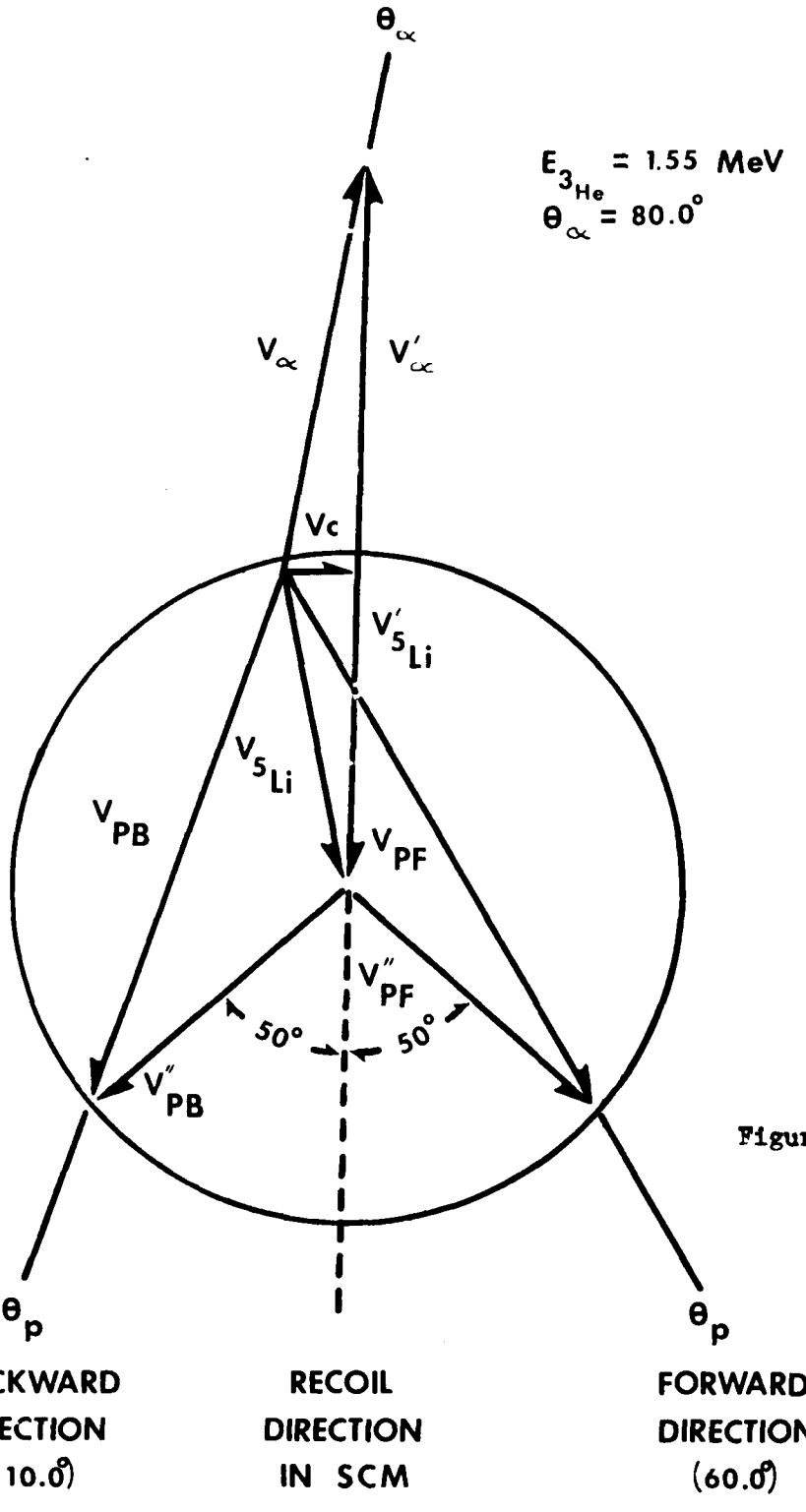

Figure 2

the 4^+ broad second excited state at 11.4 MeV, and the sharp 16.62 and 16.92 MeV states, both of a spin and parity 2^+. The energentically possible intermediate states of ^{5}Li are the $3/2^-$ ground state and the $1/2^-$ first excited state at 7.5 MeV.

Previous experimental studies [1-6] on the sequential process in the ^{6}Li + ^{3}He reaction have repeatedly indicated the formation of these states of ^{5}Li and ^{8}Be. This reaction has been shown to be predominantly a direct reaction in the first step, at some bombarding energies, for both outgoing channels. However, in the ^{8}Be channel, Vignon et. al [6] have shown that the 17.637 MeV ^{9}B compound nuclear state, shown in the energy level diagram of ^{9}B in Fig. 1, is formed in the first step, at a ^{3}He bombarding energy of 1.6 MeV. A similar study in the ^{5}Li channel has not been attempted previous to this work. However, several experimental studies involving the ^{5}Li channel have been done in order to determine the characteristics of the breakup of the ^{5}Li (g.s.) in the second step of the reaction. Specifically the work of Reimann, Martin, and Vogt[2] showed that there exists an enhancement in the yield of the protons, as measured in a forward direction with respect to the recoil direction of ^{5}Li, relative to the yield in the backward direction. These directions are indicated in Fig. 2, which is essentially a velocity vector diagram for the reaction

$$^6\text{Li} + {}^3\text{He} \longrightarrow \alpha_1 + {}^5\text{Li (g.s.)} \longrightarrow p + \alpha_2.$$

Similar observations were also made by Thompson and

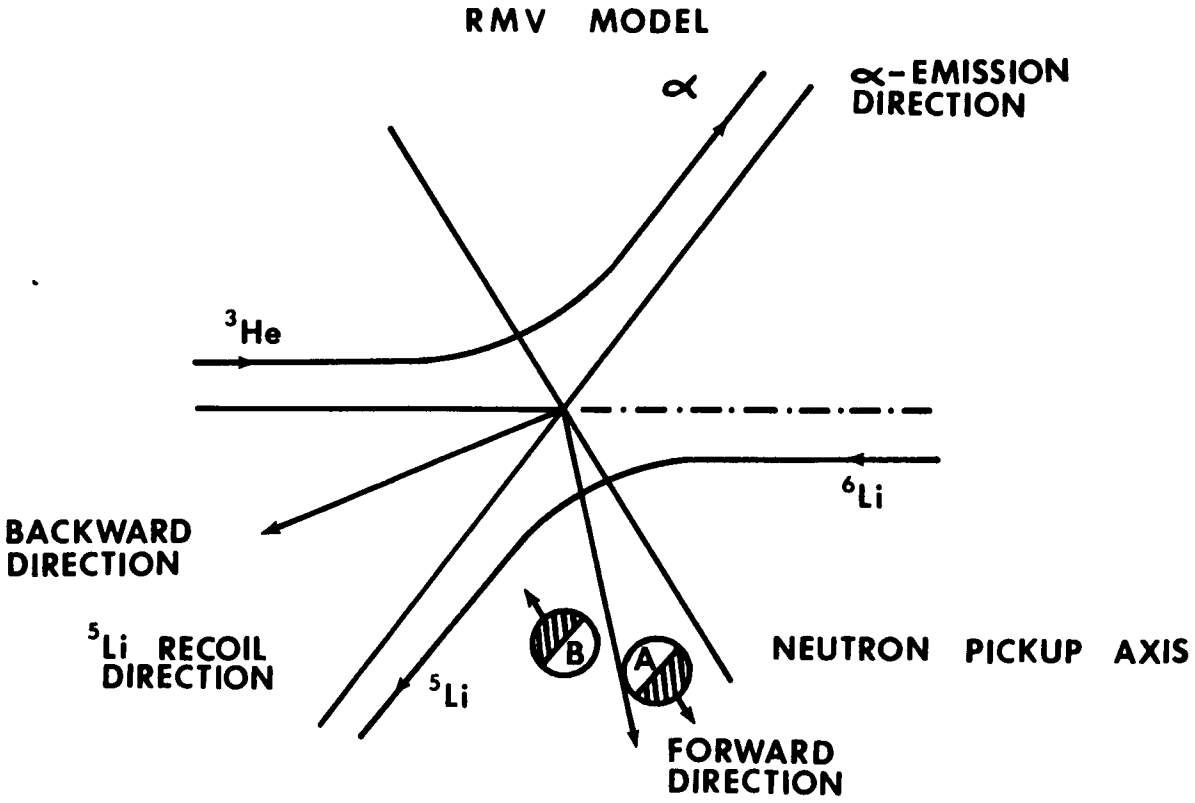

FIG. 3(a) NEUTRON TRANSFER

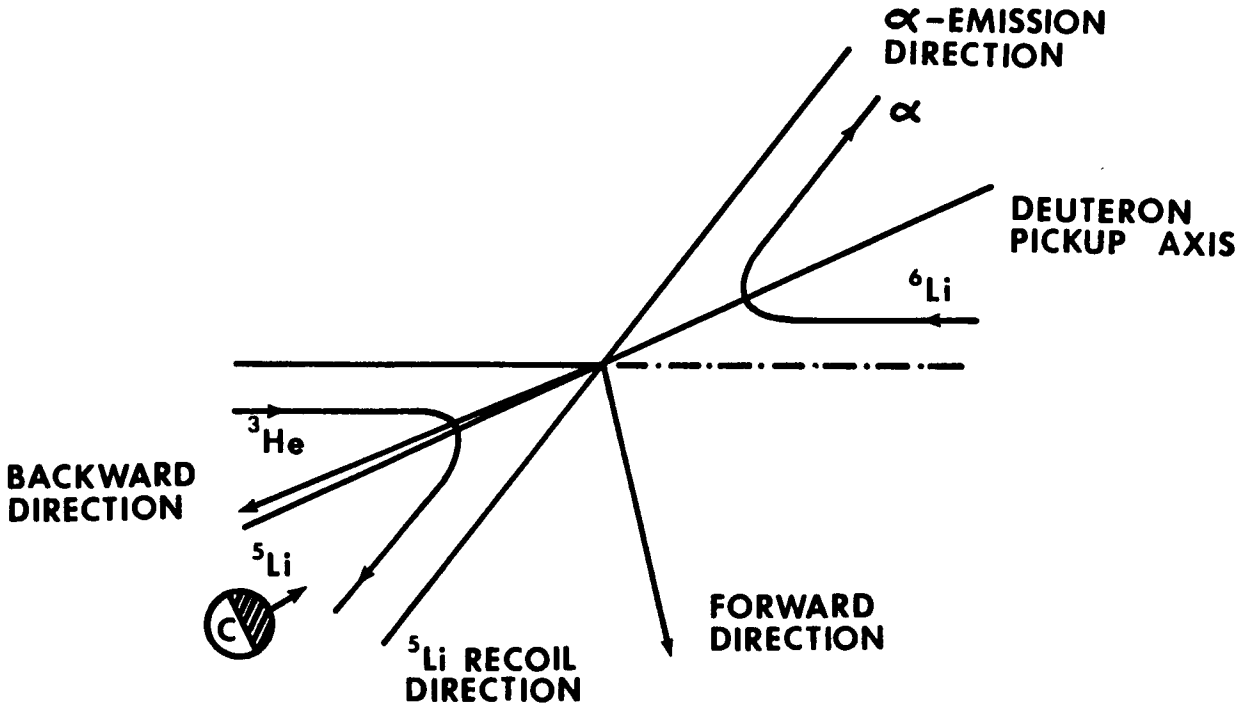

FIG. 3(b) DEUTERON TRANSFER

Tripard,[3] who measured the proton yield out of the plane formed by the incident beam and α_1.

These authors interpreted their observations as an asymmetric breakup of ^{5}Li (g.s.), and explained them on the basis of a model called the Reimann, Martin, and Vogt (RMV) model.[2]

RMV Model

The model is shown in Fig. 3. It is assumed that the first step of the sequential process is a direct reaction proceeding either by neutron transfer or deuteron transfer. The deuteron transfer can be thought of as a simultaneous transfer of a neutron and a proton. The authors argue that the neutron transfer occurs very rapidly compared to the motion of the porton in the $p_{3/2}$ shell in ^{5}Li. Consequently, after the neutron transfer, the proton is found localized in ^{5}Li. The lifetime of the ^{5}Li (g.s.) is 7×10^{-22} sec. as given in ref. 2. Therefore, an appreciable fraction of the initial localization of the proton may persist when the ^{5}Li(g.s.) nucleus decays into a proton and an alpha particle. Using a purely geometrical explanation, which does not involve correlation between the p-shell nucleons in the ground state of ^{6}Li, the authors have argued that the persistence of the localization alone would explain the observed asymmetry in the ^{5}Li decay.

Later, a more extensive angular correlation between the proton and the α- particles, at a ^{3}He bombarding energy of 1.25 MeV, was measured by Livesey and Piluso.[4] They

argued that their data showed an angular correlation pattern characteristic of the decay of a $p_{3/2}$ proton. The minimum of the proton yield appeared to be located somewhat behind the recoil axis. The authors also observed a forward - backward asymmetry in proton emission similar to that seen earlier by Reimann, Martin and Vogt. In an effort to explain the angular correlation data, Livesey and Piluso compared their results with that of Heggie and Martin,[7] who had also seen an asymmetry in the neutron breakup of ^5He in the reaction $^7Li + d \rightarrow \alpha_1 + {}^5He_{(g.s.)} \rightarrow n + \alpha_2$ at a deuteron bombarding energy of 1 MeV. In addition to the forward-backward asymmetry, their angular correlation measured between the neutron and the α_1, exhibited a shift in the minimum, similar to the one seen by Livesey and Piluso. Heggie and Martin explained their data in terms of the formation of a ^9Be compound nuclear state at an excitation energy of 17.48 MeV with a J^π of $3/2^+$, with an admixture to it arising from the tail of $5/2^-$level at 17.28 MeV, in the first step of the reaction.

Livesey and Piluso did their experiment at a ^3He bombarding energy of 1.25 MeV, which did not correspond to the excitation of any of the states in ^9B. However, it did correspond to an energy midway between the 17.19 MeV and 17.63 MeV states of ^9B. Consequently, they did not attempt to explain their data on the basis of a compound nucleus formation.

A proton-localization in the ^5Li intermediate state,

referred to earlier in the RMV model definitely implies that the intermediate state does not possess a well defined parity.[4] On the other hand, in a direct reaction it is well known that the distortion of incoming and outgoing waves may lead to a shift of the symmetry axis for the decay of the final state, even when that final state is formed in a truly sequential process, and has a well defined spin and parity.[8, 9, 10] An observation of an asymmetry about the recoil axis measured at some arbitrary forward-backward angle (see Fig. 2) may not be, in itself, an evidence for the proton localization in the ^{5}Li intermediate state. A more conclusive evidence for such an effect would be obtained by invoking the periodicity principle for a nuclear reaction, enunciated by A. Bohr in 1959.[11] The principle states that, 'In any nuclear reaction, leading to a nuclear state of well-defined parity the decay of that state must exhibit 180^{o} periodicity as measured in its own rest frame.'

The observation of such a periodicity in the proton-decay, at angles that are 180^{o} apart in the ^{5}Li recoil rest frame, would strongly suggest that ^{5}Li is formed in a state of definite parity before decaying. An observation to the contrary would tend to support the RMV concept of proton localization.

The present work is an experimental study of the sequential process in ^{6}Li + ^{3}He, going through the intermediate step of the formation of the ^{5}Li(g.s.), with the purpose of answering the following questions:

(1) What is the mechanism of the first step of the reaction? Is the ^{9}B compound nuclear state of 17.637 MeV formed at the appropriate ^{3}He bombarding nergy? What is the predominant off-resonance mechanism?

(2) What is the effect of the formation of the 17.637 MeV ^{9}B compound nuclear state on the proton-alpha angular correlation?

(3) Is a 180^{o} periodicity exhibited by the angular correlation pattern? In particular, what is the effect of the CN resonance formation, in the incoming channel, on the asymmetry in the proton-breakup of ^{5}Li(g.s.)?

The angular distribution of the first emitted α-particle would be very useful in determining the mechanism of the first step. Only one such measurement has been done in the past, at 1 MeV ^{3}He bombarding energy.[12] The data suggested a direct mechanism for the first step. Such a study near the ^{9}B resonance bombarding energy would be of particular interest.

Specifically, then, the present work describes the following three experimental studies:

(1) An alpha-alpha coincidence excitation function measured with both the detectors at a fixed angle, over a

range of ^{3}He bombarding energies around 1.6 MeV, corresponding to the 17.6 MeV state of ^{9}B in the incident channel.

(2) An alpha-proton angular correlation measurement, done with the alpha-detector at a fixed angle, for various proton-detector angles, at ^{3}He bombarding energies below, at,and above 1.6 MeV.

(3) A measurement of the angular distribution of the first emitted alpha-particle, obtained by and alpha-alpha coincidence measurement, at various angles for both the detectors, at bombarding energies below, at,and above 1.6 MeV.

CHAPTER II

EXPERIMENTAL PROCEDURE AND APPARATUS

Beam Production and Handling

Singly ionized ^{3}He beams of energies ranging from 1.25 MeV to 3.0 MeV were obtained from the Brooklyn College 3.75 MeV Dynamitron accelerator. The accelerator was equipped with a duoplasmatron ion source. Data were taken with both a straight-through configuration and the mass-analyzed configuration for the ion source. Pure ^{3}He (99.9%) was used in the straight-through configuration. A mixture of 50% ^{3}He with 50% ^{4}He was used in the mass-analyzed configuration.

After the beam was accelerated to a desired energy, it was electrostatically focused and steered into a pair of 60^{o} bending magnets which deflected the beam by 120^{o} altogether. The magnetic field of the bending magnets, measured by a NMR probe, served to define the energy of the beam. The analyzing magnetic field was calibrated using the known threshold energy for the ^{7}Li (p, n) ^{7}Be reaction of 1880.60± .07 KeV, the ^{19}F (p,d γ) resonance at 872.11± .20 KeV, and the ^{27}Al (p,γ) ^{28}Si resonance at 991.9 ± .04 KeV.[13] The spread in the energy of the beam was estimated to be less than 1 KeV. Energy stabilization was accomplished by the use of a pair of control slits at the exit of the second analyzing magnet. The beam was focused by a quadrupole lens

before it entered the scattering chamber.

Scattering Chamber

A 17" diameter scattering chamber, obtained from Rutgers University, was used for the experimental study. Detectors could be mounted on the bottom and the top turntables inside the scattering chamber. The turntables could be moved independently of each other. Detectors could also be mounted on the inside side-wall of the chamber. Thus, all reaction products were detected in the same plane.

A target ladder, with a provision for mounting four targets, could be vacuum coupled to the scattering chamber or removed from it for the convenience of preparing targets. A gate-valve was provided between the target ladder and the scattering chamber, enabling the preparation of targets and their subsequent transfer to the scattering chamber under vacuum.

The entrance port of the scattering chamber was equipped with a collimating system, which consisted of three collimators. The first collimator was a 1/4" circular copper aperture. The other two, made of tantalum, were a pair of defining collimator 1/8" in diameter and an antiscattering collimator and 5/32" in diameter, placed 1" apart. After passing through the target, the beam was finally dumped into a Faraday cup 7" deep. The charge collected in the Faraday cup was

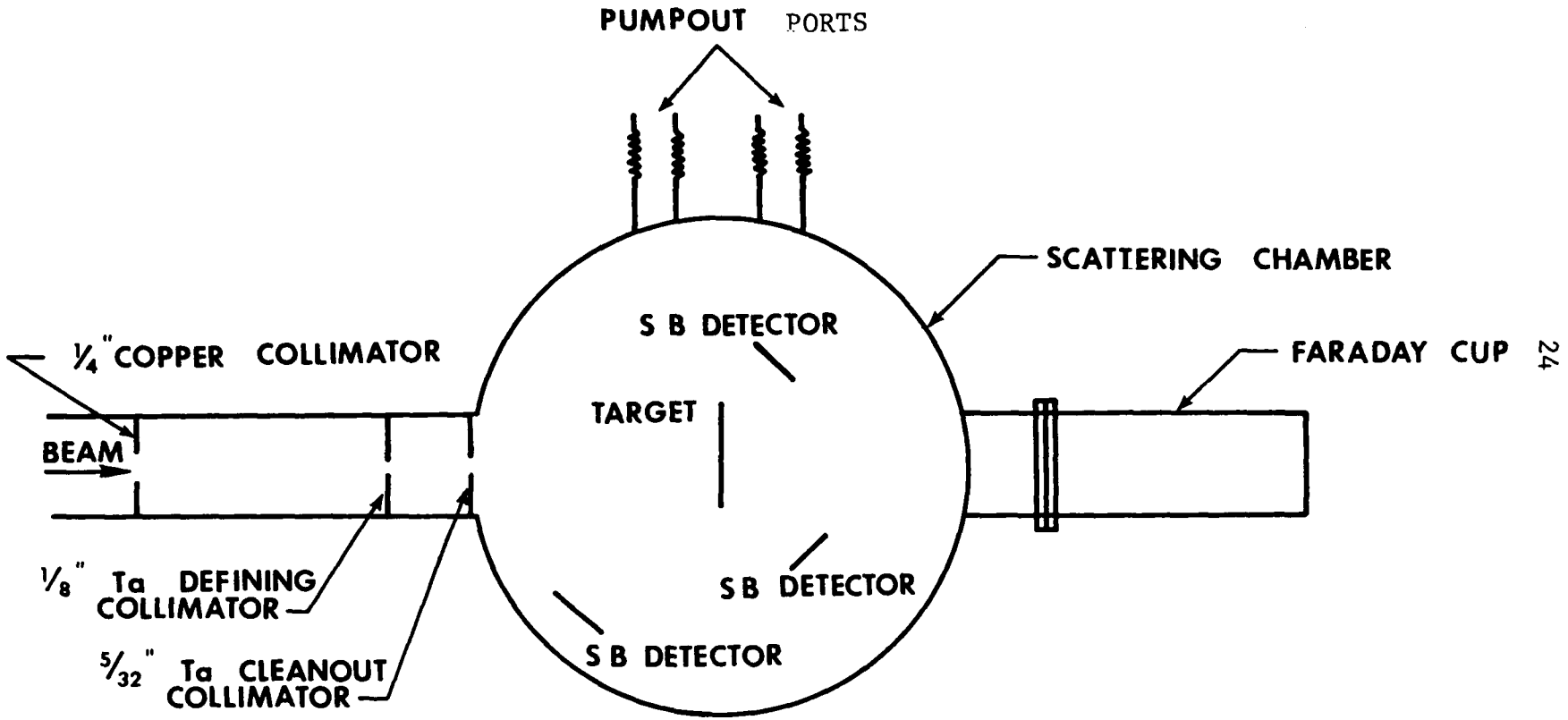

EXPERIMENTAL SET-UP

FIGURE 4

integrated by an ORTEC current digitizer.

A turbomolecular pump, TURBOVAC 350, made by Leybold Heraues, was used to produce a vacuum inside the scattering chamber. The chamber vacuum monitored by an ionization gauge, was always better than 10^{-5} Torr.

The centerline of the scattering chamber was aligned with respect to the beam transport system and the collimation system using a precision laboratory cathetometer. All detector angles could be set to an accuracy of 0.5^{o}.

The complete experimental set up for a typical measurement is shown in Fig. 4.

Detectors

Silicon Surface Barrier (SB) detectors of 50 mm^2 active area were used for charged-particle detection. The resolution of all the detectors was less than 16.6 KeV full-width at half-maximum (FWHM) for a 5.5 MeV Am^{241} alpha source.

Since a slightly different detector setup was used for coincidence, measurements between alphas and protons from that used for coincidence measurements between two alpha particles, these will be described separately.

Alpha-Alpha coincidence measurement: SB detectors of thickness 150 μ (the depletion depth) and 75 μ were used to detect α-particles of energies up to 10 MeV. They also provided discrimination between alphas and protons; the 150 μ detector discriminated between protons and alpha of energies

above 4.2 MeV, and the 75 μ detector discriminated similarly above 2.6 MeV, as the protons above these energies would not lose all their energy in the detectors. A 300 μ detector was used for some measurements.

Alpha-Proton coincidence measurement: Detection of all the protons produced in the reaction, $^{6}Li + {}^{3}He$ ranging in energy from 0 MeV to 16 MeV, would require a 1600 μ detector. However, since the energies of the protons that corresponded to a ^{5}Li (g.s.) formation in the sequential process ranged from 1.5 MeV to 7.0 MeV, a 1000 μ SB detector, capable of stopping up to 12.2 MeV protons, was used. When it was found necessary to distinguish an α particle from a proton of the same energy, one of the following two methods were employed: 1) By use of a totally depleted SB detector of a thickness 75 μ as a ΔE detector, immediately in front of a 1000 μ thickness SB detector, serving as an E detector, a particle identification was achieved. 2) Alternatively, mylar foils of thicknesses ranging from 7mg/cm^2 to 11 mg/cm^2 were placed in front of a single detector, producing much larger energy losses for the α particles than for the protons and hence resulting in an effective separation of the measured kinematic curves. The second method was found preferable as it required less complex electronics and provided adequate discrimination in almost all cases.

A detector of 300 μ thickness was used in all the runs to monitor the elastically scattered ^{3}He particles from the target nuclei.

The alpha and proton detectors were placed at a distance of 3.6 " from the target during all the experiment. The distance of the monitor detector from the target was 6.25" for the alpha-proton angular correlation, and the alpha-alpha excitation function measurements. It was 7.0" for the alpha angular distribution measurement. Brass collimators were placed in front of all the detectors in all the measurements. They were either circular or oval in shape. The dimensions of the detector collimator were decided upon by such consideration as the solid angle desired to optimize the count rate, and the maximum angular definition that could be allowed while keeping the kinematic broadening of the spectra to a minimum. Both the detectors subtended a solid angle of 2.1 mSr for all the alpha-alpha coincidence measurements, with an angular definition of 2^{o}, whereas for the alpha-proton coincidence measurement, the solid angle subtended by both the detectors was 3.7 mSr with an angular definition of 4^{o}. Whenever it was necessary, mylar foils of thickness 0.865 mg/cm^2 were placed in front of the detectors to stop the elastically scattered ^{3}He particles and the recoiling nuclei.

Targets

Targets of ^{6}LiF (^{6}Li enrichment 98.68%) were used. Carbon foils of thickness 15 to 20 μg/cm^2 were used as backings for all the targets. ^{6}LiF targets were prepared

by a vacuum evaporation of ^{6}LiF onto carbon foils mounted on aluminum frames having a 1/2" hole in the center. The target thickness was monitored using a quartz crystal thickness monitor.

Targets of ^{6}Li metal were also prepared by vacuum evaporation. These targets had to be transferred under vacuum from the vacuum evaporation system to the scattering chamber, as the ^{6}Li metal is highly reactive with oxygen. This required mounting the target ladder system onto the vacuum evaporation system by means of a vacuum collar. Target thickness could not be monitored continuously during the process of ^{6}Li metal evaporation due to the closeness of the evaporation geometry. Their thickness was determined later, after they were mounted onto the scattering chamber and the whole system was brought under vacuum, by a measurement of the energy loss of 6.19 MeV α particles, from a ^{252}Cf source, in passing through these targets. A comparison of the energy loss with the dE/dx values tabulated in ref. 14 yielded the target thickness. Targets of ^{6}Li metal of thickness of the order of 50 $\mu g/cm^2$ were used for the experiment.

Targets of ^{6}LiF were capable of tolerating up to 100na of beam current for many hours without deterioration due to beam current heating. Similarly the ^{6}Li metal targets could tolerate up to 300na of beam current.

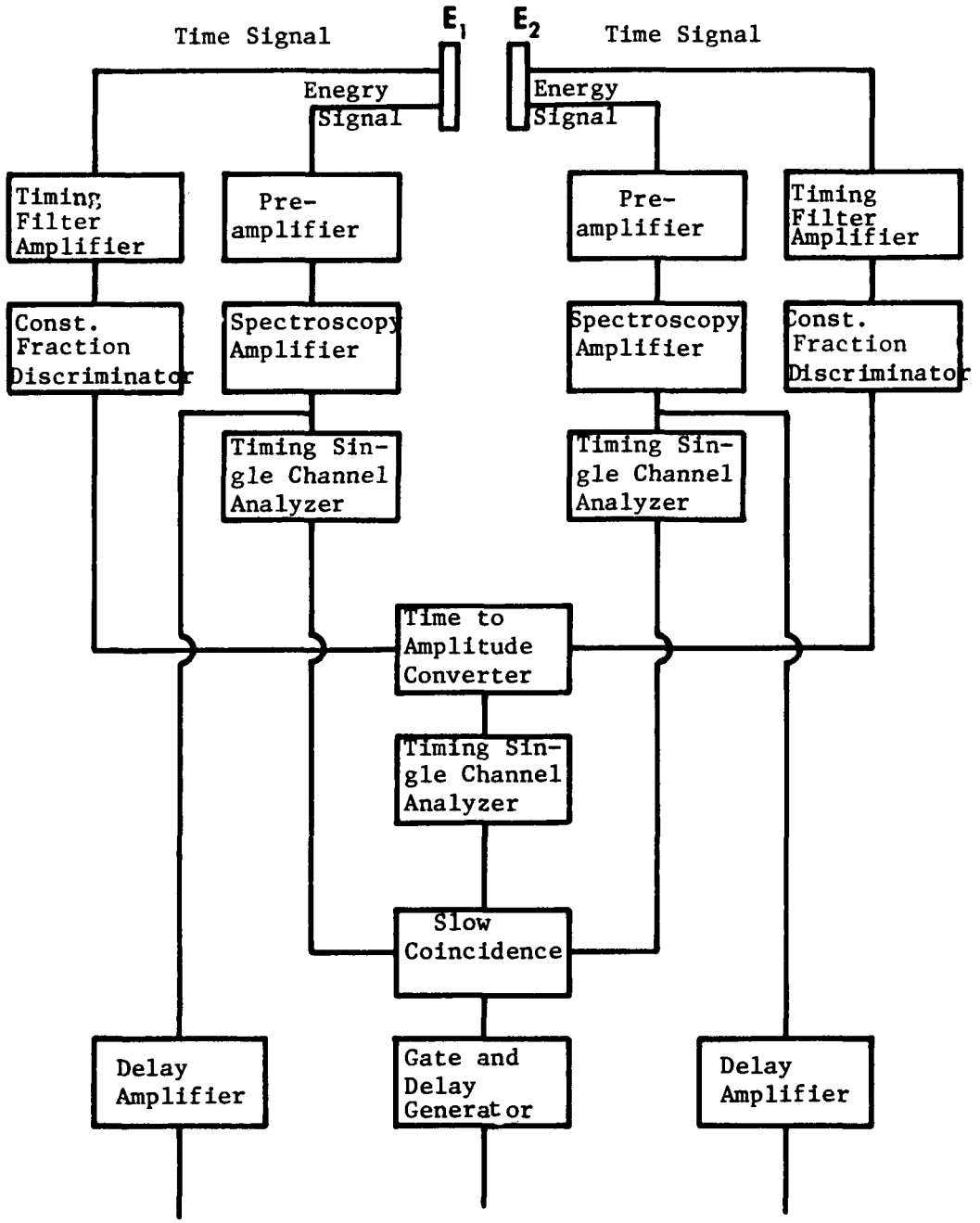

SLOW – FAST COINCIDENCE ELECTRONICS

FIGURE 5

Electronics

The coincidence measurements were performed using a slow-fast coincidence electronics shown in Fig. 5. The signals from two detectors were fed into preamplifiers which provided both an energy signal and a time signal with pulse width of ~ 50 nsec and risetime of less than 5 nsec. The time signal in each branch was passed through a timing filter amplifier and a fast discriminator. The discriminator level was set to eliminate the pulses due to detector noise. Outputs of the two fast discriminators constituted the start and stop inputs to a time - to - pulse height converter. The time spectrum showed a peak with a FWHM of 6 nsec. Random events were negligible for most of the experiment.

Energy outputs of the preamplifiers were fed into spectroscopy amplifiers in each branch. Outputs of the spectroscopy amplifiers went into timing single channel analyzers (TSCA). Slow timing was derived by establishing a slow coincidence between the logic outputs from the TSCA's. The resolving time of the slow coincidence unit was set at 200 nsec.

Outputs of the spectroscopy amplifiers were appropriately delayed and then sent to two Northern Scientific Analog to Digital converters (ADC). The inputs to the ADC's were gate pulse derived from the slow-fast coincidence timing. The 8192 channel Northern Scientific analyzer (NS 636) was used in 128 x 64 X-Y coincidence made to obtain the dual

parameter coincidence spectra. The data was printed out on a high speed Versatec printer interfaced to a PDP 11/20 computer, which was also interfaced with the NS 636. Monitor spectra were stored in a 4096-channel Northern Scientific Analyzer, which were dumped onto a magnetic tape.

Test pulses generated by an ORTEC 448 Research Pulser were fed into the preamplifiers and passed through all the electronics. The slow fast coincidence timing was set and periodically checked using these test pulses.

In all the runs signals from a fixed detector, of thickness either 150 μ or 300 μ , were scaled in a scalar after a single channel pulse height analysis. All the counts scaled within a single channel window between 7 MeV and 10 MeV corresponded to products from a $^{3}He + ^{6}Li$ reaction. This allowed a very convenient normalization for each run which was independent of contaminants and thickness variations in the targets.

Data were collected for a fixed value of total charge collected in the Faraday cup, with beam currents ranging from 100 na to 300 na. Data collection time for coincidence measurement was between 40 min and 120 min. A single spectrum was taken in each detector before and after each coincidence to check for gain shifts in the electronics. The singles count rate in each of the two detectors (with .8625 mg/cm^2 of mylar in front of them) varied from 10^3 counts/sec to 10^4 counts/sec, depending on the target thickness, beam current, and the angle of the detector. Dead time in all the ADC's was kept below 5%.

Chapter III

KINEMATICS AND REACTION MECHANISM

In the following discussion, the kinematics of three body final state reactions will be considered. Such a reaction can be written as

$$a + A \rightarrow 1 + 2 + 3 .$$

No restrictions are placed on the order of emission or the reaction mechanism. Since all studies were performed in a single plane (the reaction plane), the kinematics will be considered only in the reaction plane. Particle 1(2) will be understood to be detected at laboratory angle θ_1 (θ_2), angle being measured with respect to the direction of the incident beam. Particle 3 is undetected. All the quantities in the following discussion are described in a laboratory frame.

Conservation Equation

The non-relativistic conservation equations for momentum and energy take the form

$$p_a = \sum_{i=1}^{3} p_i \cos \theta_i \qquad (1)$$

$$o = \sum_{i=1}^{3} p_i \sin \theta_i \qquad (2)$$

$$T_a + Q = \sum_{i=1}^{3} T_i \qquad (3)$$

where

$$Q = (m_a + M_A - \sum_{i=1}^{3} m_i)c^2$$

since $T_i = p_i^2/2m_i$, equations (1) - (3) constitute three equations in terms of 6 parameters; p_1, p_2, p_3, and θ_1, θ_2 and θ_3.

Four of these p_1, p_2, θ_1 and θ_2 are determined experimentally. This leaves two unknown quantities and three equations to determine them, causing the problem to appear overdetetmined. However, one does require four quantities experimentally to resolve double-valved solutions.

The Kinematic curve

The parameters p_3 and θ_3 of the undetected particle may be elimiated from equations (1) - (3) in a straighforward manner. The resulting expressions may be written as

$$Ap_2^2 + Bp_2 + C = 0 \qquad (4)$$

with

$$A = \frac{1}{2m_2} + \frac{1}{2m_3}$$

$$B = \frac{p_1}{m_3}(\sin\theta_1 \sin\theta_2 + \cos\theta_1 \cos\theta_2) - \frac{p_a}{m_3}\cos\theta_2$$

$$C = \frac{p_1^2}{2m_1} + \frac{p_a^2 + p_1^2}{2m_3} - \frac{p_a p_1}{m_3} - \cos\theta_1 - \frac{p_a^2}{2m_a} - Q$$

Acceptable solutions will be limited to positive real roots of equation (4), given by

$$p_2^{\pm}(p_1) = \frac{-B \pm \sqrt{B^2 - 4AC}}{2A}$$

Negative values of p_2 will correspond to particles moving away from the detector and hence must be discarded.

The above solution defines a curve in the $p_1 - p_2$ kinematic plane. Experimentally, one measures kinetic energies rather than momenta, so it is of interest to express the above relation in terms of T_1 and T_2. This is also straightforward and the result is

$$A'T_2 + B' T_2^{\frac{1}{2}} + C' = 0 \qquad (5)$$

with $A' = 1 + \frac{m_2}{m_3}$

$$B' = \frac{2\sqrt{m_1 m_2 T_1}}{m_3}(\sin\theta_1 \sin\theta_2 + \cos\theta_1 \cos\theta_2) - \frac{2\sqrt{m_a m_2 T_a}}{m_3}\cos 0$$

$$C' = T_1\left(1 + \frac{m_1}{m_3}\right) + T_a\left(\frac{m_a}{m_3} - 1\right) - \frac{2\sqrt{m_a m_1 T_a T_1}}{m_3}\cos\theta_1 - Q$$

Allowed values of $T_2^{\frac{1}{2}}$ are the real and positive solutions of equation (5) given by

$$T_2^{\frac{1}{2}}(T_1) = \frac{-B' \pm \sqrt{B'^2 - 4A'C'}}{2A'} \qquad (6)$$

The relationship in the E_1-E_2 plane, given by (6), will herinafter be referred to as the kinematic curve.

In the most general cases all three particles are distinguishable and detectable, and if no particle discrimi-

nation is employed six kinematic curves are obtained, one for each distinguishable permutation of two detectable particles. For other combinations of particles, it is possible to have one, two or three curves, e.g. two identical particles in the final state lead to three different kinematic curves.

Sequential Decay Kinematics

If the nuclear reaction $a + A \rightarrow i + j + k$ proceeds through an intermediate state in which two of the final particles are bound, the process can be written as a sequence of two reactions

(a) $a + A \rightarrow i + (jk)$

(b) $i + (jk) \rightarrow i + j + k$

For step (a), the energy conservation equation is

$$E_a + Q_i = T_i + T_{jk} + E_{jk} \qquad (7)$$

where $Q_i = (m_a + M_A - m_i - m_{jk})\, c^2$

T_{jk} is the kinetic energy of the cluster (jk) and the E_{jk} is the excitation energy of the state in (jk), involved in the step (a).

It is assumed throughout that particles i, j, and k remain in their ground state. Restating the convention adopted for labelling particles, the first emitted particle strikes detector 1 (2) if i = 1 (2), and the first emitted particle is undetected if i = 3.

Since step (a) results in a two-body final state, the reaction takes place in a plane, therefore conservation of momentum is expressed by

$$P_a = p_i \text{ Cos } \theta_i + P_{jk} \text{ Cos } \theta_{jk} \qquad (8)$$

$$P_i \text{ Sin } \theta_i = P_{jk} \text{ Sin } \theta_{jk} \qquad (9)$$

Using $T_i = \frac{p_i^2}{2m_i}$ and $T_{jk} = \frac{p^2_{jk,}}{2m_{jk}}$ the parameters T_{jk}, p_{jk} and θ_{jk} may be eliminated from equation (6) - (8). The result is

$$E_{jk} = Q_i + E_a \left(1 - \frac{m_a}{m_{jk}}\right) - E_i \left(1 + \frac{m_i}{m_{jk}}\right) + \frac{2\ m_a\ m_i\ T_a\ T_i}{m_{jk}} \text{ Cos } \theta_i \qquad (10)$$

The three equations, represented by equation (10), may be expressed in terms of E_1, p_1, and p_2, by using relationships developed in the preceding sections.

For each value of E_1, the possible excitation energies of the intermediate nucleus are given by

$$E_{23} = E_a + Q_1 - E_1 - \frac{1}{2m_{23}} (p_a^2 + p_1^2 - 2\ p_a\ p_1 \text{ Cos } \theta_1)$$

$$E_{13} = E_a + Q_2 - E_1 - \frac{1}{2m_{13}} (p_a^2 + p_2^2 - 2\ p_a\ p_2 \text{ Cos } \theta_2)$$

$$E_{12} = E_a + Q_3 - \frac{p_a^2}{2\ m_3} + \frac{p_a}{m_3} (p_1 \text{ Cos } \theta_1 + p_2 \text{ Cos } \theta_2) - \frac{1}{2} \left(\frac{1}{m_3} + \frac{1}{m_{12}}\right) (p_1^2 + p_2^2 + 2\ p_1\ p_2 \times (\text{Sin } \theta_1 \text{ Sin } \theta_2 + \text{Cos } \theta_1 \text{ Cos } \theta_2)).$$

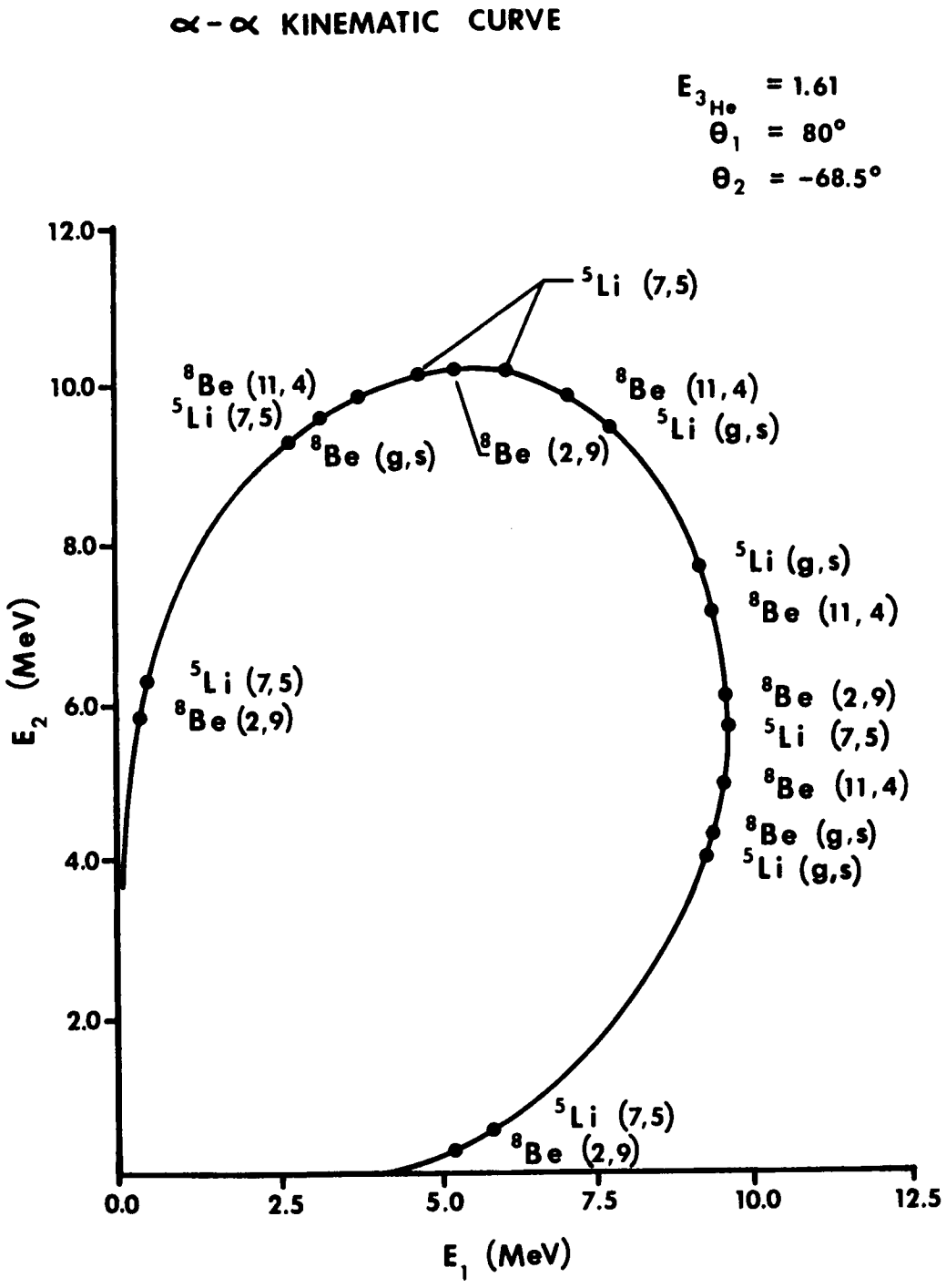
α - α KINEMATIC CURVE
$E_{3_{He}}$ = 1.61
θ_1 = 80°
θ_2 = -68.5°
12.0
10.0
8.0
6.0
4.0
2.0
E_2 (MeV)
0.0
2.5
5.0
7.5
10.0
12.5
E_1 (MeV)
^{5}Li (7,5)
^{8}Be (11,4)
^{5}Li (7,5)
^{8}Be (g,s)
^{8}Be (2,9)
^{8}Be (11,4)
^{5}Li (g,s)
^{5}Li (g,s)
^{8}Be (11,4)
^{5}Li (7,5)
^{8}Be (2,9)
^{8}Be (2,9)
^{5}Li (7,5)
^{8}Be (11,4)
^{8}Be (g,s)
^{5}Li (g,s)
^{5}Li (7,5)
^{8}Be (2,9)

FIGURE 6

A state in ^{5}Li or ^{8}Be appears as a segment on these kinematic curves. The length of the segment is determined by the width of the state. Fig. 6 shows a kinematic curve, calculated using the expression (6) for a ^{3}He bombarding energy of 1.55 MeV, with the locations of ^{5}Li and ^{8}Be states, calculated using the expressions (10), shown on it.

Phase Space Distribution

As mentioned in Chapter I, two distinct mechanisms leading to the three-particle final state are possible: (1) simultaneous breakup into three particles and (2) sequential breakup proceeding through states of an intermediate nucleus. The qualitative features of the projected coincidence spectrum allow the determination of the relative importance of the two possible decay modes, and in the case of sequential processes the relative contributions of different states of the intermediate nucleus can be measured.

If the reaction proceeds via simultaneous breakup into three particles, the projected coincidence spectrum would be expected to reflect a uniform population of the available phase space. Several authors[15,16] have treated this problem. The resulting spectrum formed by the projection of the kinematic curve onto E_1 (or E_2) axis is a smoothly increasing function of E_1 (or E_2), which attains its maximum value at the point of vertical tangency of

PHASE SPACE DISTRIBUTION WITH THE ASSOCIATED KINEMATIC CURVE

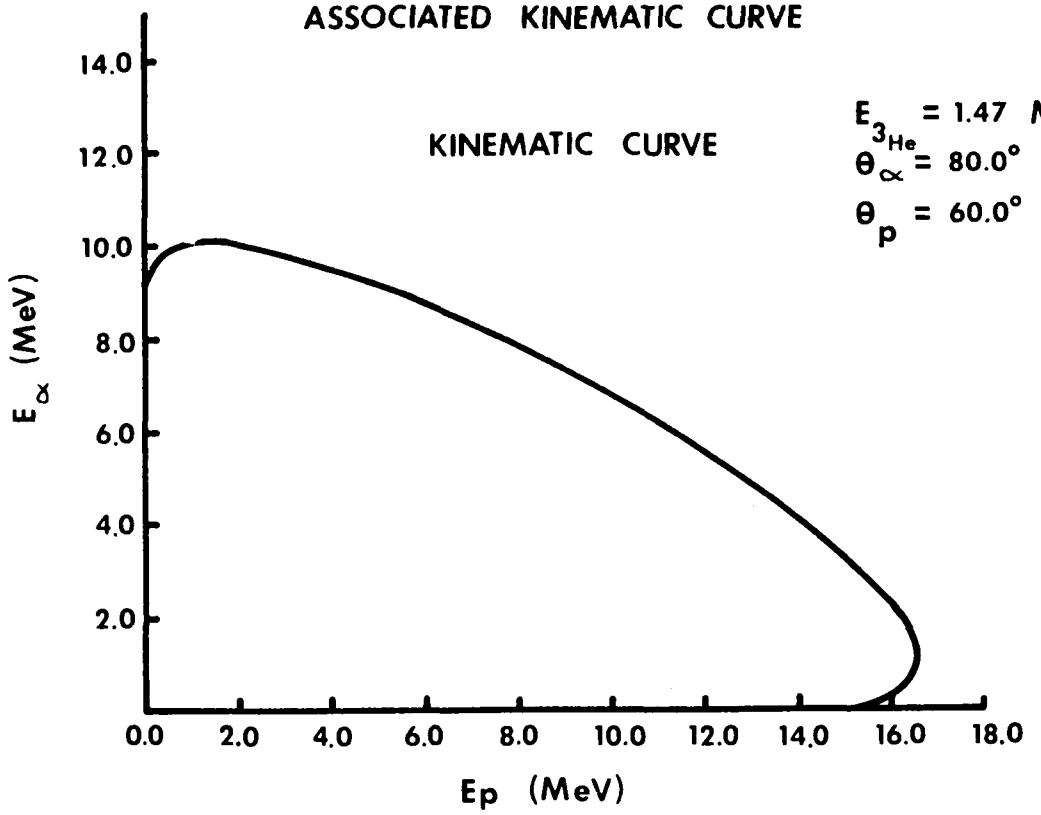

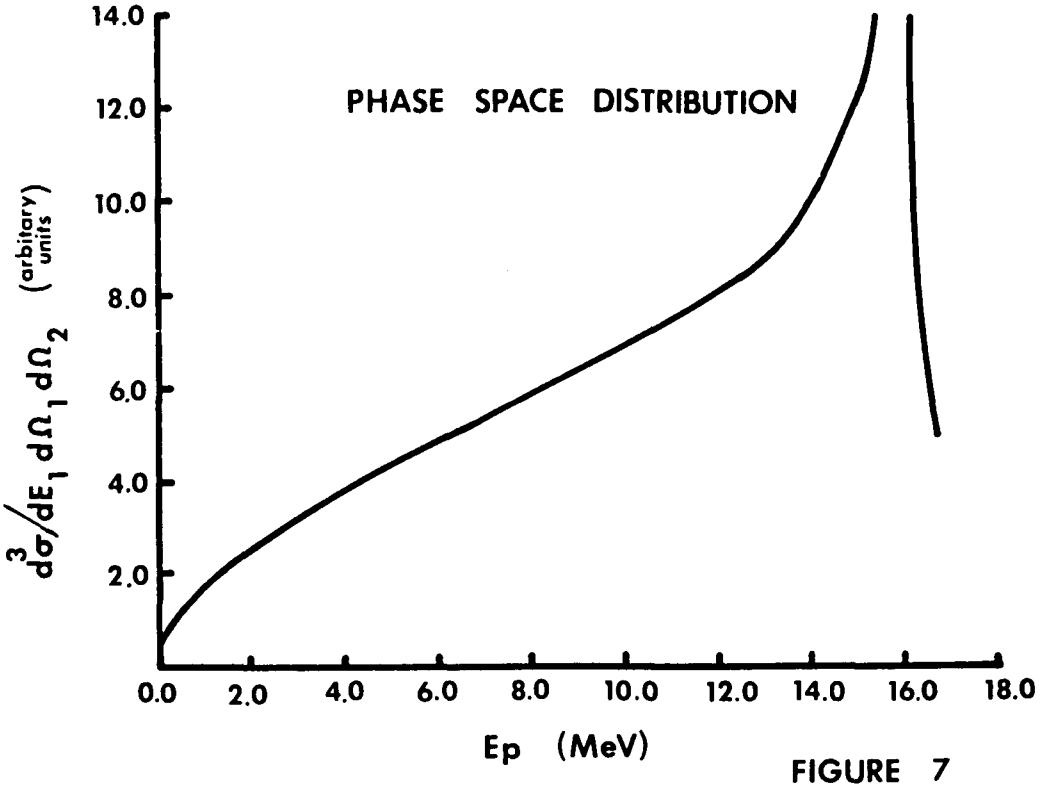

FIGURE 7

VELOCITY VECTOR DIAGRAM

FOR ^{6}Li (^{3}He, α) ^{5}Li (g.s.) $\rightarrow$ p + α

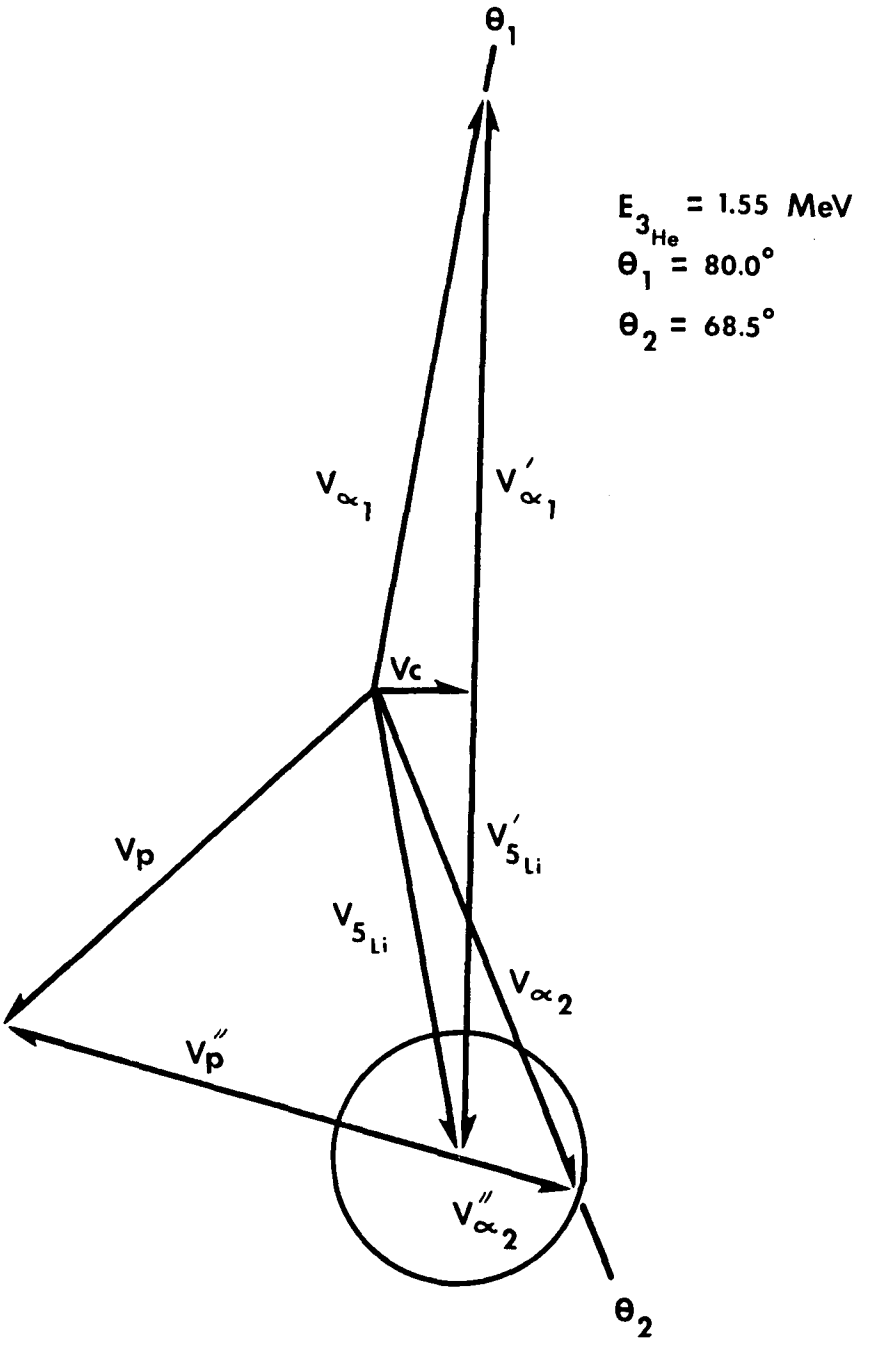

FIGURE 8

the kinematic locus.

Even when angular momentum and coulomb effects complicate the calculations, the smooth character of the projected spectrum is retained.[17] The mathematical expression, for coplaner final states, is

$$\frac{d^3\sigma}{dE_1 d\Omega_1 d\Omega_2} = \text{const.} \frac{m_3 p_1 p_2^2}{\left| p_2\left[\frac{m_2 + m_3}{m_2}\right] + p_1 \cos\Delta_{12} - p_a \cos\theta_2 \right|} \quad (11)$$

where Δ_{12} is the angle between the two detectors. An example of such a phase space distribution with the associated kinematic curve is shown in Fig. 7.

On the other hand, if the reaction mechanism leading to the three body final state were sequential in nature, the projected coincidence spectrum would be expected to exhibit manifestation of the intermediate nuclear states involved. The shape of such peaks would largely be determined by the width of the energy level involved.

Therefore, the qualitative appearance of the coincidence spectrum can signal definite indications of the mechanisms which contribute to the formation of a three-particle final state.

Velocity Vector Diagram

Mathematical expressions for the velocities of the outgoing particles 1, 2 and 3 in various frames of references are summarized in Appendix A. A velocity vector diagram using these velocities is shown in Fig. 8.

CHAPTER IV

EXPERIMENTAL DATA

Excitation Function Measurement

As it was generally difficult to resolve the α peaks due to the ^{5}Li states from the α continuum under them in a single detector spectrum, the excitation function measurement was done using an alpha-alpha coincidence method. Coincidences between the two α particles were measured in two detectors, set at angles of 80° and -68.5°, as a function of ^{3}He bombarding energy. Targets of ^{6}LiF of a thickness 33 $\mu g/cm^{2}$ on a 20 $\mu g/cm^{2}$ carbon backing were used for the measurement. Other experimental details have been described earlier in Chapter II.

The experimental geometry is illustrated in Fig. 9 by a velocity vector diagram for the reaction $^{6}Li + {}^{3}He \rightarrow \alpha_{1} + {}^{5}Li\ (g.s.) \rightarrow p + \alpha_{2}$, drawn for a ^{3}He bombarding energy of 1.55 MeV. The recoil direction of the ^{5}Li nuclei, for an α_{1} going into 80° detector is -79°. By choosing an angle of -68.5° for the α_{2} detector, contributions from the 16.66 MeV and the 16.92 MeV states of ^{8}Be to the $\alpha - \alpha$ coincidence curve are totally excluded. Then, the main contribution to the $\alpha - \alpha$ coincidence curve comes from the ^{5}Li (g.s.).

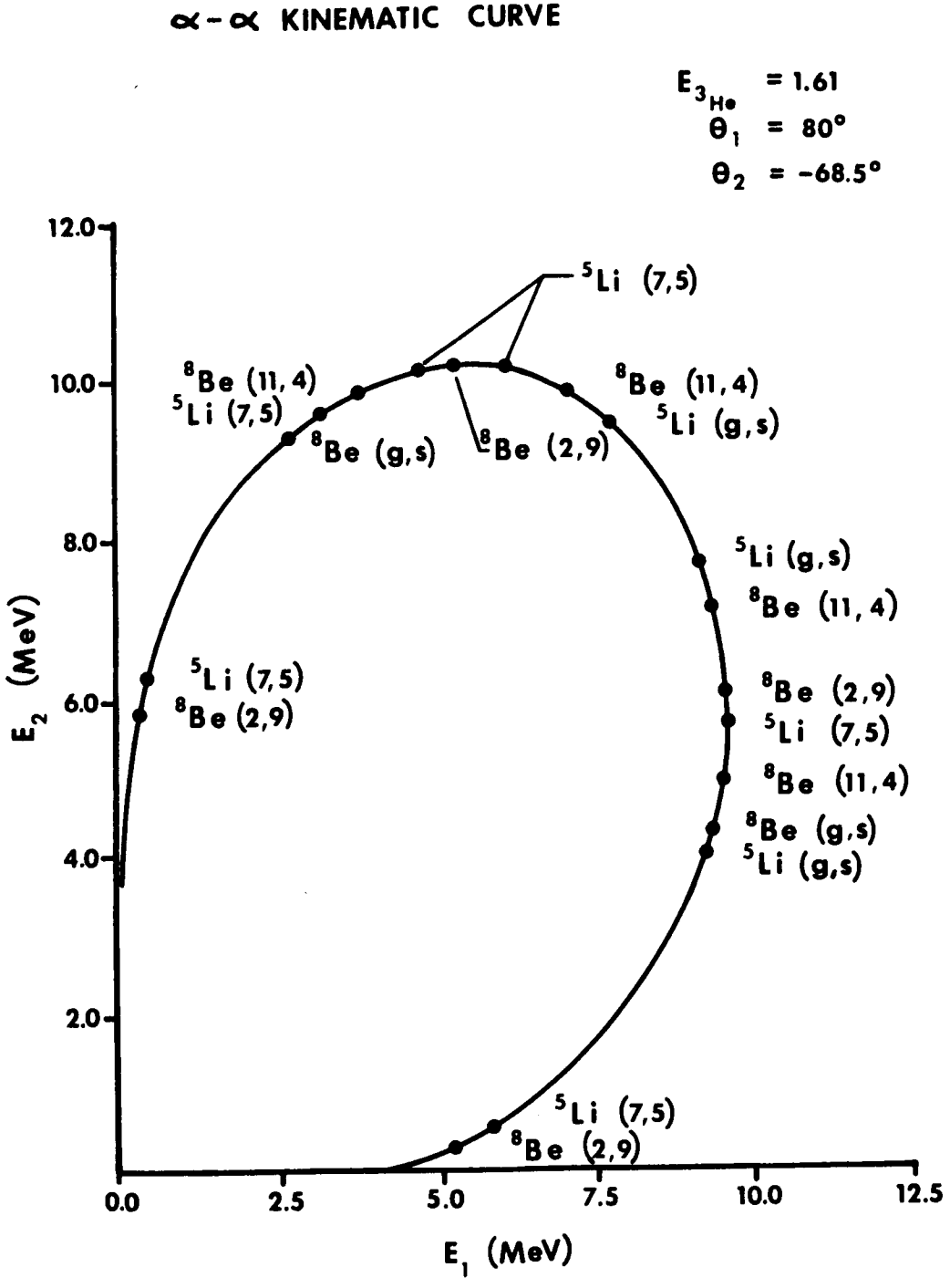
α - α KINEMATIC CURVE
$E_{3_{He}}$ = 1.61
θ_1 = 80°
θ_2 = -68.5°
12.0
10.0
8.0
6.0
4.0
2.0
E_2 (MeV)
0.0
2.5
5.0
7.5
10.0
12.5
E_1 (MeV)
^{5}Li (7,5)
^{8}Be (11,4)
^{5}Li (7,5)
^{8}Be (g,s)
^{8}Be (2,9)
^{8}Be (11,4)
^{5}Li (g,s)
^{5}Li (g,s)
^{8}Be (11,4)
^{5}Li (7,5)
^{8}Be (2,9)
^{8}Be (2,9)
^{5}Li (7,5)
^{8}Be (11,4)
^{8}Be (g,s)
^{5}Li (g,s)
^{5}Li (7,5)
^{8}Be (2,9)

FIGURE 9

FIGURE 10

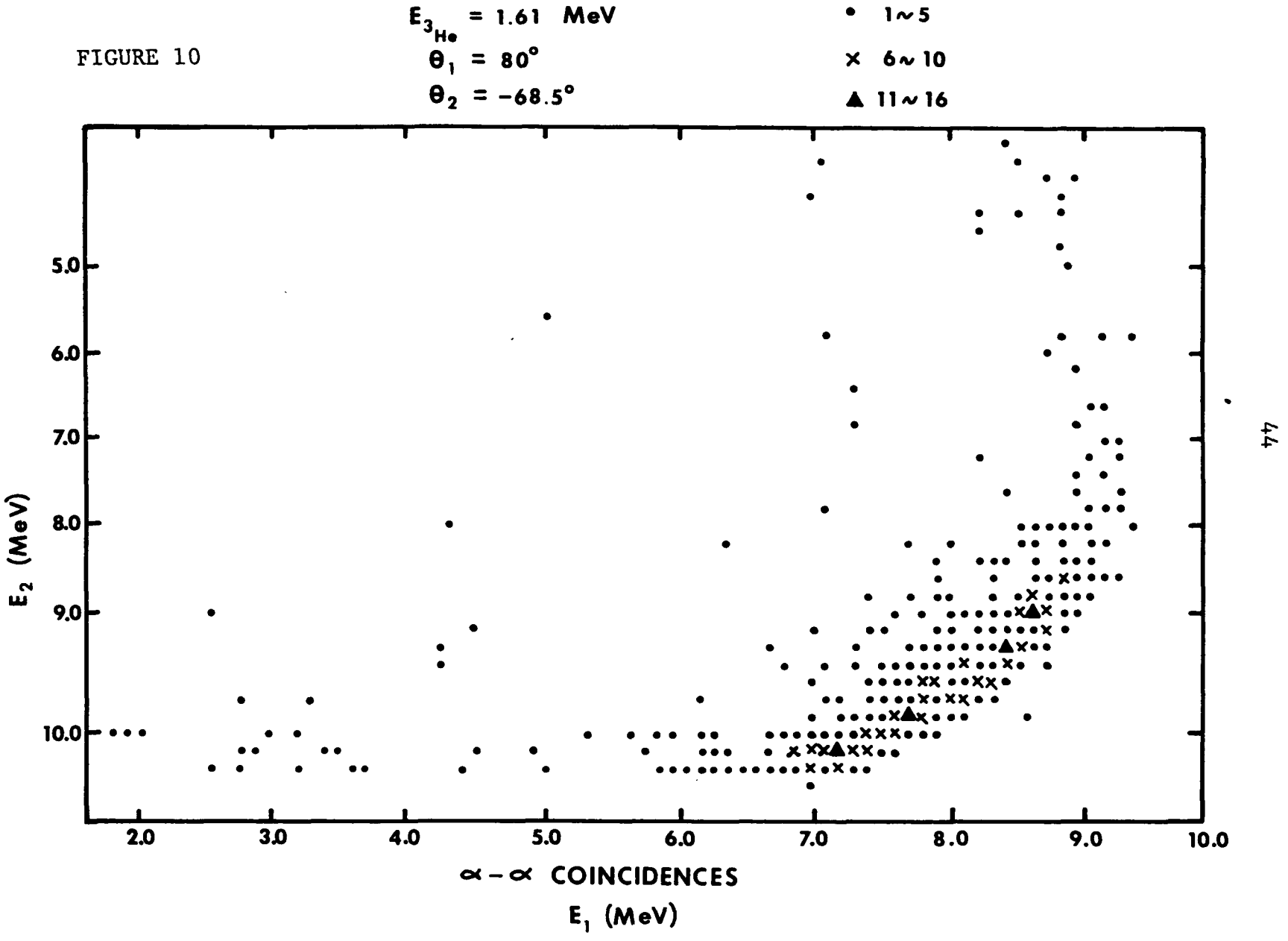
$E_{^3He}$ = 1.61 MeV
θ_1 = 80°
θ_2 = −68.5°
• 1∼5
× 6∼10
▲ 11∼16
5.0
6.0
7.0
8.0
9.0
10.0
E_2 (MeV)
2.0
3.0
4.0
5.0
6.0
7.0
8.0
9.0
10.0
α − α COINCIDENCES
E_1 (MeV)

Fig. 9 is a calculated alpha-alpha kinematic curve for a ^{3}He bombarding energy of 1.61 MeV showing the locations of various ^{5}Li and ^{8}Be states on it. There are four possible locations for the ^{5}Li (g.s.). Two of these occur towards the middle of the curve. Such alpha-alpha coincidence data were obtained experimentally for ^{3}He bombarding energies ranging from 1.47 MeV to 1.75 MeV. One of these is shown in Fig. 10, which is taken at a ^{3}He bombarding energy of 1.61 MeV. The data at the other ^{3}He bombarding energies is very similar to it except for minor shifts of the kinematic curve along the two energy axes, due to the changes in bombarding energy. A large concentration of counts is seen in all the data at the two middle locations corresponding to ^{5}Li (g.s.). The spread along the curve is due to the width of the ^{5}Li (g.s.) which is 1.5 MeV. Another possible contribution to the spectrum in this region could result from the formation of ^{8}Be 11.4 MeV state, which kinematically could produce an enhancement in the counting rate near the ^{5}Li (g.s.) locations, as seen in the calculated kinematic curve in Fig. 9. However, an examination of the data near the calculated location of the ^{8}Be state shows that this contribution is negligible.

Contributions to the coincidence data may also be expected from the simultaneous break-up process. Previous studies [2, 3] have shown that at low bombarding energies,

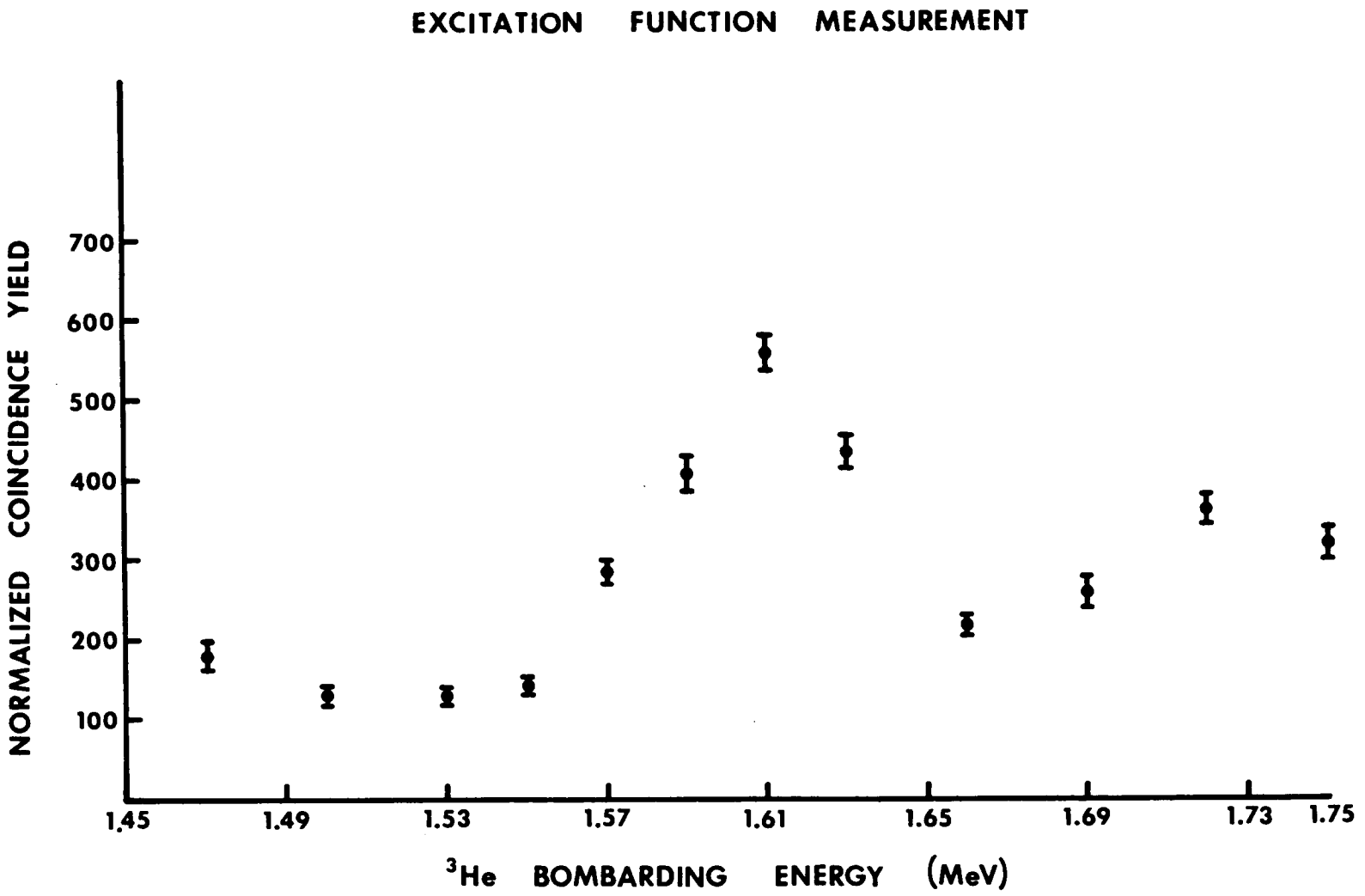
EXCITATION FUNCTION MEASUREMENT
NORMALIZED COINCIDENCE YIELD
700
600
500
400
300
200
100
1.45
1.49
1.53
1.57
1.61
1.65
1.69
1.73
1.75
^{3}He BOMBARDING ENERGY (MeV)

FIGURE 11

such contributions are less than 10%. The present data are found to be in agreement with this estimate.

The normalization to the data was obtained by measuring the elastically scattered ^{3}He particles from ^{19}F nuclei, detected in a 300 μ SB detector. This detector was located at a backward angle of 130^{o} with respect to the incident beam direction. ^{3}He elastic scattering from ^{19}F nuclei is largely Rutherford, and is not expected to vary significantly over the range of ^{3}He incident energies for which the excitation function was measured.

The coincidence yields obtained by adding up counts on the coincidence curve between E_1 = 5.9 MeV to E_1 = 9.6 MeV and E_2 = 6.5 MeV to E_2 = 10.2 MeV (Fig. 10) were normalized to ^{3}He elastically scattered from ^{19}F. These have been plotted as a function of ^{3}He bombarding energy in Fig. 11.

The error in each data point is mainly due to the coincidence counting statistics. An enhancement is seen in the excitation function curve at 1.61 MeV. After taking into account the target thickness, which was 70 ± 20 KeV of ^{3}He energy loss at 1.61 MeV ^{3}He incident energy, the width of ^{9}B resonance from this measurement is 70 ± 20 KeV. Both the energy and width are in good agreement with previously measured values of the ^{9}B compound state as obtained from an excitation function measurement on the ^{7}Be (d,p) ^{8}Be reaction.[18]

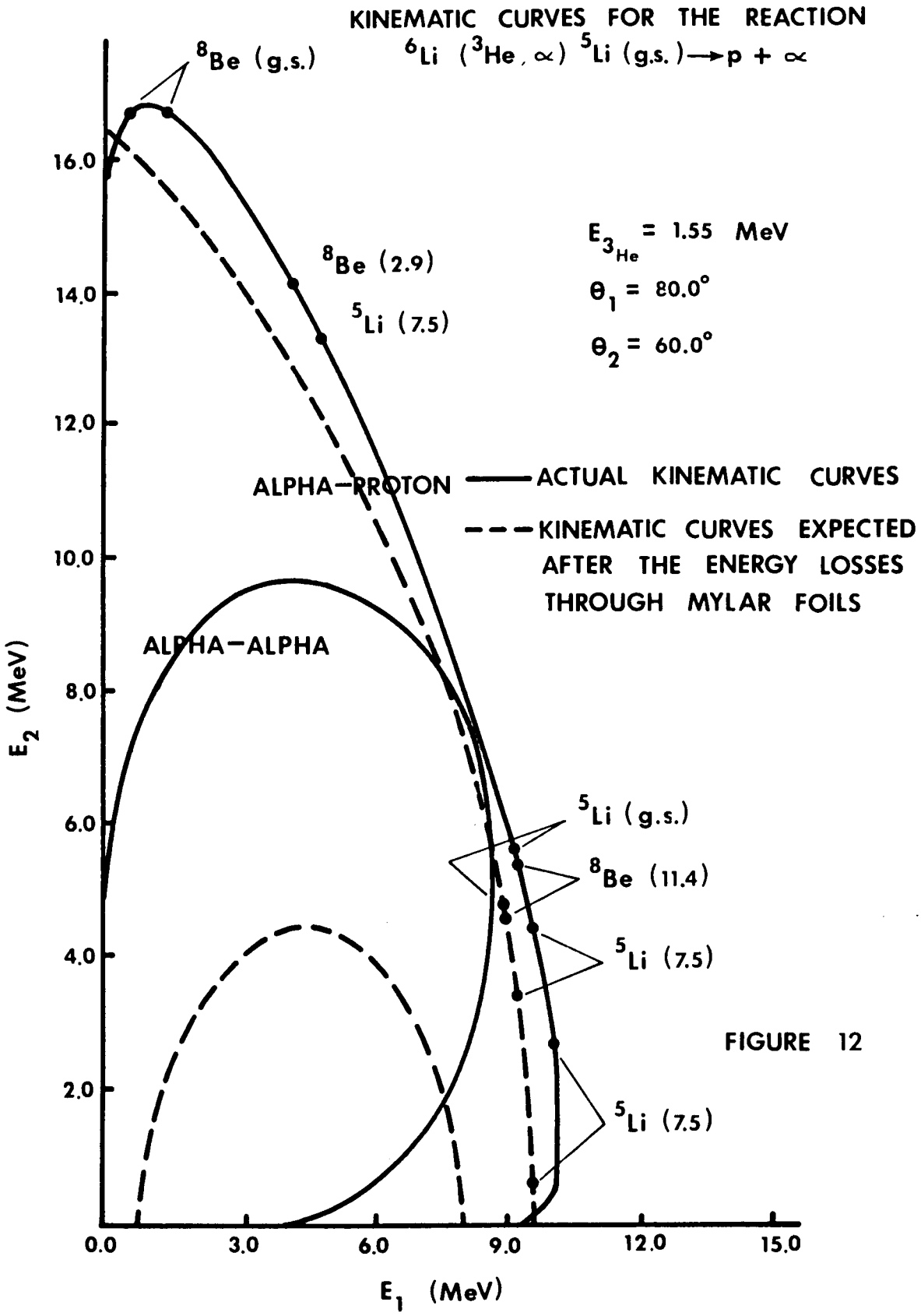
KINEMATIC CURVES FOR THE REACTION
^{6}Li (^{3}He, α) ^{5}Li (g.s.) $\rightarrow$ p + α
^{8}Be (g.s.)
$E_{3_{He}}$ = 1.55 MeV
θ_1 = 80.0°
θ_2 = 60.0°
^{8}Be (2.9)
^{5}Li (7.5)
ALPHA–PROTON
ALPHA–ALPHA
ACTUAL KINEMATIC CURVES
KINEMATIC CURVES EXPECTED AFTER THE ENERGY LOSSES THROUGH MYLAR FOILS
^{5}Li (g.s.)
^{8}Be (11.4)
^{5}Li (7.5)
^{5}Li (7.5)
E_2 (MeV)
E_1 (MeV)
16.0
14.0
12.0
10.0
8.0
6.0
4.0
2.0
0.0
3.0
6.0
9.0
12.0
15.0

FIGURE 12

FIGURE 13

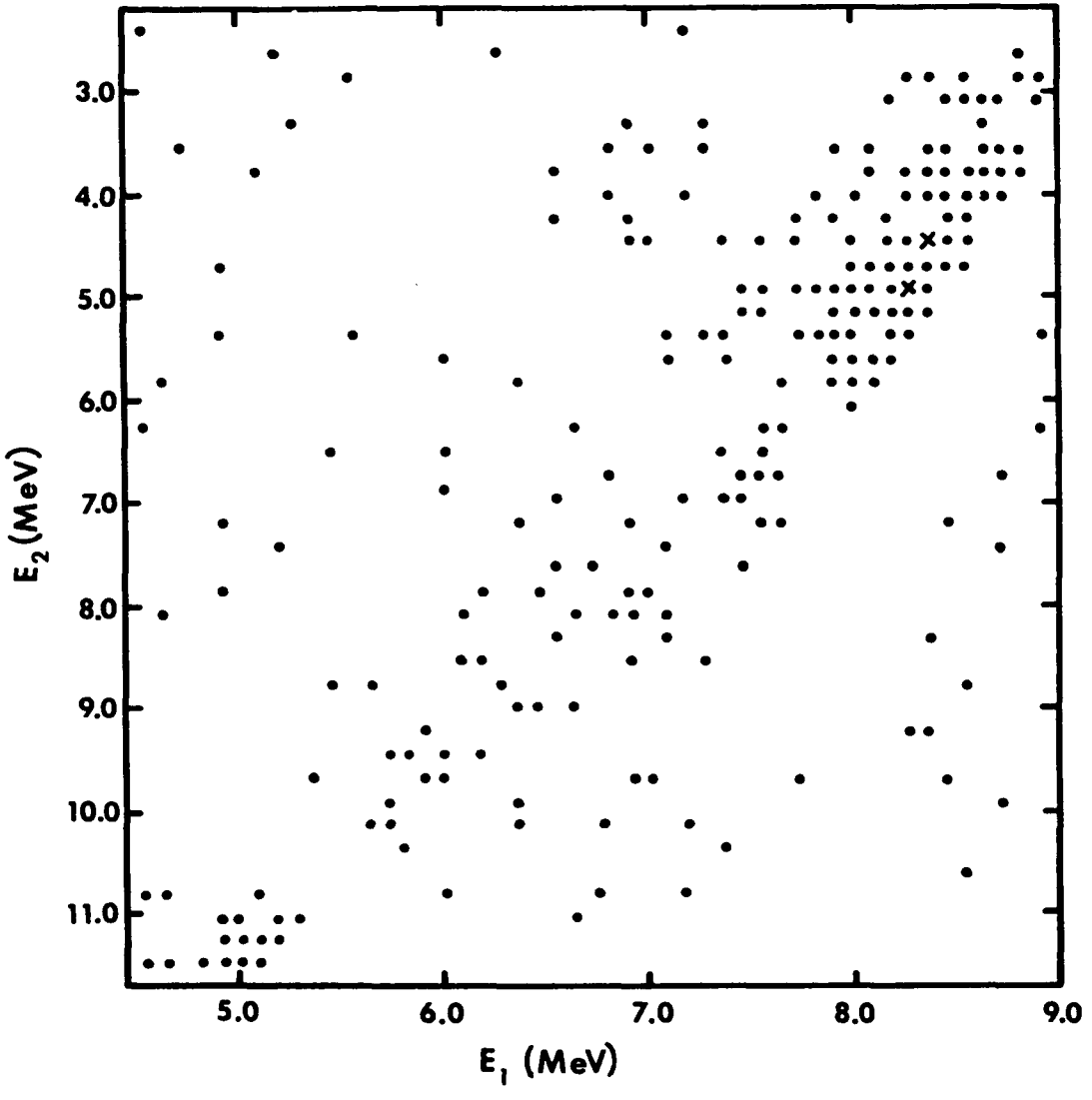
3.0
4.0
5.0
6.0
7.0
8.0
9.0
10.0
11.0
E2 (MeV)
5.0
6.0
7.0
8.0
9.0
E1 (MeV)
E3He = 1.47 MeV
θα = 80°
θ = −79°
• 1~4
× 5~8

FIGURE 14

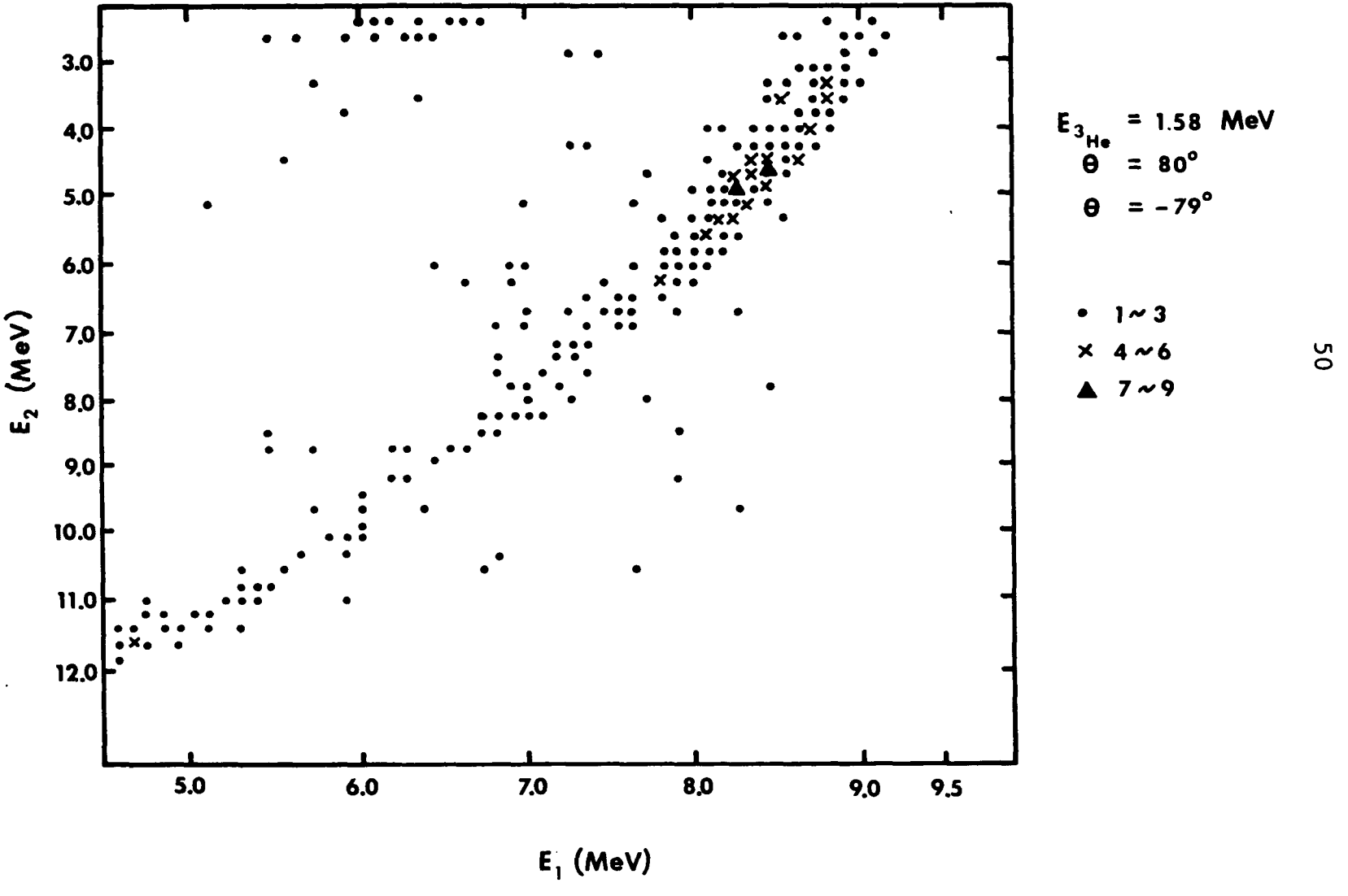
3.0
4.0
5.0
6.0
7.0
8.0
9.0
10.0
11.0
12.0
E_2 (MeV)
5.0
6.0
7.0
8.0
9.0
9.5
E_1 (MeV)
$E_{^3He}$ = 1.58 MeV
θ = 80°
θ = -79°
• 1~3
× 4~6
▲ 7~9

FIGURE 15

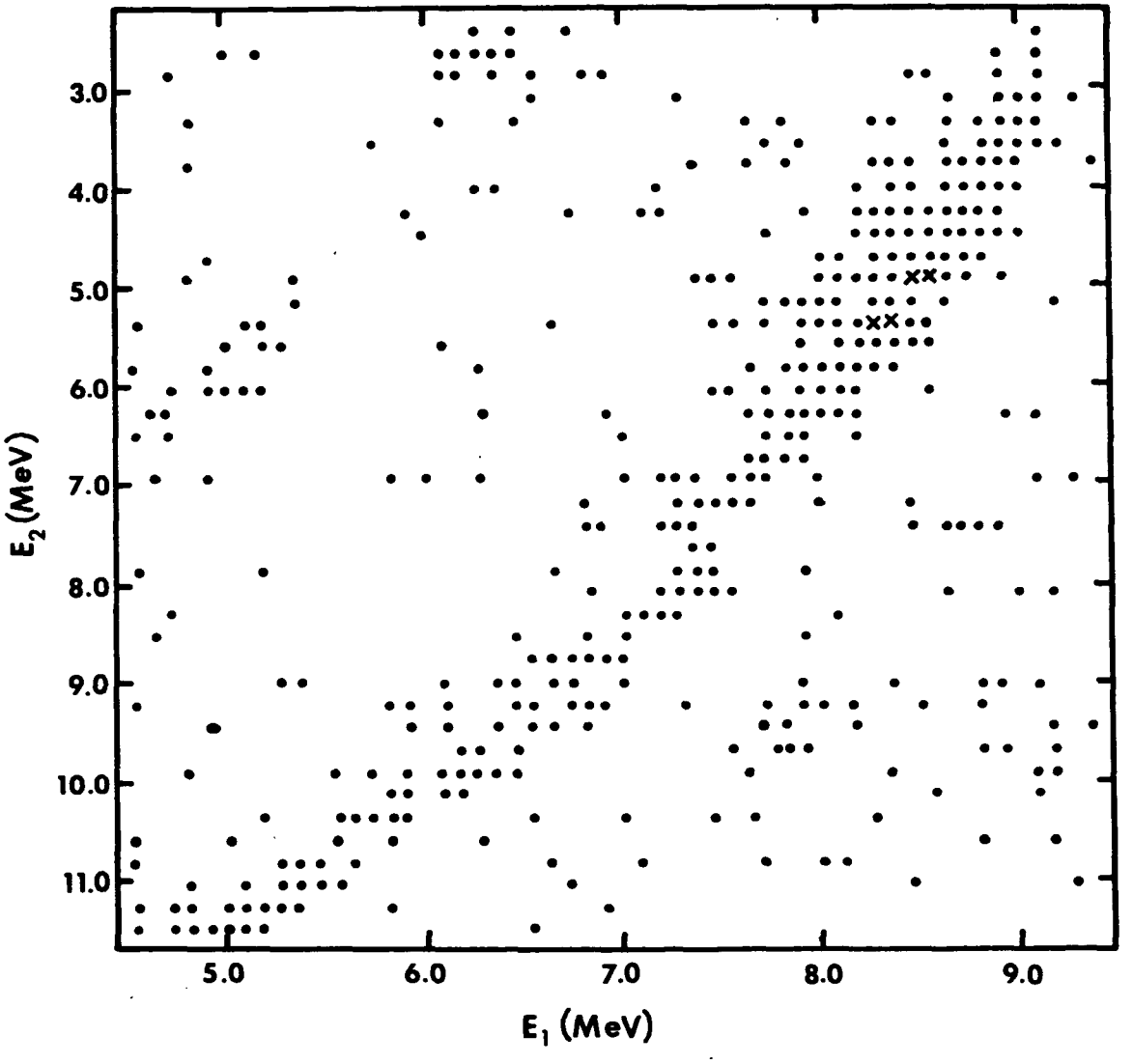
3.0
4.0
5.0
6.0
7.0
8.0
9.0
10.0
11.0
E_2 (MeV)
5.0
6.0
7.0
8.0
9.0
E_1 (MeV)
$E_{^3He}$ = 1.69 MeV
θ_α = 80°
θ = -79°
• 1 ~ 8
× 9 ~ 16

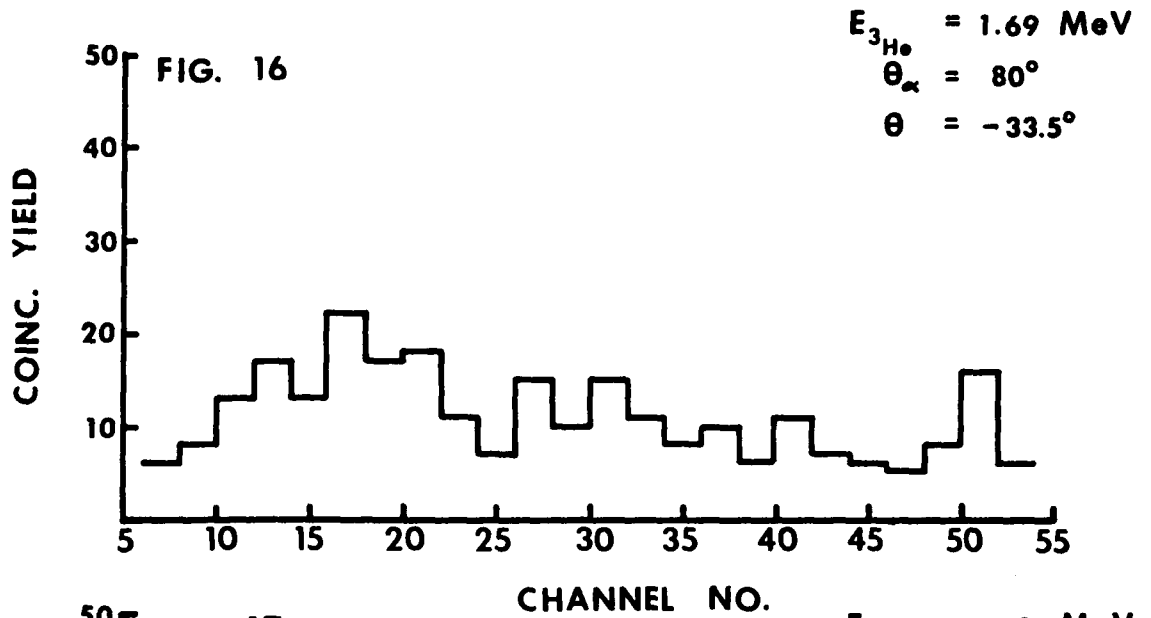
FIG. 16
$E_{^3He}$ = 1.69 MeV
θ_α = 80°
θ = −33.5°
COINC. YIELD
CHANNEL NO.

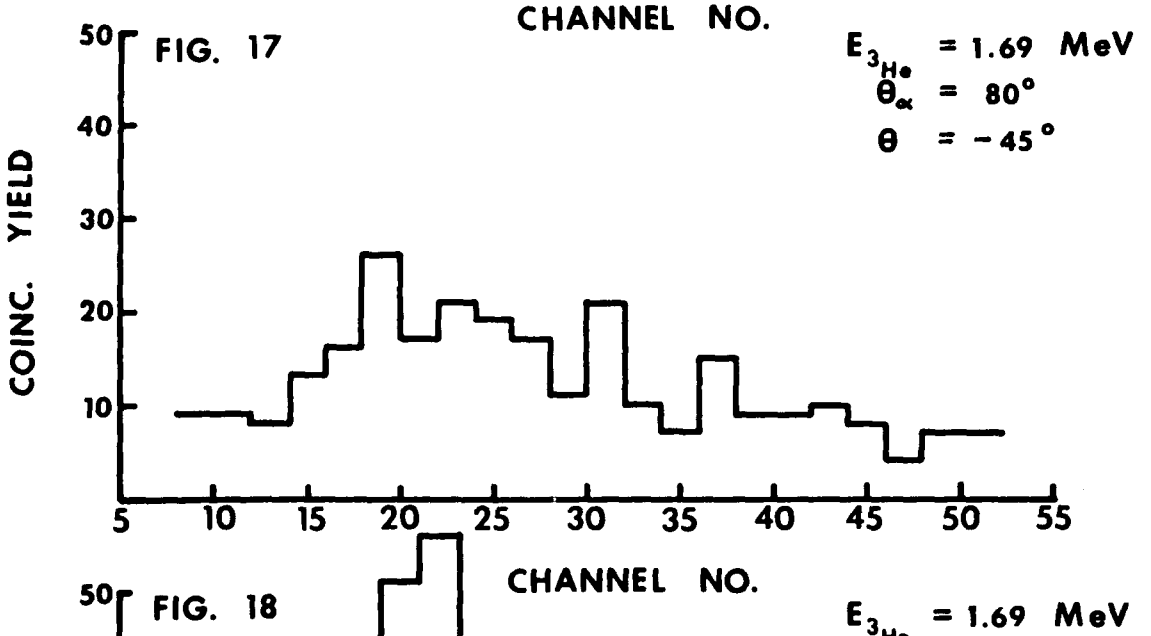
FIG. 17
$E_{^3He}$ = 1.69 MeV
θ_α = 80°
θ = −45°
COINC. YIELD
CHANNEL NO.

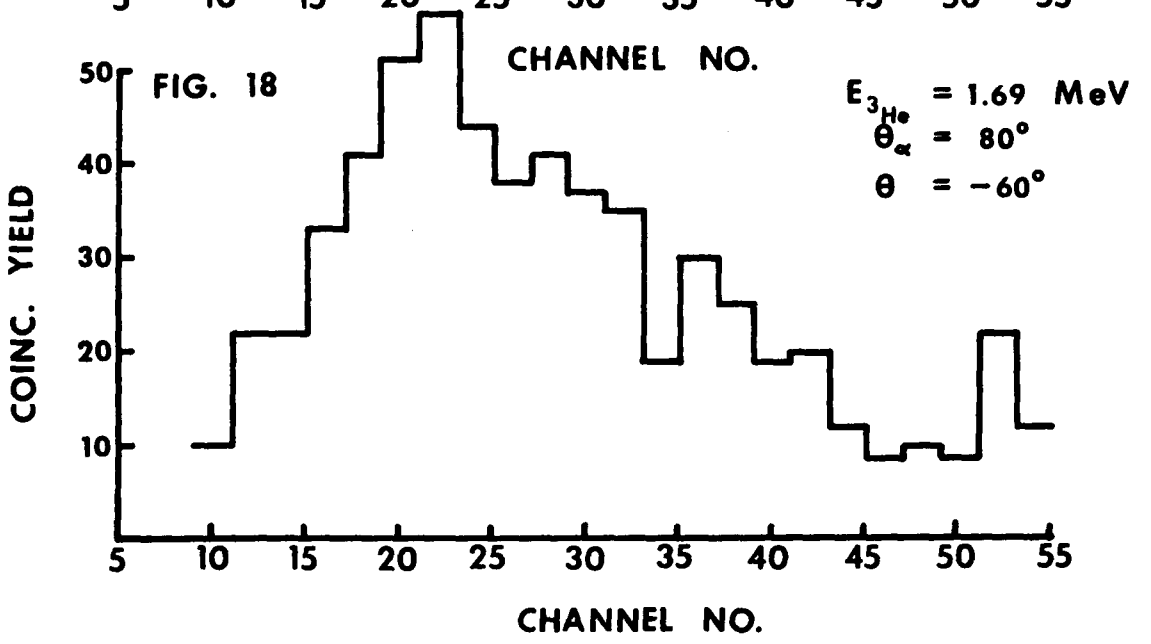
FIG. 18
$E_{^3He}$ = 1.69 MeV
θ_α = 80°
θ = −60°
COINC. YIELD
CHANNEL NO.

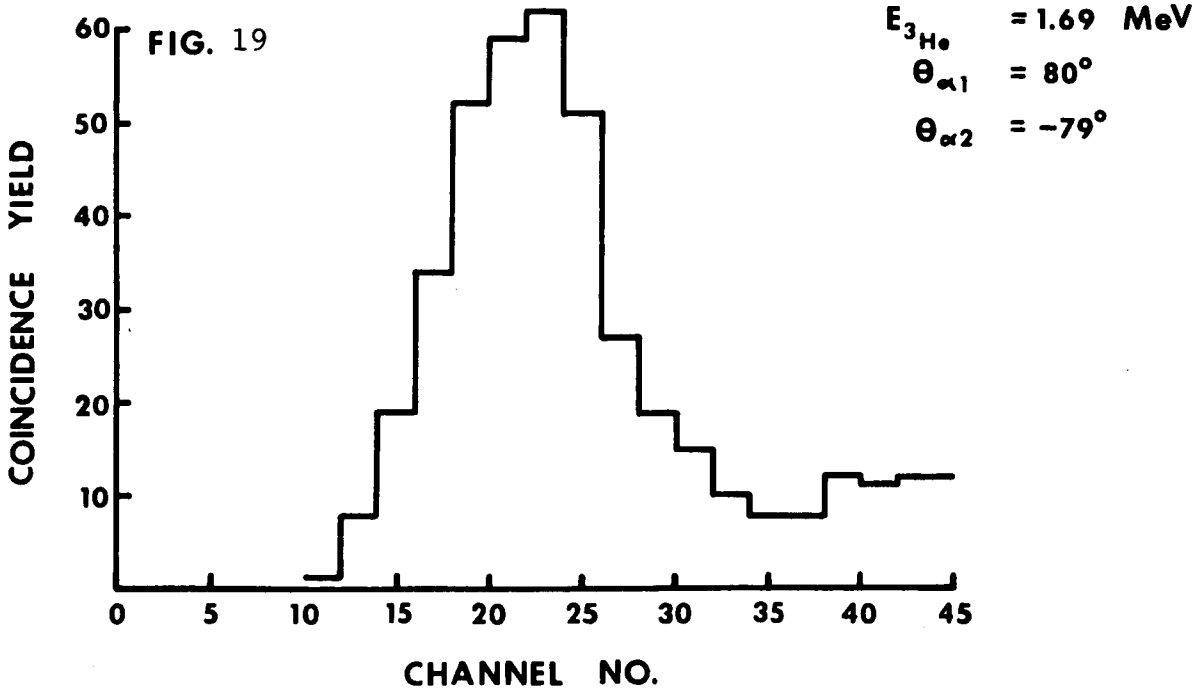
FIG. 19
$E_{^3He}$ = 1.69 MeV
$\theta_{\alpha 1}$ = 80°
$\theta_{\alpha 2}$ = −79°
COINCIDENCE YIELD
CHANNEL NO.

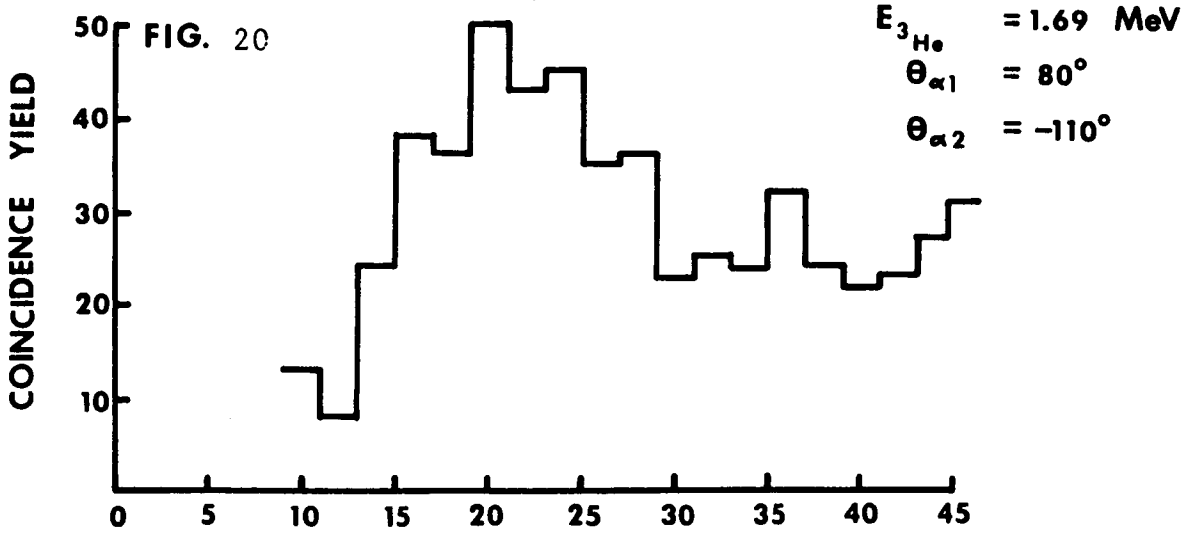
FIG. 20
$E_{^3He}$ = 1.69 MeV
$\theta_{\alpha 1}$ = 80°
$\theta_{\alpha 2}$ = −110°
COINCIDENCE YIELD
CHANNEL NO.

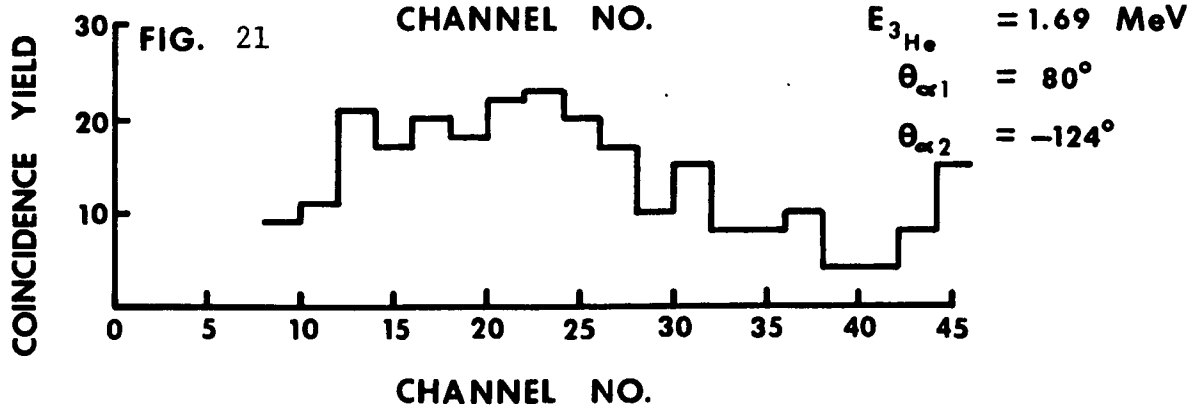
FIG. 21
$E_{^3He}$ = 1.69 MeV
$\theta_{\alpha 1}$ = 80°
$\theta_{\alpha 2}$ = −124°
COINCIDENCE YIELD
CHANNEL NO.

Alpha Proton Angular Correlation Measurement

Alpha proton angular correlations were measured at ^{3}He incident energies of 1.47 MeV, 1.58 MeV and 1.69 MeV with ^{6}Li metal targets. These bombarding energies corresponded to below, on, and above the resonance in ^{9}B. The effective resonance bombarding energy was determined for a particular ^{6}Li metal target, before it was used for taking the data on resonance. Target thickness for the off resonance measurements was 50 $\mu g/cm^2$ of ^{6}Li metal on 20 $\mu g/cm^2$ of carbon. For the on-resonance measurement, it was of the order of 25 $\mu g/cm^2$ of ^{6}Li metal on 20 $\mu g/cm^2$ of carbon.

A 150 μ SB detector was fixed at an angle of 80^{o} to detect the α particles. The other SB detector, of a total thickness 1075 μ, was moved between -33.5^{o} and -124^{o} to detect protons. This covered a range of 180^{o} in the system in which the recoiling ^{5}Li (g.s.) was at rest (the recoil center of mass, RCM). In the labroatory frame, however, this corresponded to 45^{o} on either side of the ^{5}Li (g.s.) recoil direction, which was equal to -79^{o}. Mylar foils of a total thickness 11 mg/cm^2 were placed in front of the latter detector to distinguish the protons from alpha for proton detector angles between -68^{o} and -102^{o}. For the other settings, a similar discrimination was achieved using a 7 mg/cm^2 thick mylar foil in front of the proton detector.

A separation of the α-α kinematic curve from the α-p kinematic curve, calculated using the energy loss data for the protons and the alpha particles for their passage through mylar, given in ref. 15, is shown in Fig. 12. The locations of the ^{5}Li and ^{8}Be states are also shown on it.

Experimentally obtained α-p coincidence curves for the proton detector angle set at -79^{o}, the direction of the recoiling ^{5}Li (g.s.), for incident energies of 1.47 MeV, 1.58 MeV, and 1.69 MeV are shown in Fig. 13, Fig. 14, and Fig. 15, respectively. At this particular angle, the counts due to ^{5}Li (g.s.) are seen to be well separated from all the other states. The α-α coincidence curve is also seen to be well separated from the α-p coincidence curve. The projections of the α-p coincidence curve onto the proton energy axis, for a ^{3}He bombarding energy of 1.69 MeV, are plotted in Fig. 16 through Fig. 21. There are two types of contributions under the ^{5}Li (g.s.) peak; (1) from the other intermediate states found in the sequential process, notably the ^{5}Li (7.5 Mev) and ^{8}Be (2.9 MeV) states whose widths (Γc.m.) are 2.5 MeV and 1.5 MeV respectively, and (2) from the simultaneous process. For the proton detector angles between -45^{o} and -110^{o} the contribution from (1) is either not significant or indistinguishable from (2) which is, however, present at all the proton detector angles.

As the contribution from the simultaneous process goes smoothly to zero as a function of decreasing energy, when projected along the proton energy axis, as can be seen in Fig. 7, it can easily be estimated in the region where the ^{5}Li (g.s.) is located. In order to do so, the average shape of the background between 7.5 MeV and 10.5 Mev has been smoothly extrapolated to zero MeV. This procedure, also substracts the contributions of type (1) when they are indistinguishable from the continuum background along the kinematic curve. For the proton detector settings of -33.5^{o}, -39^{o} and -124^{o}, contribution of type (1) are significant and do show up as a peak near the ^{5}Li (g.s.) peak. After substracting the average background, as explained above, this additional contribution has been substracted by extrapolating the shapes of the ^{5}Li (7.5 Mev) and the ^{8}Be (2.90 MeV) peaks under the ^{5}Li (g.s.) region.

The ^{5}Li (g.s.) coincidence yields have been obtained by adding up counts under the ^{5}Li (g.s.) peak, and subtracting the contributions of types (1) and (2). These coincidence yields, normalized to the singles from the reaction ^{6}Li + ^{3}He, have been plotted as a function of the proton detector angle as measured in the ^{5}Li (g.s.) recoil center of mass frame (θ_{RCM}). The solid angle correction in going from the laboratory frame to the recoil center of mass frame was further applied to the data. The normalized and

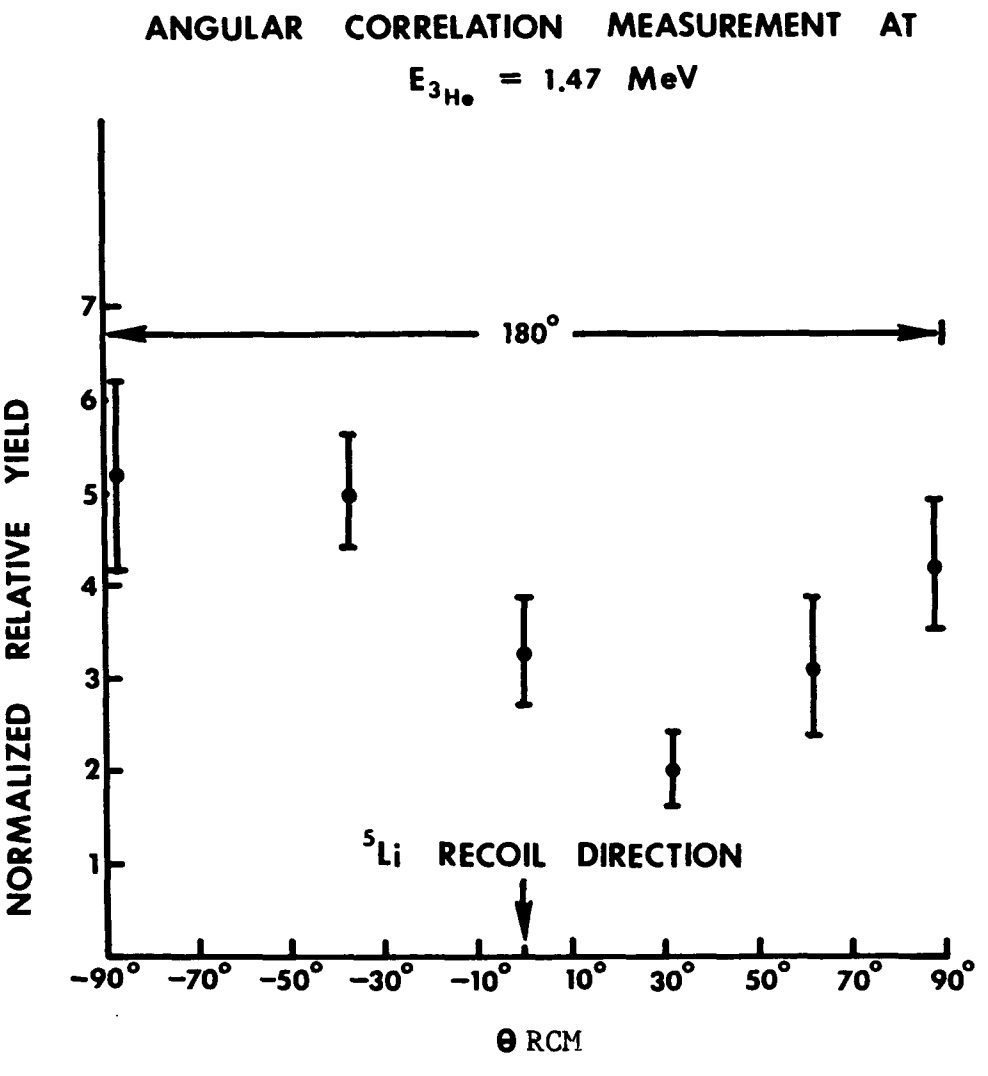
ANGULAR CORRELATION MEASUREMENT AT
$E_{^3He}$ = 1.47 MeV
NORMALIZED RELATIVE YIELD
7
6
5
4
3
2
1
180°
^{5}Li RECOIL DIRECTION
-90° -70° -50° -30° -10° 10° 30° 50° 70° 90°
θ RCM

FIGURE 22

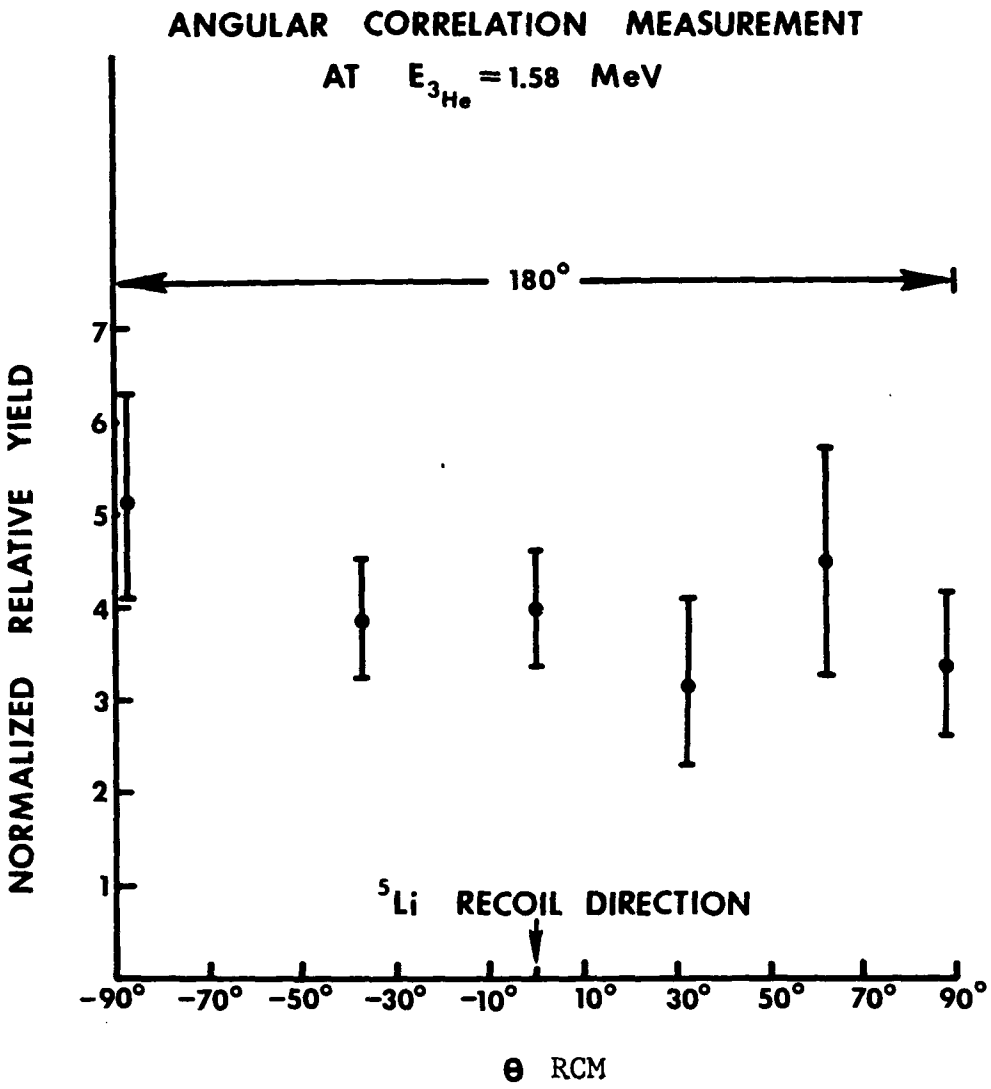
ANGULAR CORRELATION MEASUREMENT
AT $E_{^3He}$ = 1.58 MeV
180°
NORMALIZED RELATIVE YIELD
7
6
5
4
3
2
1
^{5}Li RECOIL DIRECTION
-90° -70° -50° -30° -10° 10° 30° 50° 70° 90°
θ RCM

FIGURE 23

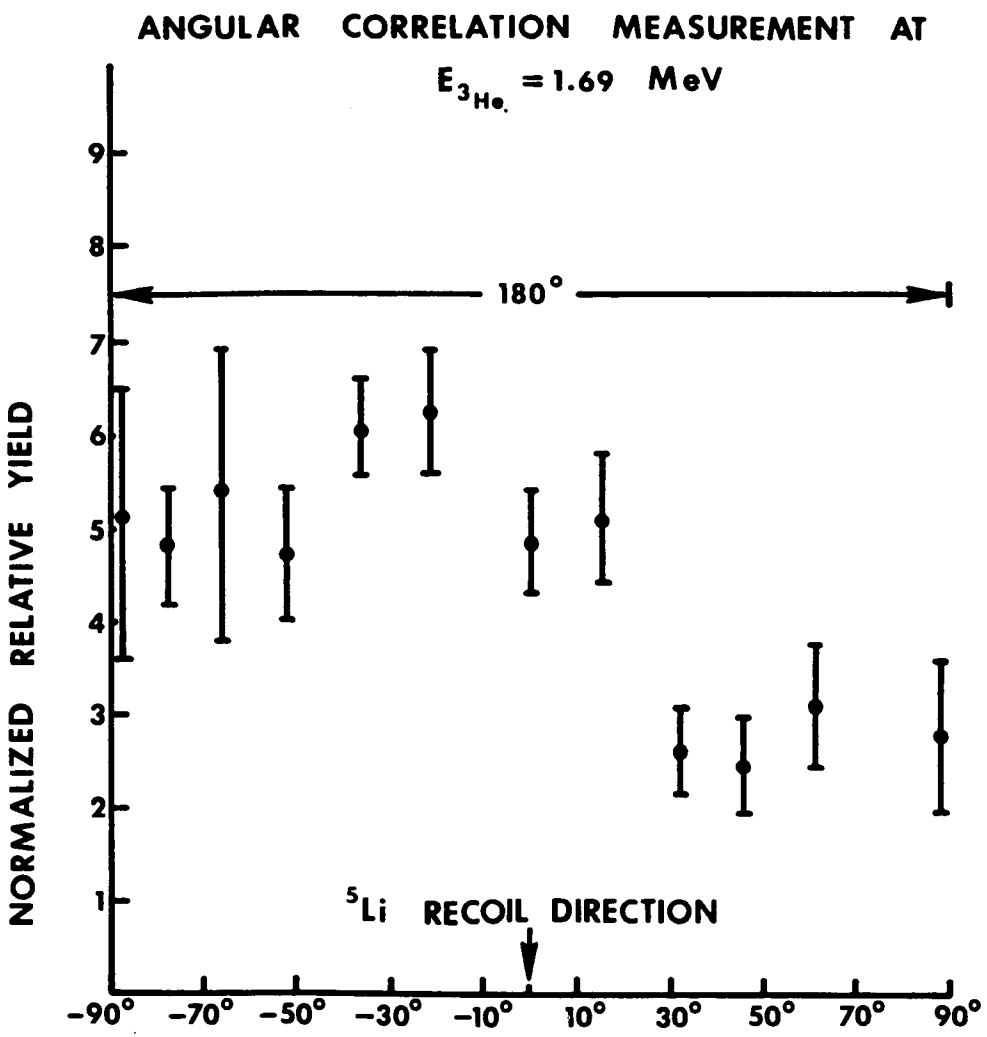
ANGULAR CORRELATION MEASUREMENT AT
$E_{^3He.}$ = 1.69 MeV
NORMALIZED RELATIVE YIELD
180°
^{5}Li RECOIL DIRECTION
1
2
3
4
5
6
7
8
9
-90°
-70°
-50°
-30°
-10°
10°
30°
50°
70°
90°
θ RCM

FIGURE 24

corrected yields are shown in Figs. 22 , 23, and 24 for the 1.47 MeV, 1.58 MeV and 1.69 Mev bombarding energies respectively. Errors are mainly due to counting statistics and background substraction. Due to the limitations on target thickness, required for a well-defined resonance measurement, the α-p coincidence count rate due to the ^{5}Li (g.s.) was of the order of 2 - 3 cts. per min. Time for each run was of the order of 60 min. to 120 min. Consequently, a large error is seen in all the data due to poor counting statistics.

Angular Distribution Measurements

In order to measure the angular distribution of the first emitted α particle, an α-α coincidence method was used. The method is similar to the excitation function measurement in the following respect. For a given direction of emission of α_1, say θ_1, the α_2 is detected at an angle θ_2, which is about 10^{o} forwards with respect to the recoil direction of ^{5}Li. In addition to eliminating the contributions from ^{8}Be (16.66 MeV) and ^{8}Be (16.91 MeV) states to the α-α kinematic curve, this choice for θ_2 also produces a separation in the two ^{5}Li (g.s.) locations, which would have overlapped if the α_2 detector were set along the recoil direction of ^{5}Li (g.s.). A kinematic analysis of the α-α kinematic curve, as described earlier in Chapter III shows that one of the two peaks lying midway on the kinematic curve

corresponds to a coincidence between the first emitted α_1 going into the detector at θ_1, and the ^{5}Li (g.s.) breakup α_2 going into the detector at θ_2. The other peak corresponds to the detection of α_1 at θ_2 and α_2 at θ_1. A further analysis, using the velocity vector diagrams, shows that if θ_2 differs from the ^{5}Li (g.s.) recoil angle (for an α_1, emitted along θ_1) by a certain angle, say θ_a; then θ_1 differs from the ^{5}Li (g.s.) recoil angle (for an α_1 emitted along θ_2) by the same angle θ_a (to within one degree). Thus in this way, comparable data can be obtained for two different directions of emission of the first emitted α particle, namely θ_1 and θ_2, by doing a single measurement.

Coincidences between α_1 and α_2 were measured for the values of (θ_1, θ_2) equal to (20^o, -141^o), (30^o, -127^o), (40^o, -113^o), (50^o, -101^o), (60^o, -89^o), (70^o, -79^o). This covered a range of α_1 angles in the system center of mass frame from about 25^o to 155^o. ^{3}He bombarding energies were chosen to be 1.47 MeV, 1.61 MeV and 1.69 MeV, which were below, on and above the ^{9}B compound state at 17.64 MeV. The measurement at 1.61 MeV was performed using ^{6}LiF targets of thickness 25 μg/cm^2 deposited on carbon foils of thickness 20 μg/cm^2. The other two measurements were performed using ^{6}Li metal targets of thickness 50 μg/cm^2, deposited on carbon foils of 20 μg/cm^2. The use of ^{6}LiF targets for the on-resonance measurement was necessitated by the fact that the

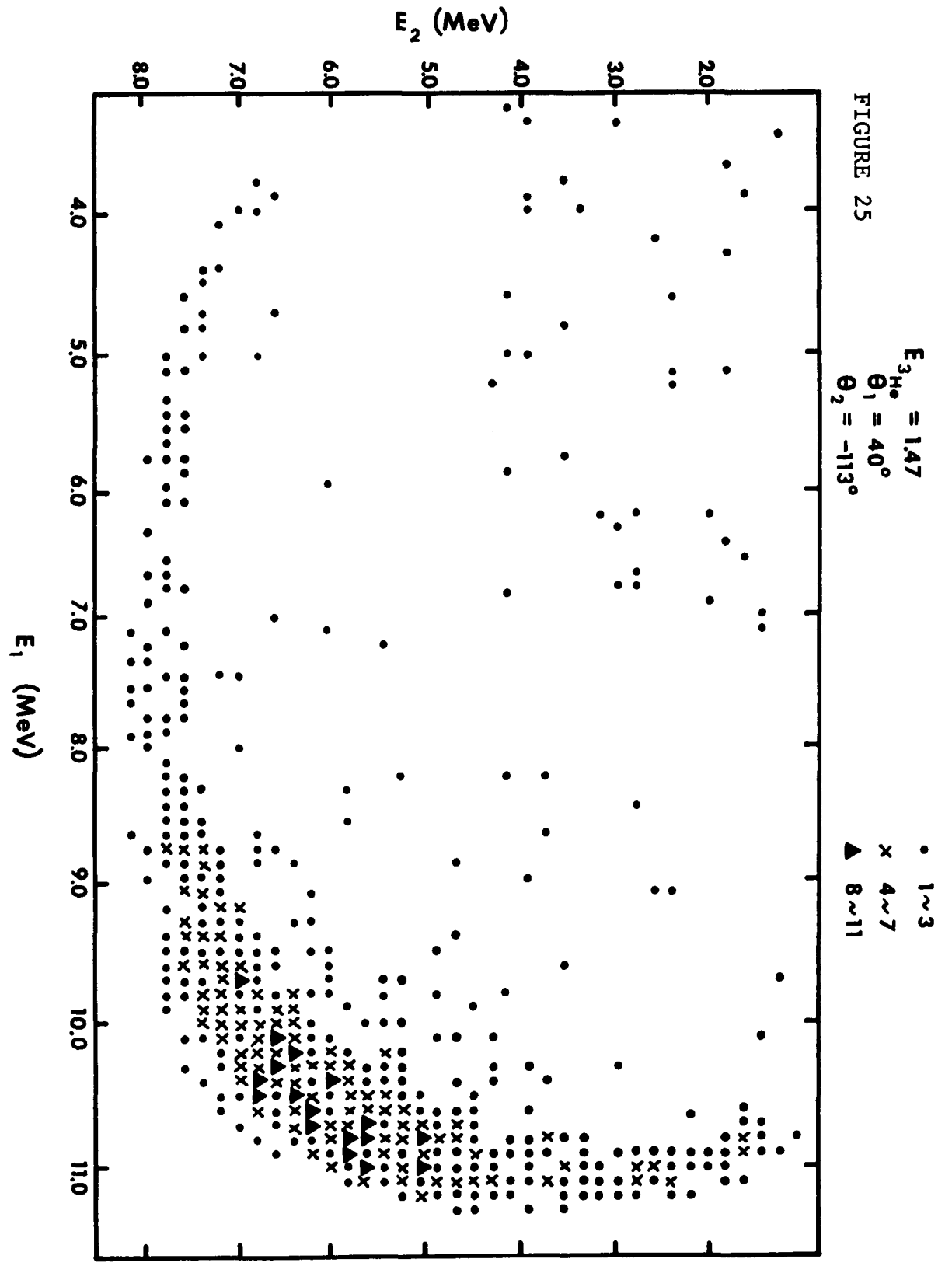

FIGURE 25

FIGURE 26

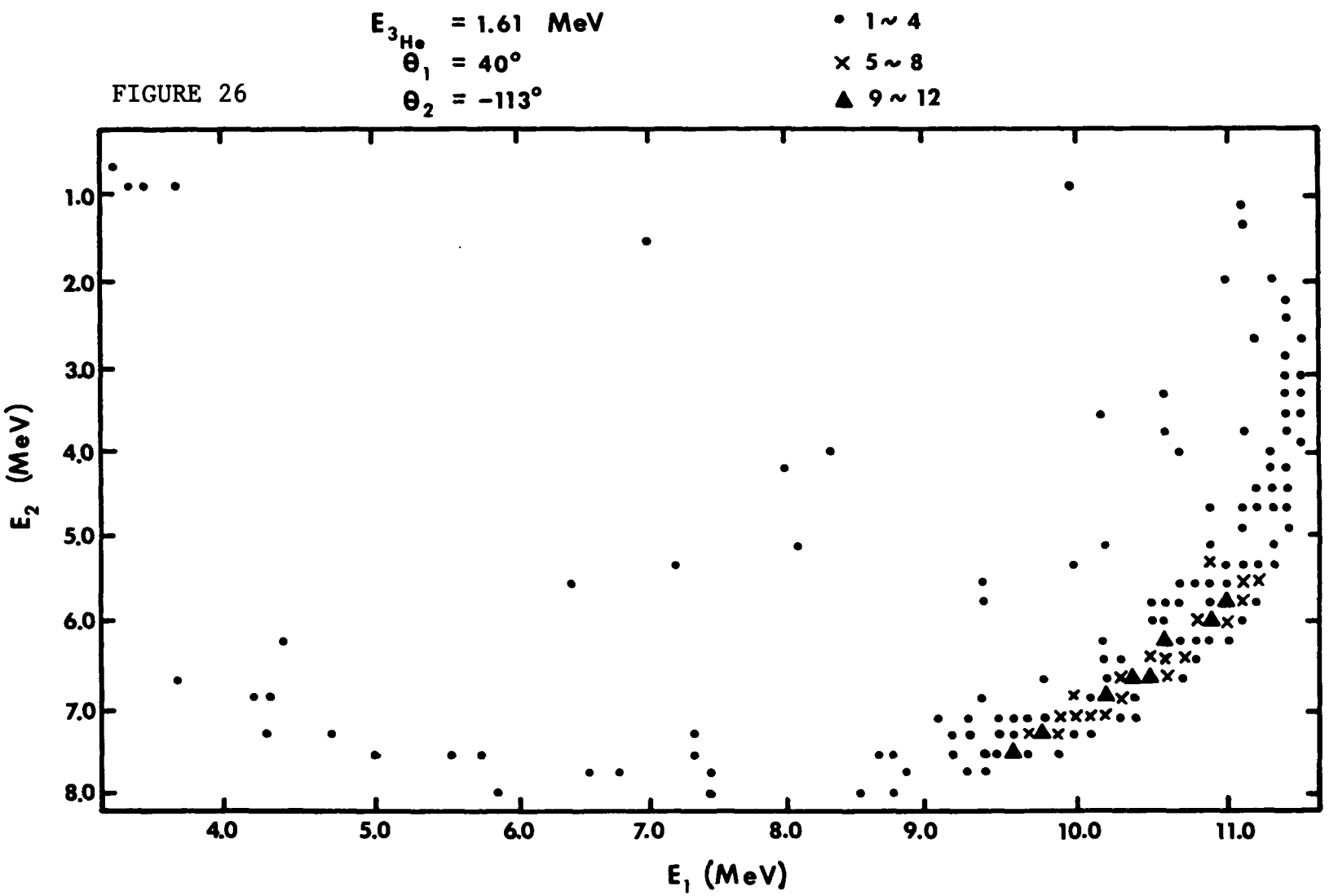
$E_{^3He}$ = 1.61 MeV
θ_1 = 40°
θ_2 = −113°
• 1 ~ 4
× 5 ~ 8
▲ 9 ~ 12
1.0
2.0
3.0
4.0
5.0
6.0
7.0
8.0
E_2 (MeV)
4.0
5.0
6.0
7.0
8.0
9.0
10.0
11.0
E_1 (MeV)

FIGURE 27

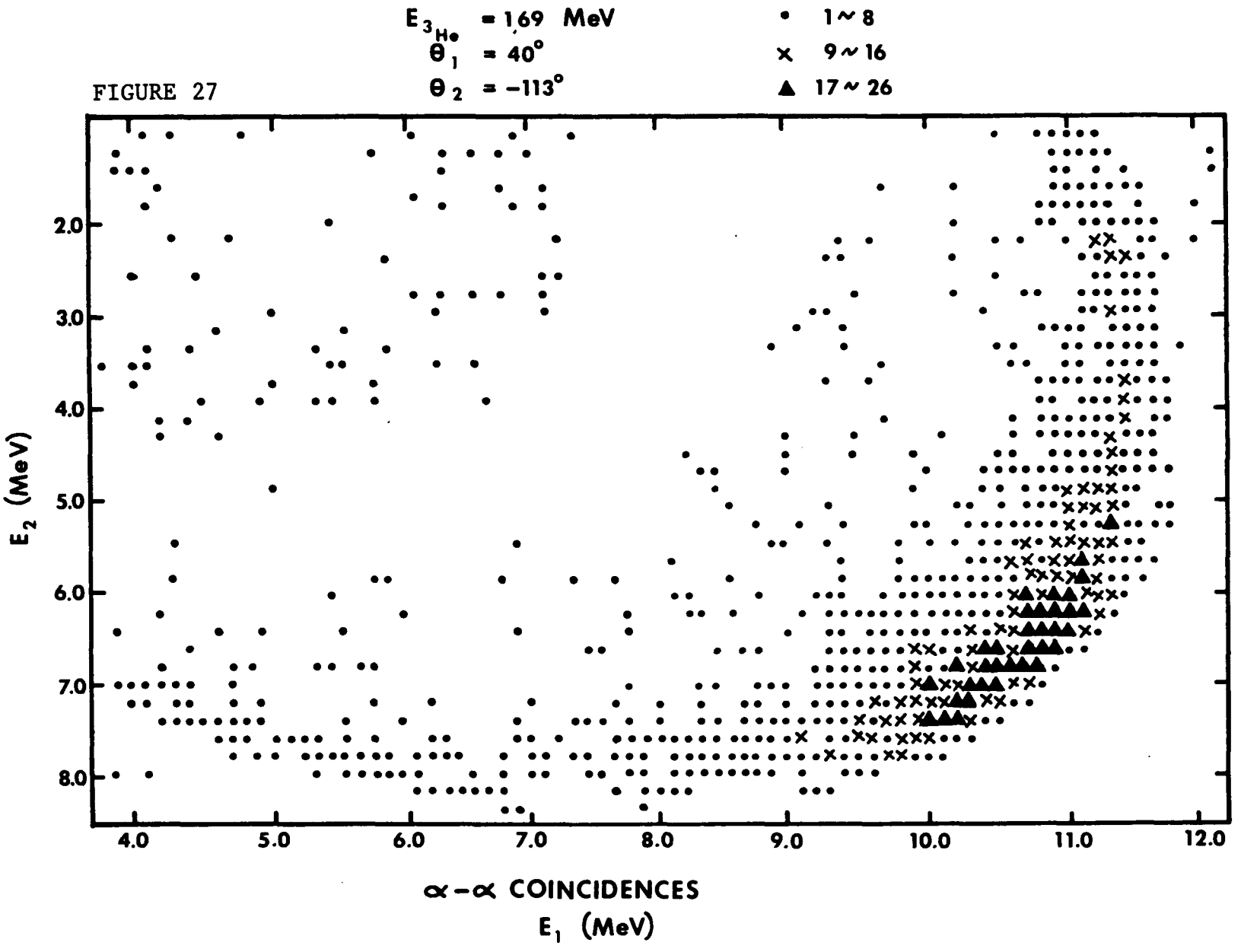
$E_{^3He}$ = 1.69 MeV
θ_1 = 40°
θ_2 = −113°
• 1 ~ 8
× 9 ~ 16
▲ 17 ~ 26
2.0
3.0
4.0
5.0
6.0
7.0
8.0
E_2 (MeV)
4.0
5.0
6.0
7.0
8.0
9.0
10.0
11.0
12.0
α − α COINCIDENCES
E_1 (MeV)

FIGURE 28

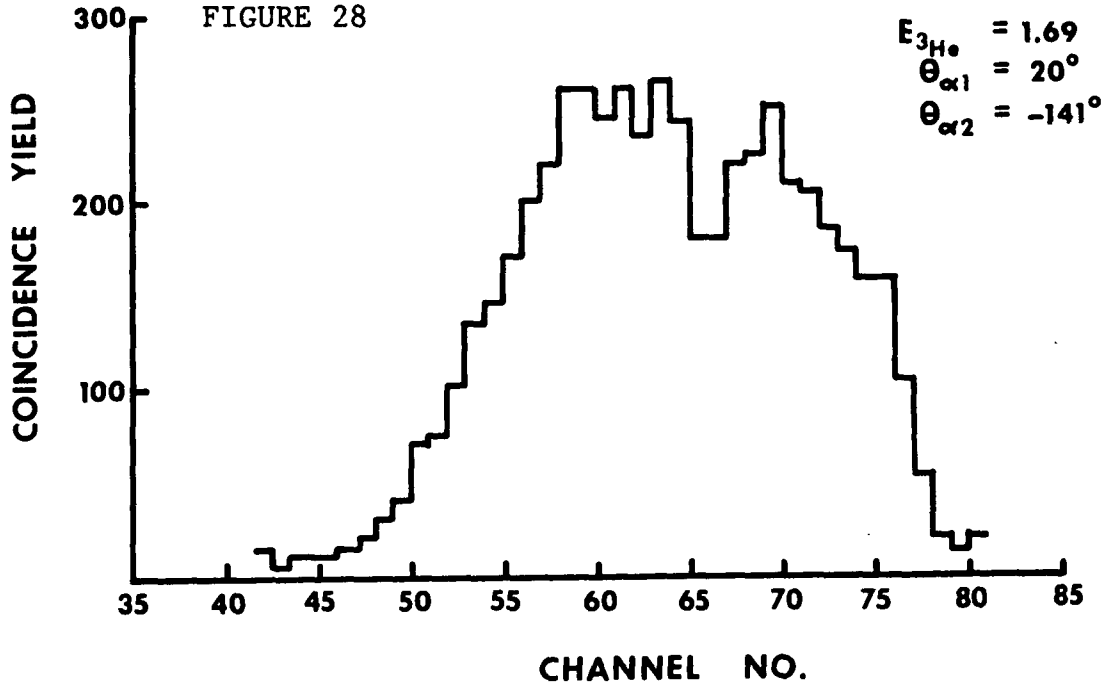

FIGURE 29

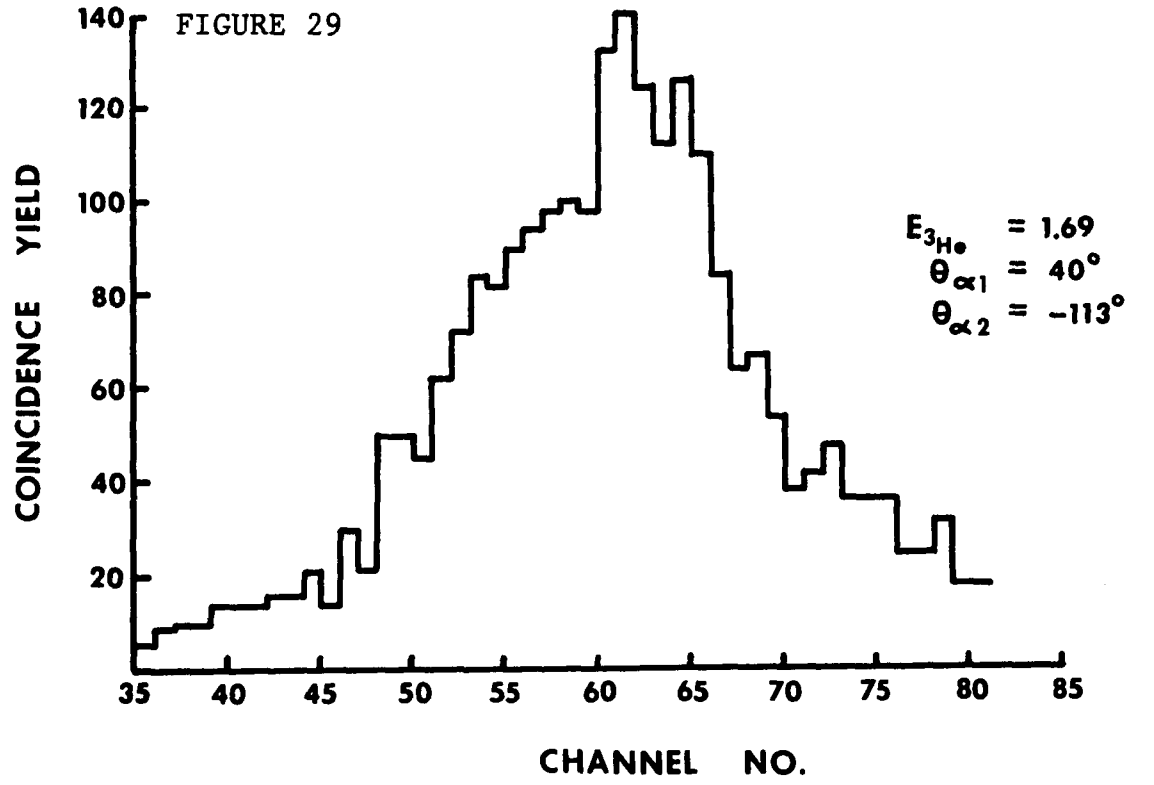

FIGURE 30

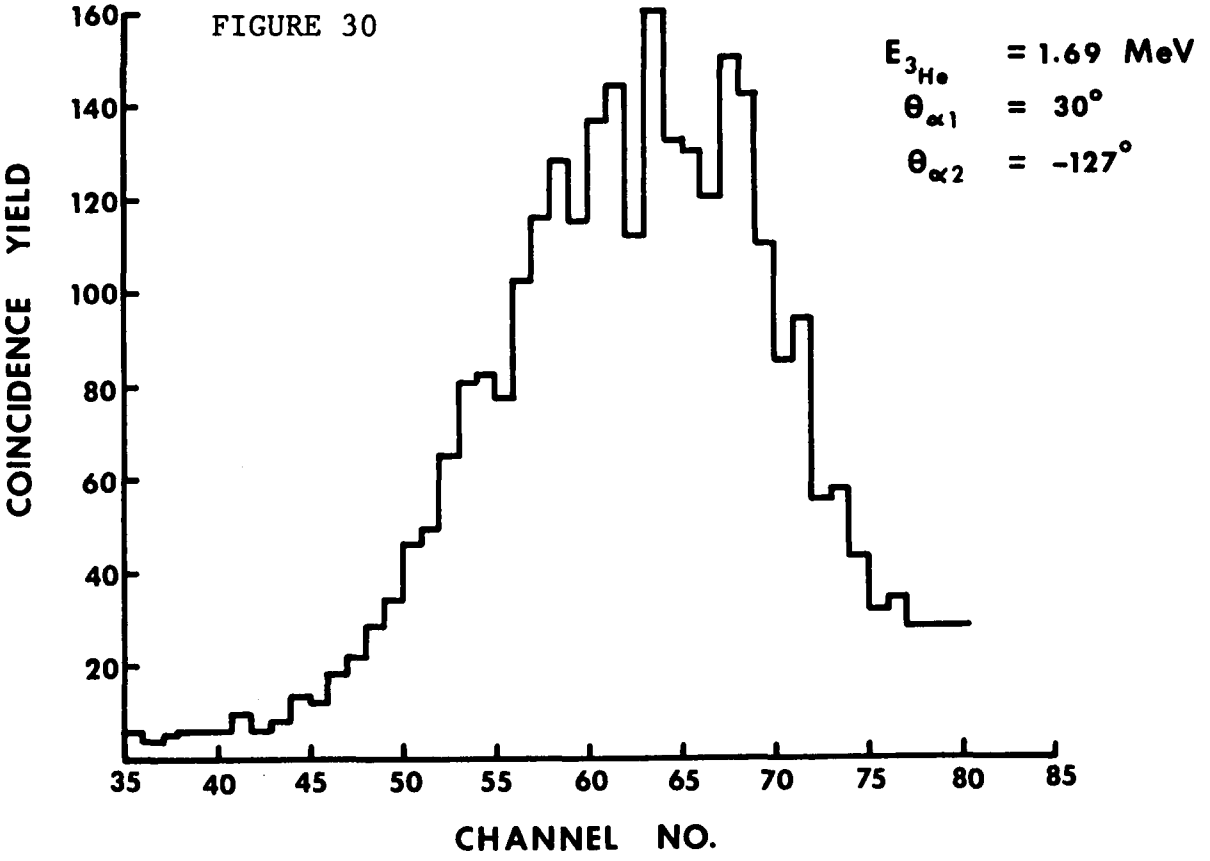

FIGURE 31

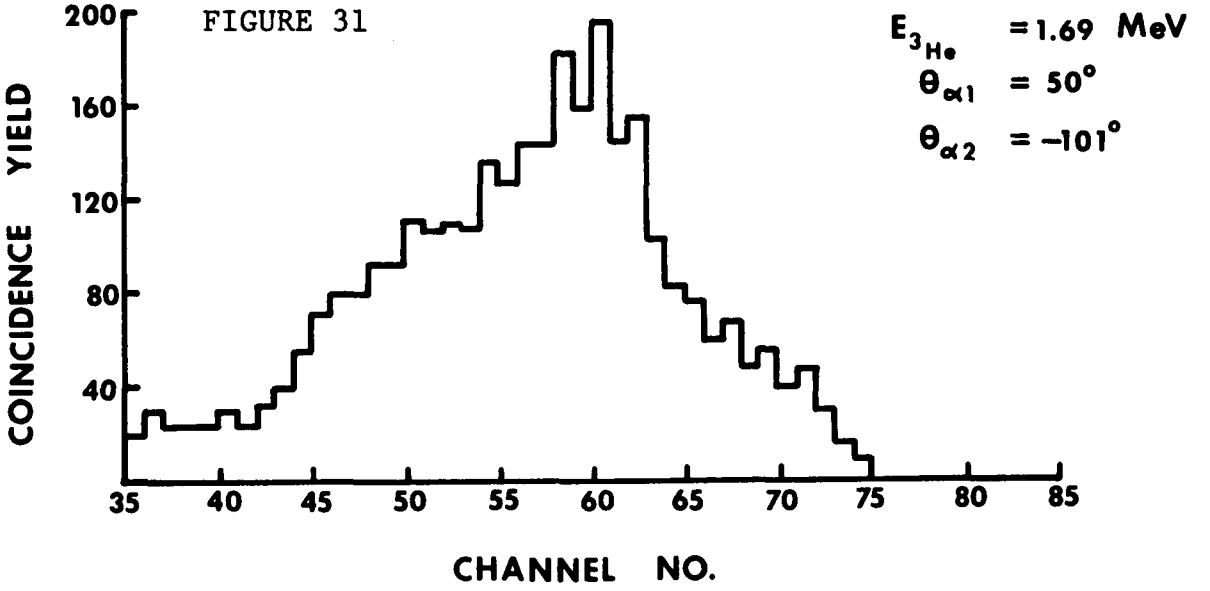

FIG. 32

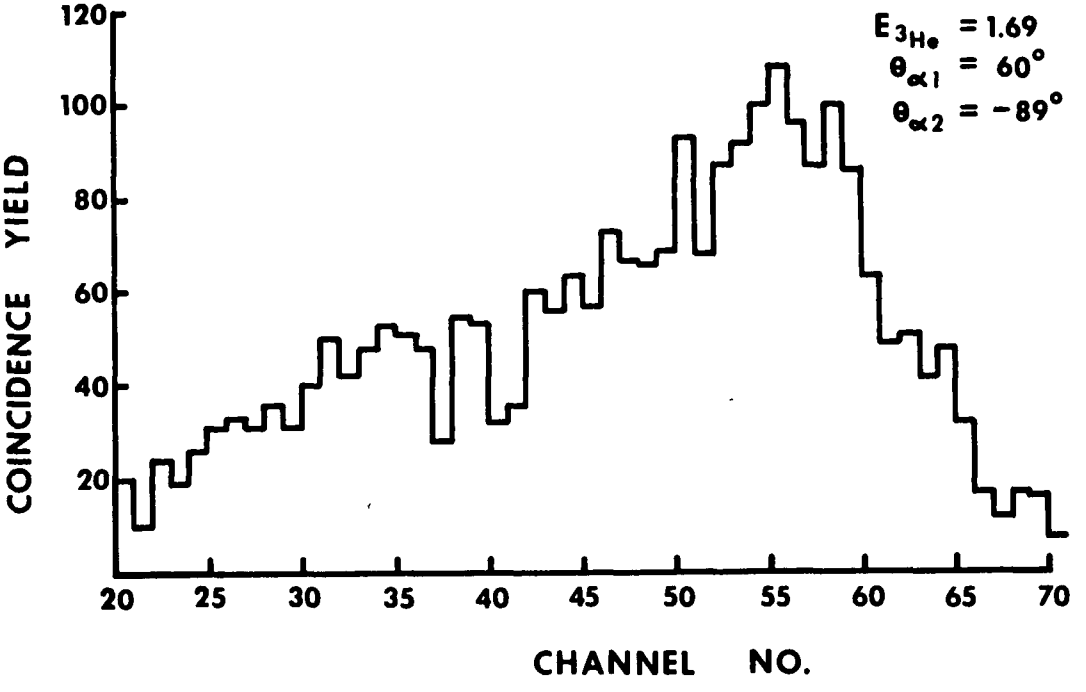
$E_{^3He}$ = 1.69
$\theta_{\alpha 1}$ = 60°
$\theta_{\alpha 2}$ = −89°
COINCIDENCE YIELD
120
100
80
60
40
20
20 25 30 35 40 45 50 55 60 65 70
CHANNEL NO.

FIG. 33

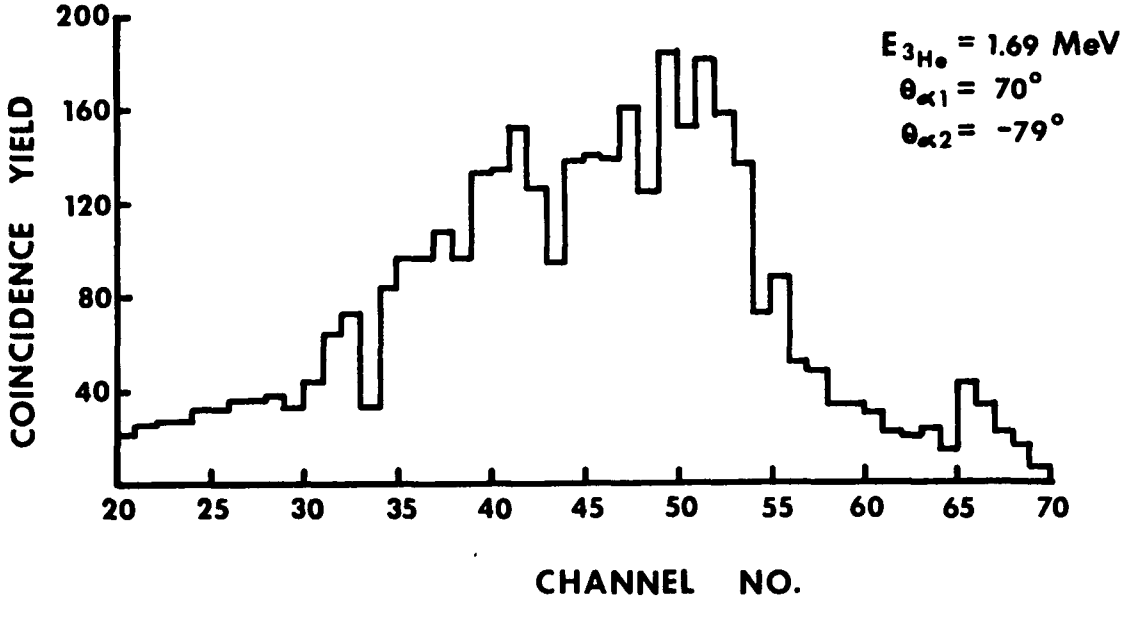
$E_{^3He}$ = 1.69 MeV
$\theta_{\alpha 1}$ = 70°
$\theta_{\alpha 2}$ = −79°
COINCIDENCE YIELD
200
160
120
80
40
20 25 30 35 40 45 50 55 60 65 70
CHANNEL NO.

^{6}Li metal targets did not exhibit a uniformity sufficient to insure a completely on-resonance measurement. However, by using them for the off-resonance measurements, a significantly higher coincidence counting rate was achieved which considerably reduced the data collection time. Other experimental details have been described earlier in Chapter II.

Experimentally obtained coincidence curves for the detectors setting of (40^{o}, -113^{o}), for the ^{3}He bombarding energies of 1.47, 1.61 and 1.69 MeV are shown in Fig. 25, Fig. 26 and Fig. 27 respectively. These show a large concentration of counts near the two ^{5}Li (g.s.) locations which are towards the middle of the kinematic curve.

The projections of such coincidence data shown in Fig. 28 to Fig.33 were obtained by subdividing the band of counts along the kinematic curve by means of slots of equal width, drawn so that any given slot would be perpendicular to a tangent to the kinematic curve which is drawn at the location of the slot. This procedure of drawing projections would give a maximum separation between the two peaks corresponding to ^{5}Li (g.s.), which are nonetheless found to overlap considerably due to a 1.5 MeV width of the ground state.

The counts under the two peaks were separated by assuming that each of them has a gaussian shape, whose FWHM is equal to the FWHM of the ground state. The center of the

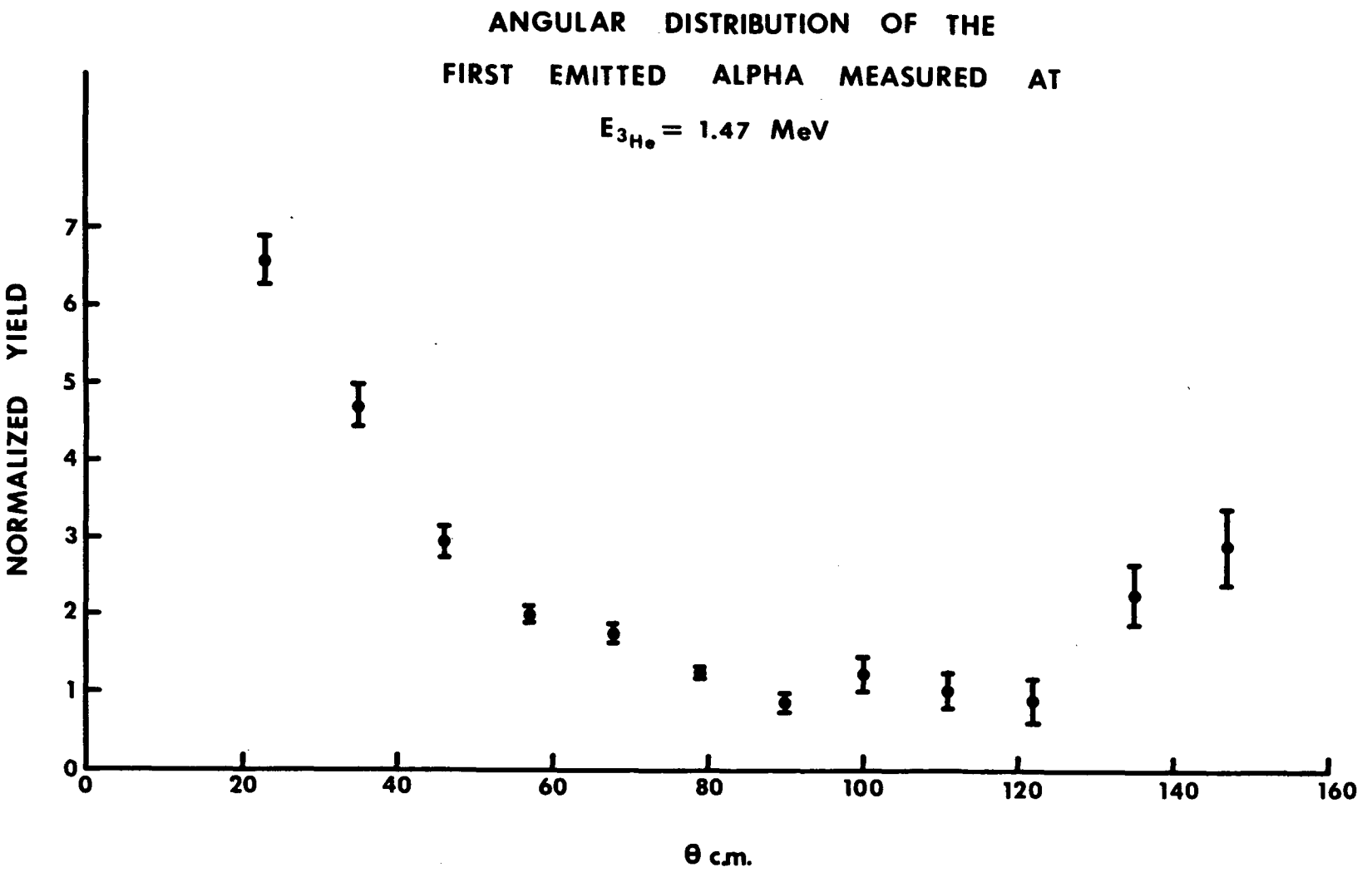
ANGULAR DISTRIBUTION OF THE
FIRST EMITTED ALPHA MEASURED AT
$E_{^3He}$ = 1.47 MeV
NORMALIZED YIELD
0
1
2
3
4
5
6
7
0
20
40
60
80
100
120
140
160
θ c.m.

FIGURE 34

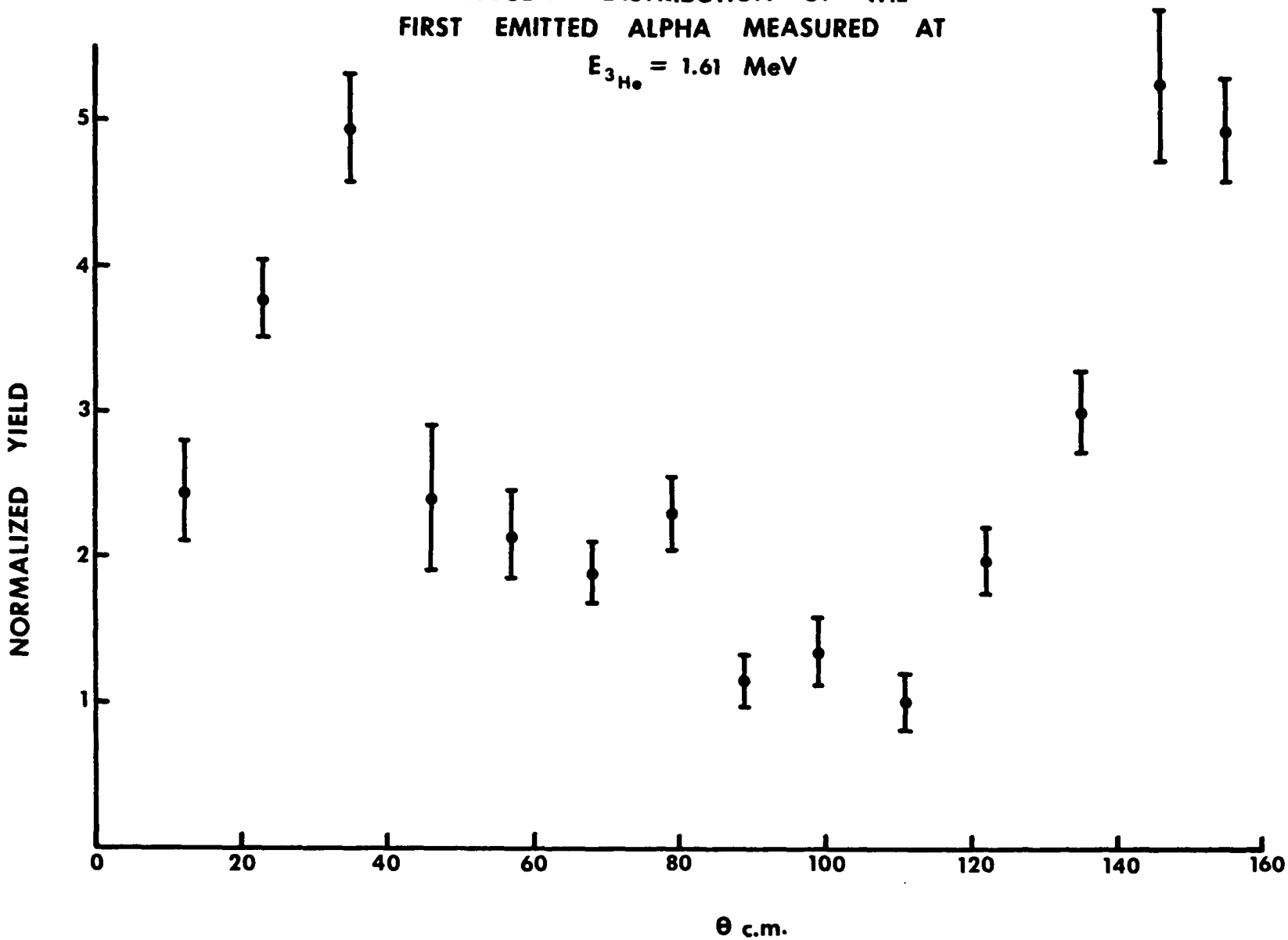
ANGULAR DISTRIBUTION OF THE
FIRST EMITTED ALPHA MEASURED AT
$E_{^3He}$ = 1.61 MeV
NORMALIZED YIELD
1
2
3
4
5
0
20
40
60
80
100
120
140
160
θ c.m.

FIGURE 35

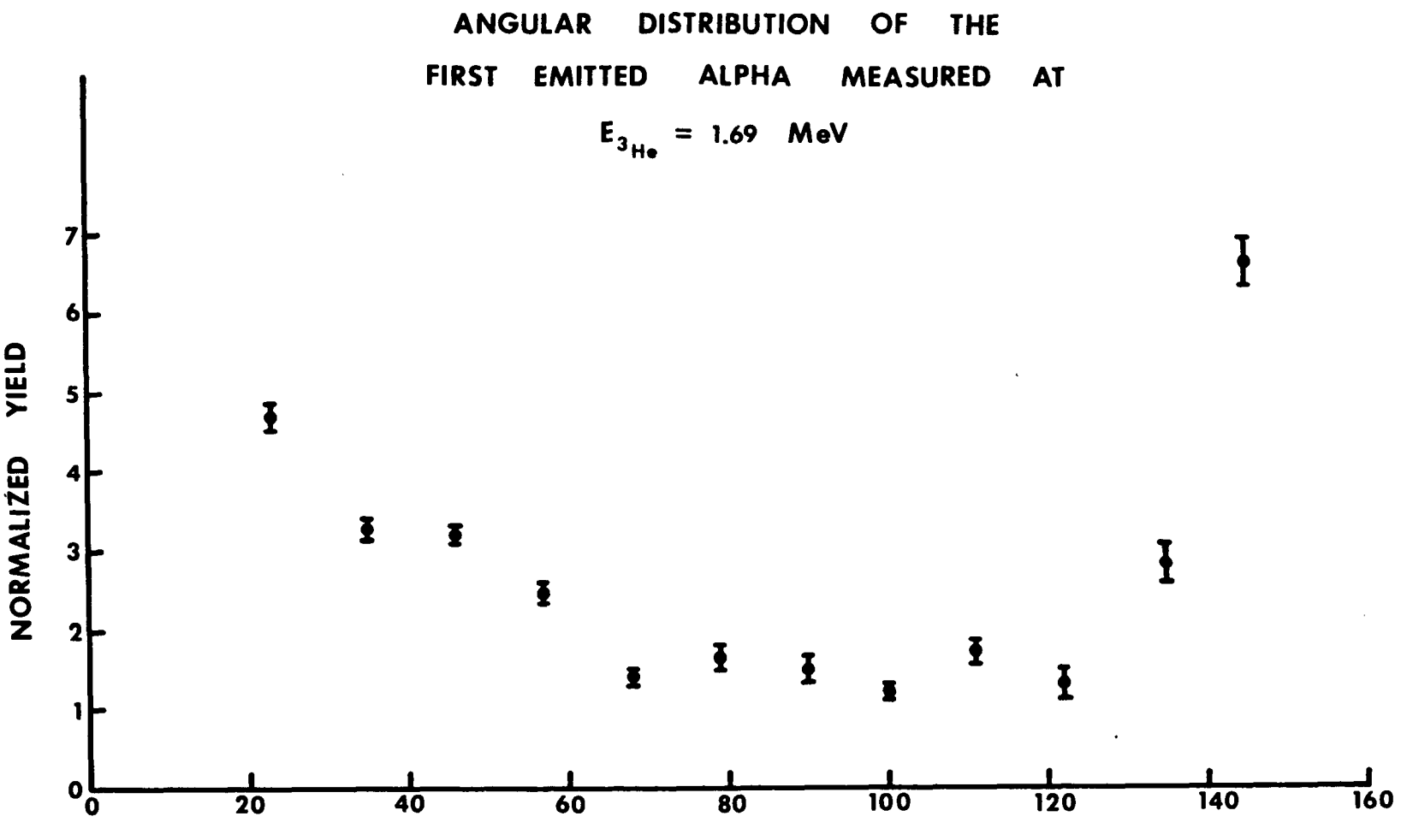
ANGULAR DISTRIBUTION OF THE
FIRST EMITTED ALPHA MEASURED AT
$E_{^3He}$ = 1.69 MeV
NORMALIZED YIELD
0
1
2
3
4
5
6
7
0
20
40
60
80
100
120
140
160
θ c.m.

FIGURE 36

peak was taken to be the center of gaussian. Thus, by fitting an overlap of two gaussians of appropriate heights located at calculated positions of the centers of the two peaks and of widths equal to the calculated widths of the peaks, to the actual data, counts under each of the two peaks were separated.

Contributions from the simultaneous process to the ^{5}Li (g.s.) peaks is seen to be negligible as evidenced by examining the data in the region where the counts are only from the simultaneous process. The contribution from the ^{5}Li (7.5 MeV) and ^{8}Be (2.9 MeV) states are expected towards the tails of the ^{5}Li (g.s.) peaks. Since the data that was used to obtain the maximum height of the gaussian was a sum of counts in a half-width at half-maximum of the peak, taken from the center of the peak, the procedure excluded any contributions, arising from the ^{5}Li (7.5 MeV) and ^{8}Be (2.9 MeV) states, to the data.

The angular distribution of the first-emitted alpha particle has been plotted as a function of angle of its emission as measured in the system center of mass (θ_{CM}), in Figs. 34, 35, and 36 for ^{3}He bombarding energies of 1.47 MeV, 1.61 MeV and 1.69 MeV respectively. The 1.47 MeV and 1.69 MeV data, which was taken with the ^{6}Li metal targets was normalized to ^{6}Li + ^{3}He singles integrated above 7 MeV. The 1.61 MeV data taken with a ^{6}LiF target, was normalized

to the ^{3}He elastically scattered from ^{19}F. Data at each energy was normalized individually and they cannot be interrelated to each other in a simple way. The solid angle correction, for a transformation between the laboratory frame and the system center of mass frame has not been applied to the data as it was computed to be less than 1% .

The errors shown in these figs. are mainly due to the coincidence counting statistics associated with each peak. In most of the data one of the two peaks was very obvious. Therefore, for those data a gaussian was fitted to only one peak which was clear from the data and the sum under the other peak was obtained by subtracting the sum of counts under the peak which was correctly fitted to a gaussian, from the total number of counts under the two peaks. This, however, gave somewhat larger errors for the peak for which a gaussian fit was not made.

CHAPTER V

THEORETICAL MODELS

In this chapter theoretical models relevant in the study of the angular distribution of the first-emitted particle and the alpha-proton angular correlation in the reaction $^{6}Li\ (^{3}He, \alpha_1)\ ^{5}Li(\ g.s.) \rightarrow \alpha_2 + p$, will be described.

First the theory relating to the angular distribution will be described.

Angular Distribution of the First-Emitted α Resulting From a ^{9}B CN Formation

Consider the reaction,

$$a + A \rightarrow (CN) \rightarrow b + B.$$

The system before collision is described by three numbers: the channel index α, the channel spin s, and the orbital angular momentum l. Let the spin of the target be I, and the spin of the incident projectile be i, so that $\vec{s} = \vec{I} + \vec{i}$. Let the spin of the compound nuclear state that is formed be J. After the CN-breakup, the system is described by the same quantities, with similar labels with primes on them, i.e., by α', s', l', I', and i'. The differential cross-section for such a reaction at a given energy E can be expressed as follows, [19]

$$d\sigma_{\alpha\alpha'}(E, \theta) = \frac{\lambda_\alpha^2}{(2i + 1)(2I + 1)} \sum_{l=0}^{L_{max}} B_L(\alpha'; \alpha) P_L (\text{Cos } \theta) \, d\Omega \quad (12)$$

where $\lambda_\alpha = \lambda_\alpha / 2\pi = (k_\alpha)^{-1} = \left(\frac{2\mu_\alpha E_\alpha}{\hbar^2}\right)^{-\frac{1}{2}}$

$$B_L(\alpha'; \alpha) = \sum_{s=|I-i|}^{I+i} \sum_{s'=|I'-i'|}^{I'+i'} R_L(\alpha' s'; \alpha s),$$

where $R_L(\alpha' s'; \alpha s)$ is defined as

$$R_L(\alpha' s'; \alpha s) = \frac{(-1)^{s'-s}}{4\left((E - E_0)^2 + (\tfrac{1}{2}\Gamma)^2\right)} \sum_{l_1=|J_0 - S|}^{J_0 + s}$$

$$\sum_{l_2=|J_0 - s|}^{J_0 + s} \sum_{l_1'=|J_0 - s'|}^{J_0 + s'} \sum_{l_2'=|J_0 - s''|}^{J_0 + s'} Z(l_1 J_0 l_2 J_0, s l) x$$

$$Z(l_1' J_0 l_2' J_0, S'L) \, x \, g_{sl_1} g_{sl_2} g_{'s'l'_1} g_{'s'l'_2} \, x$$

$$\text{Cos}\left(\xi_{\alpha l_1} - \xi_{\alpha l_2} + \xi_{\alpha' l_1'} - \xi_{\alpha' l_2'}\right) \text{ (for } (\alpha s) \neq (\alpha' s')\text{)}$$

Here $g_{\alpha sl} = \pm (\Gamma_{\alpha sl})^{\frac{1}{2}}$ where $\Gamma_{\alpha sl}$ are the partial widths, E_o is observed resonance energy of the CN state, and Z - coefficients are defined as follows:

$$Z (l_1 J_1 l_2 J_2, s L) = i^{L - l_1 + l_2} (2l_1 + 1)^{\frac{1}{2}} (2l_2 + 1)^{\frac{1}{2}} x$$

$$(2J_1 + 1)^{\frac{1}{2}} (2J_2 + 1)^{\frac{1}{2}} W(l_1 J_1 l_2 J_2, s L) x$$

$$(l_1 l_2 00 | l_1 l_2 L O) ,$$

where W is the Racah coefficient defined in ref. 20 (see Appendix C). The ξ_1 are the phase-shifts for a hard-sphere potential scattering defined as

$$\exp (2i \xi_1) = \exp (2i \sigma_1) \frac{G_1 (R) - i F_1 (R)}{G_1 (R) + i F_1 (R)}$$ (for charged particles)

σ_1 is the usual coulomb phase-shift and G_1 and F_1 are conventional regular & irregular solutions of the radial wave equation outside the nuclear surface.

Angular Distribution of the First-Emitted α Particle Resulting From a Direct Reaction

There are two different ways in which the reaction $^6Li (^3He, \alpha) ^5Li(g.s.)$ can proceed by a direct mechanism. One is by a neutron pickup, and the other is by a deuteron pick-up or more generally a two particle transfer involving

a neutron and a proton. A distorted wave theory for both types of reaction exists, 21 - 24 and will be summarized in this section.

<u>One-particle transfer reaction</u>: The differential cross-section for a direct reaction a + A → b + B proceeding by a single particle transfer between the incoming and outgoing channels α and β respectively, is given by

$$\frac{d\sigma}{d\Omega} = \frac{\mu_\alpha \mu_\beta}{(2\pi\hbar^2)^2} \frac{k_\beta}{k_\alpha} \frac{N_\beta}{N_\alpha} \frac{(2J_B + 1)}{(2J_A + 1)(2s_a + 1)} \sum_{lsj} |A_{slj}|^2 \times \sum_m \left|\beta_{sj}^{lm}\right|^2 \quad (13)$$

Here $\mu_\alpha = \frac{m_a m_A}{(m_a + m_A)}$, m being the masses of the subscripted variable $N_\alpha = \frac{(n_a + n_A)!}{n_a! n_A!}$, n being the number of nuclides in the nucleus, J_A and J_B are the target and the residual nuclear spins respectively, s_a is the spin of the incoming particle a, $k_\alpha = \sqrt{\frac{2\mu_\alpha E_\alpha}{\hbar^2}}$, and l, s, and j are the orbital, spin and total angular momenta of the transferred particle respectively. The A_{lsj} are referred to as spectroscopic coefficients and the β_{sj}^{lm} are called reduced amplitudes defined by the equation

$$(2l + 1)\ i^{l}\ \beta^{lm}_{sj} = \int d^3\vec{r}_\alpha \int d^3\vec{r}_\beta\ \chi_\beta^{(-)*}\ (\vec{k}_\beta, \vec{r}_\beta)\ x$$

$$f_{lsjm}\ (\vec{r}_\beta, \vec{r}_\alpha)\ \chi_\alpha^{(+)}\ (\vec{k}_\alpha, \vec{r}_\alpha) \quad (14)$$

Where the $\chi_\alpha^{(+)}$ and $\chi_\beta^{(-)}$ are distorted waves for the incoming and outgoing channels, and f_{lsjm} is referred to as the form factor. The spectroscopic coefficient includes such quantities as the fractional parentage coefficients for the initial or final nuclear states and the interaction strength. The form factor depends on the bound wave function of the transferred particle with the residual nucleus, the nuclear interaction between the transferred particle and the incoming and outgoing nuclei, and their internal wave function.

Zero-Range Approximation: Equation 14 is a six-dimensional integral over the two channel displacement variables $\vec{r}_\alpha$ and $\vec{r}_\beta$. For a direct reaction involving any sort of rearrangement, such an integration, almost all of which has to be handled numerically, becomes extremely difficult. The above difficulty is removed by the assumption that the form factor is proportional to an interaction that has a small range. This zero-range approximation has a physical meaning that the light particle in channel β, particle b, is assumed to be emitted at the same point, at which the light particle in channel α, particle a, is absorbed. If the reaction should involve the transfer of a particle x, then the zero-range

approximation means

$$\vec{r}_a = \vec{r}_b = \vec{r}_X$$

which implies $\vec{r}_\beta = \frac{M_A}{M_B} \vec{r}_\alpha$

The form-factor can then be written as,

$$f^{(zero)}_{lsjm} (\vec{r}_\beta, \vec{r}_\alpha) = \delta(\vec{r}_\beta - \frac{M_A}{M_B} \vec{r}_\alpha) \times$$

$$\int f_{lsjm} (\vec{s} + \frac{M_A}{M_B} r, r)\, d^3s$$

$$= F_{lsj} (\vec{r}_\alpha)\, Y^m_l (\hat{r}_\alpha)\, \delta (\vec{r}_\beta - \frac{M_A}{M_B} \vec{r}_\alpha). \quad (15)$$

In the zero-range approximation the reduced amplitudes β^{lm}_{sj} can be written as

$$(2l + 1)\, i^l\, \beta^{lm}_{sj} = \int d^3r\, \chi^{(-)*}_\beta (\vec{k}_\beta, \frac{M_A}{M_B} \vec{r}) \times$$

$$F_{lsj}(r)\; Y^m_l (\hat{r})\; \chi^{(+)}_\alpha (\vec{k}_\alpha, \vec{r}) \qquad (16)$$

The zero-range approximation calculation for the distorted waves, can be easily computer-coded and one such code DWUCK has been used to perform calculations on the ^{6}Li (^{3}He,α) ^{5}Li (g.s.) reaction.

Form-Factor for a (^{3}He,α) Reaction: It can be shown easily that the form-factor for a (^{3}He,α) reaction is given by

$$A_{lsj}\, f_{lsjm} \propto D^{(4,3)}\,(r_{n_0\,{}^3He})\;\; Y_l^{m\,*}\,(r_{n_0B})\;x \;\; R_{lj}^{\alpha_B\,J_B}\,(r_{n_0B})\;\; s,\tfrac{1}{2} \qquad (17)$$

where

$$D^{(4,3)}\,(r) = \int d^3r_{{}^3He}\;\; \varphi_{{}^3He}(r_{\,{}^3He})\;\; V_{n_0\,{}^3He}\;\; \varphi_{{}^4He}\,(r, r_{{}^3He})$$

where $V_{n_0{}^3He}$ is the interaction between stripped neutron and each of the particles in ^{3}He. For the internal wave function φ of ^{3}He and ^{4}He, Irving-Gunn wavefunction given in ref. 27 can be used.

The zero-range approximation is not so obvious for a (^{3}He,α) reaction. A finite-range calculation for this reaction can be done, by employing the method used by Bassel for a (t, d) reaction, [28] described as follows: In the first stage the volume integral of $D^{(4,3)}$ (r) is computed, i.e.,

$$D_0^{(4,3)} = \int D^{(4,3)}\,(r)\; d^3r$$

Then one replaces the $D^{(4,3)}$ (r) by the following

$$D^{(4,3)}_{(r)} = D_0^{(4,3)}\; f(r).$$

In the second stage of calculation, the second moment of the (noramlized) fuction f(r) is computed. Then the extent to which the subsequent DW calculation is sensitive to the range of f(r) is tested by replacing f(r) by a normalized gaussian that has the same second moment.

Finite range effects tend to reduce the cross-section at forward angle, and modify the angular distribution at large angles for a (t, d) reaction. Similar finite-range effects may be expected in a (^{3}He, α) reaction.

Two-Particle Transfer Reaction: A two particle transfer, for example the transfer of a proton and a neutron, can be described by the formalism given in ref. 23 and 24. For the reaction a + A → b + B, the differential cross-section is given by

$$\frac{d\sigma}{d\Omega} = \frac{(2J_A + 1)\ \mu_\alpha\ \mu_\beta\ \ k_\beta}{(2J_B + 1)\ (2\pi\hbar^2)^{\ 2}\ k_\alpha} \times (fC)^2 \times \sum_{LSJM} \frac{b_s}{2s + 1} \times$$

$$\left| \sum_{\gamma} A_{LSJ\gamma}\ \beta^{M}_{\gamma L} \right|^2 \qquad (18)$$

J_A, J_B, μ_α, μ_β, k_α, k_β have the same meaning as for a one-particle transfer reaction. Here $f = \frac{1}{2}\left(\frac{n_a!\ (n_A - 2)!}{(n_a - 2)!\ n_A!}\right)^{\frac{1}{2}}$

and $C = (T_a\ M_{T_a},\ T_A\ M_{T_A} \mid T_B\ M_{T_B})$, where n is equal to the number of nuclides and T is the isospin of the subscripted nucleus. $b_s^2 = \frac{1}{4}\delta_{sl}$ for a deuteron-transfer. The quantity $A_{\gamma LSJ}$ arises from an overlap integral between the initial and final nuclear states, and like the single nucleon transfer spectroscopic factor - contains the nuclear structure information. Here, γ refers to the quantum nos. of the stripped nucleons, including the single particle quantum nos. $\beta_{\gamma\ L}^{\ M}$ are the usual distorted wave reduced amplitude. The above formulation has also been coded in the DWUCK program in a zero-range approximation, with a provision for applying a finite range correction to the cross-section.

In the remainder of this chapter, the theories needed to describe the alpha-proton angular correlation will be discussed.

The RMV Model

The RMV model was party described in Chapter I. In this chapter, the geometrical explanation used by RMV to explain the enhancement of the proton emission in the forward direction with respect to the ^{5}Li recoil direction is described.

According to the RMV model, a proton localization is produced in ^{5}Li at the time of its formation which persists at the time of its decay. The RMV model for the neutron transfer is described in Fig. 3(a) and for the deuteron

transfer in Fig. 3(b). In these Figs. the possible location of the proton in ^{5}Li after the primary reaction is shown by a shading of that particular side of the ^{5}Li nucleus. There are two possibilities for the location of the proton in ^{5}Li, namely A and B, when a neutron transfer initiates the reaction, and only one possibility, namely C, when a deutron transfer initiates the reaction. This is a consequence of the primary reaction being a direct reaction, as can be seen easily from Figs. 3(a) and 3(b). The arrows point in a direction in which the proton is most likely to emerge upon the decay of ^{5}Li. In order to understand the relative probabilities with which A, B and C can occur in the RMV model consider the ensemble of all the reactions involving a neutron and a deuteron transfer. For all the reactions in this ensemble, the transferred neutron common to both the kinds of transfer, is necessarily located on the side of ^{6}Li which is directly facing the incoming ^{3}He projectile. The proton, however, can be found, with equal probability, on either side of ^{6}Li. As a deuteron transfer cannot occur when proton is located opposite to the side from which the neutron is being picked up, which will occur at least 50% of the time, implies that a pure neutron transfer leading to A in Fig. 3(a) will occur in a 50% of the reactions in the ensemble. Out of the remaining 50% of the reactions in the ensemble, in which the proton is located on the same side as the neutron which is being picked, a simultaneous

transfer of proton and neutron may take place only half the time. Thus a 25% of the reactions result in a deuteron transfer leading to C in Fig. 3(b). The remaining 25% leads to B in the Fig. 3(a).

Thus A entirely compensates for the effect of B and then both A and C lead to a predominant peaking in the forward direction as implied by the directions of the arrows in which protons are likely to emerge in the cases A and C.

Bohr's Symmetry Principle

It was stated in Chapter I that a 180^{o} periodicity is expected in the decay pattern of ^{5}Li (g.s.), as measured in its own rest frame, if the ^{5}Li (g.s.) is formed in a state of well-defined parity. This is a result of applying Bohr's symmetry principle to the reaction. The principle can be described as follows:

Consider a collision between two particles with relative momentum p_i, leading to a final state of two particles emerging with a relative momentum p_f. Then, provided the interactions are parity conserving and the particles can be assigned intrinsic parities, the collision exhibits reflection symmetry with respect to the planes containing p_i and p_f.

If we denote the reflection operator by R, then for a reaction that involves particles with spin, R can be

represented as a parity inversion followed by a rotation of 180^{o} about a vector $\vec{n}$ which is defined to be perpendicular to the collision plane (p_i, p_f). If S_n is the sum of spin components along $\vec{n}$ then

$$R = P\, e^{i\pi S_n}$$

where P is the parity operator. We thus have a conservation law

$$P_i\, e^{i\pi S_{n_i}} = P_f\, e^{i\pi S_{n_f}}, \qquad (19)$$

and this also implies that both the initial and final state wave functions possess a 180^{o} periodicity.

In the decay of ^{5}Li (g.s.), if the parity of ^{5}Li (g.s.) is well-defined, the principle stated above can be applied to its decay. Consequently, the wave function for the final state resulting from the decay of ^{5}Li (g.s.), must possess a 180^{o} periodicity, leading to a 180^{o} periodicity in the angular correlation pattern.

The Angular Correlation Function for the First Step of the Sequential Process Being A Direct Reaction

The angular correlation theory described in the following is applicable only for a direct reaction involving one-nucleon transfer. Such a theory for a two-nucleon transfer

would be prohibitively complicated and has not been described. Since the measured angular correlation does not possess a symmetry about the ^{5}Li (g.s.) recoil direction, the plane wave description will not be adequate. The theory therefore involves a distorted wave description. On the basis of only the spin and parity of the initial and final nuclei (1^{+} and $3/2^{-}$) the angular mementum transfer is restricted to l = 1, 3 for a simple neutron pickup reaction. The angular distribution for the first emitted α particle from ^{6}Li ($^{3}He,\alpha$) ^{5}Li (g.s.) has a large beak in the forward direction characteristic of l = 1 transfer. Moreover, if one assumed that the last neutron in ^{6}Li is in a p 3/2 shell, an l = 1 transfer pickup process would be expected. Consequently, the observed angular correlations were compared to the predictions of DWBA theory based upon the assumption that the initial reaction occurs via a l = 1 neutron pickup reaction.

The angular correlation function formulated in ref. 10, 25, and 26, is applicable for this reaction under the above assumptions. The angular correlation function for a two-step sequential process in which the first step proceeds by a direct reaction mechanism followed by the decay of the residual nucleus is given by

$$W(\theta, \theta, k_a, k_b) = \sum_{K,Q} \left(\frac{4}{(2k+1)}\right)^{\frac{1}{2}} \rho_{KQ}(J_B, J_B)\, F_K\, Y_{KQ}(\theta, \phi) \qquad (20)$$

where $F_K = \sum_{L\,L'} D_L\, D_{L'}\, F_K(L\,L'\,J_C J_B)\quad b_K(LL')$

Thus for a process A (a, b) $B^* \longrightarrow$ C + c, W describes the angular distribution of c measured in coincidence with b emitted along $\vec{k}_b$. The angle (θ, ϕ) represents the relative angle between b and c.

The separation of W into the products of ρ_{KQ} and $F_K Y_{KQ}$ consists in representing the properties of the intermediate state (i.e., its m-state population) by ρ_{KQ} and properties of subsequent decay by $F_K Y_{KQ}$. The angular coordinates have been defined in the RCM with the x axis taken along the recoil direction of B* and the z axis is along $\vec{k}_a \times \vec{k}_b$. The factor D_L denotes the reduced matrix element, which selects the contribution to the various angular momentum components of radiation. The γ-angular correlation coefficients F_K (L L', $J_B J_C$) and the parameters b_k which refer to particle emission rather than γ decay have been tabulated by Biedenharn and Rose.[25] The order of W is limited by $k \leqslant 2l, j + j', L + L'$ or $2J_B$, where l and j are the appropriate orbital and total angular momentum transfer associated with the initial reaction. J_B represents the spin of the intermediate state B* , and L denotes the relative angular momentum of the emitted radiation. The ρ_{KQ} $(J_B J_B)$ are statistical tensors describing the polarization of B* after its has been formed. The ρ_{KQ} $(J_B J_B)$ are

expressible in terms of ρ_{kq} (1, 1') where 1 and 1' refer to the orbital angular momentum transfer in the initial reaction.

$$\rho_{KQ}(J_B J_B) = \frac{(2J_B + 1)^{\frac{1}{2}}}{2(2J_A + 1)} \sum_{jlj'l'} x$$

$$\frac{\theta_{jl}\ \theta_{j'l'}(-1)^{l'}\ \eta_K\ (jj' J_A J_B)\ \rho_{kq}(l,l')}{(l0,l'0\ k0)} \qquad (21)$$

where the θ_{jl}'s are the reduced width amplitude, and the η_K (products of Wigner and Racah Coefficients have been tabulated in ref. 26. The tensor ρ_{kq} (1,1') is formed from the density matrix $\rho_{lm,l'm'}$ is the following way

$$\rho_{kq}(l,l') = \sum_{m,m'} (-1)^{l'-m'} (lm,l'-m' \mid kq)\ \rho_{lm;l'm'}$$

where $\rho_{lm;l'm'} = \beta_{lm}\beta_{l'm'}$.

Here the β_{lm} are the reduced amplitudes defined earlier for a one particle transfer DWBA.

The above expression for angular correlation, when applied to the ^{6}Li (^{3}He,α) ^{5}Li (g.s.) $\rightarrow$ p + α reaction, assuming a reflection symmetry through the reaction plane for the function W, reduces to

$$W(\theta,\phi)\ 1 + A_2^0\ P_2^0\ (\text{Cos}\ \theta) + A_2^2\ p_2^2\ (\text{Cos}\ \theta)\ \text{Cos}\ 2\ (\phi-\phi_2) \qquad (22)$$

This equation depicts a process in which an 1 = 1 neutron is picked up from a ^{6}Li ($J_A = 1^+$) target to form ^{5}Li (g.s.) ($J_B = 3/2^-$) which then decays by proton emission with L = 1 to a final α- particle state ($J_C = 0^+$). The value of K is, therefore, restricted to 2. The theoretical parameters β_{1m} are contained in A_2^0, A_2^2 as follows

$$A_2^0 = -\tfrac{1}{2} \sum_{jj} \frac{\theta_{1(\frac{1}{2})j}\ \ \theta_{1(\frac{1}{2})\,j'}}{|\theta_{1(\frac{1}{2})\,j}|^2}\ \eta_2\ (jj'\ J_A J_B)\ x$$

$$\sum_{LL'} C_L C_{L'}\ \ F_2\ (LL'\ J_C J_B)\ b_2\ (LL')$$

$$\frac{-2A_2^2}{A_2^0} = \frac{2}{\frac{B_{1-1}}{B_{11}} + \frac{B_{11}}{B_{1-1}}} = \lambda$$

$$2\phi_2 = \text{Arg}\left(-\frac{B_{1-1}}{B_{11}}\right)$$

Since the measurement was done in a reaction plane ($\theta = \pi/2$), we have finally

$$W(\theta, \phi) \propto 1 + A_2^2 \cos 2(\phi - \phi_2) \qquad (23)$$

Angular Correlation Function When the First Step of the Reaction Proceeds by a CN Formation

A shift in the minimum of the angular correlation pattern away from the recoil direction of ^{5}Li can be produced by a CN formation in the first step of a sequential process provided two CN states of opposite parities take part in the reaction.[7] Such a possibility exists in the ^{6}Li (^{3}He, p$\alpha\alpha$) reaction at 1.61 MeV ^{3}He bombarding energy, where the 17.64 MeV ^{9}B state ($J^\pi = 3/2^-$ or $5/2^-$) is formed in the first step of the reaction. At such a bombarding energy either the 17.20 MeV level in ^{9}B (width 120 ± 40 KeV and $J^\pi = 1/2^+$ or $3/2^+$), and/or the 18.6 MeV level (width 1 MeV J^π = not known) may be excited.

The uncertainties in the spins of the state involved make it pointless to attempt writing an angular correlation function, as at least one of the spin must be known which will determine the spin of the other state through a fitting procedure. However, this reaction bears many similarities to a ^{7}Li (d,α) ^{5}He (g.s.) $\rightarrow$ n + α,[7] which had been shown to proceed by a ^{9}Be CN formation, with states of opposite parities being excited at a deutron bombarding energy of 1 MeV, and which resulted in a shift in the minimum of the

angular correlation function away from the ^{5}Li (g.s.) recoil direction. Therefore, it will be worthwhile comparing the angular correlation for ^{6}Li (^{3}He,α) ^{5}Li (g.s.) $\rightarrow$ p + α at 1.6. MeV ^{3}He bombarding energy with the angular correlation applicable for the ^{7}Li + d reaction. From ref. 7, this function was shown to be a simple expression, i.e.,

$$W(\theta) = k_1 + k_2 \, Sin^2 (\theta - \theta_0) \qquad (24)$$

where k_1, k_2 and θ are parameters which can be related to theoretical quantities.

CHAPTER IV

RESULTS AND DISCUSSION

Mechanism of the First Step in ^{6}Li ($^{3}He,\alpha$) ^{5}Li (g.s.) $\rightarrow$ p + α

As was mentioned earlier in Chapter IV, the 17.64 MeV level in the ^{9}B compound nucleus is formed in the reaction ^{6}Li ($^{3}He,\alpha$) ^{5}Li (g.s.) at a ^{3}He incident energy of 1.580$\pm$ 0.20 MeV. The width of the ^{9}B state is 0.070$\pm$ 0.020 MeV.

The mechanism of the first step of the sequential process in the reaction ^{6}Li ($^{3}He,\alpha$) ^{5}Li (g.s.) $\rightarrow$ p + α at 1.61 MeV ^{3}He bombarding energy is primarily the formation of the ^{9}B compound nucleus. As seen from Fig. 27, it leads to an angular distribution of the first emitted α which is symmetric about 90^{o} in the system center of mass (SCM), where the angles are measured with respect to the ^{3}He incident beam direction. The first emitted angular distribution measured at off-resonance ^{3}He bombarding energies, i.e. at 1.47 MeV and 1.69 MeV, (Figures 34 and 36 respectively), does not possess such a symmetry about 90^{o} in the SCM. Consequently, the mechanism of the first step at off-resonance bombarding energies has a contribution in it which is a direct reaction. As mentioned in Chapter V, there are two

types of direct reaction that can occur in the first step, a neutron transfer or a deuteron transfer from the ^{6}Li nucleus to the ^{3}He. Both the types of reaction will contribute to the resulting angular distribution. Differential cross-sections have been calculated using DWBA theory described in Chapter V for each of these transfers with the aid of the computer code DWUCK3,[29] which uses a zero-range approximation. Optical model parameters used in performing these calculations have been tabulated in tables I and II. Table I lists optical model parameters for a neutron transfer calculation. The calculated differential cross-section has been plotted as a function of the center of mass angle of the first emitted α- particle in Figure 37, which shows a forward peaked function expected for a l = 1 neutron transfer. The effect of varying the optical model parameters on the differential cross-section was examined and it was found that the shape of the curve was not sensitive to reasonable variation of parameters.

Applying the additional finite range correction to the differential cross-section increased the magnitude of the cross-section by about a factor of 2.5 without changing the shape appreciably. Table II

FIGURE 37

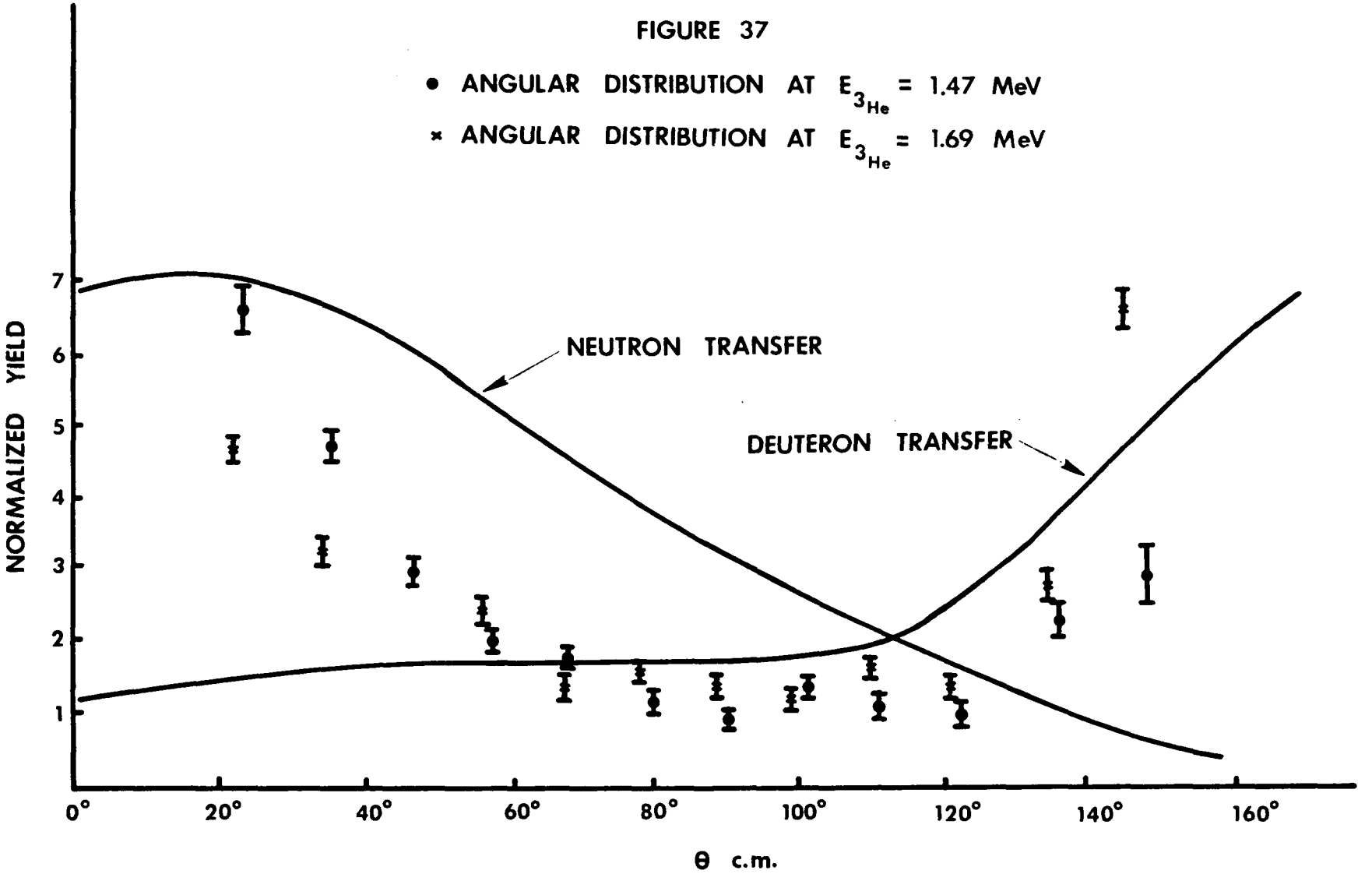
• ANGULAR DISTRIBUTION AT $E_{^3He}$ = 1.47 MeV
× ANGULAR DISTRIBUTION AT $E_{^3He}$ = 1.69 MeV
NEUTRON TRANSFER
DEUTERON TRANSFER
NORMALIZED YIELD
1
2
3
4
5
6
7
0°
20°
40°
60°
80°
100°
120°
140°
160°
θ c.m.

lists the optical model parameters used for the deuteron transfer calculation. A microscopic two-particle transfer type of calculation was performed in this case. The calculated differential cross-section is shown in Figure 37 .

This cross-section shows a backward peaking in the center of mass for a l = 0 deuteron transfer. On making the imaginary surface potential for the transferred particle equal to-67.0 MeV, keeping all the other parameters constant the calculated $d\sigma/d\Omega$ showed a dip at about $\theta_{CM} = 50^{o}$. Reasonable variation of the other parameters did not affect the cross-section in any appreciable way.

A comparison of the experimentally measured angular distributions (in Figures 34 and 36) with the calculated curves in Figure 37 suggests that both the neutron transfer and the deuteron transfer mechanisms are taking part in the reaction.

Proton-Alpha Angular Correlation

A 180^{o} aperiodicity is exhibited by all the angular correlation data as seen in Figures 22-24 . Application of Bohr's symmetry principle suggests that the ^{5}Li state formed in the first step of the reaction does not possess a well-defined parity quantum no.,

at any of the incident energies, i.e., 1.47 MeV, 1.58 MeV, and 1.69 MeV. This result tends to support the RMV concept of proton-localization in ^{5}Li for both a direct reaction mechanism as well as a CN formation in the first step. The RMV-model, however, assumes a direct reaction for the first step. Therefore, the aperiodicity at the on-resonance ^{3}He incident energy may be due to the direct reaction component of this reaction in order for it to be consistent with the RMV model.

The asymmetry ratio, defined as the ratio between the α - p coincidence yield in the forward direction to the same quantity in backward direction, where these quantities are 180^{o} apart in the recoil center of mass (RCM) frame, have been tabulated in table III. The ratios are shown at each bombarding energy using coincidence yields before and after background subtraction. These values have been compared with previously measured values, measured similarly, of Reimann, Martin, and Vogt (RMV) and those of Thompson and Tripard (TT) who had obtained their asymmetry ratios without a background subtraction. The asymmetry ratios from the present work are not very different from previously measured values. The asymmetry ratios after the background subtraction have much larger

absolute errors, therefore a comparison of these at different bombarding energies is difficult to make. The existence of an asymmetry after the background subtraction, which may be concluded from the table III for at least 1.58 MeV and 1.69 MeV ^{3}He incident energies may be uniquely associated with ^{5}Li (g.s.). Similar asymmetry effects are also seen in the background which may be related to asymmetric breakup of ^{5}Li (7.5) state. Thompson and Tripard[3] reported an assymmetry ratio of $1.84\pm.4$ in the ^{5}Li (7.5) breakup which is a significant part of the background in the present data at the forward and backward angles.

A significantly lower asymmetry is seen at on-resonance bombarding energy in the data which includes background, as compared with the off-resonance data. Formation of a ^{9}B CN may therefore produce a ^{5}Li state which does not have a strong proton localization, and thus the direct reaction may be predominatly responsible for the asymmetry. This will be in agreement with the RMV model.

The 1.47 MeV angular correlation function (Figure 22) is very similar to the measurement of Livesey and Piluso at 1.25 MeV. The shift in the minimum of the correlation function in the present measurement is 15^{o} as measured in the laboratory compared with the shift

of 13^{o} in the Livesey and Piluso measurement. As the major mechanism at 1.47 MeV ^{3}He energy from previous data appears to be a direct reaction, such a shift in the minimum as well as the entire shape of the angular correlation curve may be explained within the framework of a direct reaction in the first step of the ^{6}Li ($^{3}He,\alpha$) ^{5}Li (g.s.)$\rightarrow$ p + α. The shape of the curve as was pointed out by Livesey and Piluso, apart from a shift in the minimum, is due to the emission of a p 3/2 proton from a ^{5}Li (g.s.)

The on-resonance angular correlation function does not have a shape similar to the one at 1.47 MeV, although it does show the aperiodicity as pointed out earlier.

The angular correlation at 1.69 MeV has a shape similar to the measurement at 1.47 MeV indicating that the direct reaction mechanism may be largely responsible for its shape. The magnitude of the shift in minimum is of the order of 20^{o} as measured in the laboratory which is somewhat larger than the value at 1.47 MeV.

Although the present work does not make it completely clear, whether the shift in the minimum of the angular correlation curve is due to a direct reaction in the first step or as was suggested by

Livesey and Piluso, due to formation of ^{9}B compound nucleus with an admixture to it from another ^{9}B level, it has been shown that a ^{9}B CN is formed at the appropriate bombarding energy and that the off-resonance mechanism is largely a direct reaction.

Table I

Optical Model Parameters for a Neutron Transfer at $E_{^3He}$ = 1.55 MeV.

Quantity	Transferred Particle	Initial State	Final State
R_o	1.25 f	2.25 f	2.10 f
a	0.65 f	0.50 f	0.50 f
V_o	-1.00 MeV	-99.00 MeV	-95.0 MeV
R_o'	0	0	0
a'	0	0	0
W'	0	0	0
R_o''	0 f	1.23 f	1.23 f
a''	0 f	0.76 f	0.76 f
W''	0 MeV	-10.0 MeV	-10.0 MeV
R_o'''	0	0	0
a'''	0	0	0
V_{so}	10 0	0	0
W_{so}	0	0	0
R_c	1.113f	1.113f	1.113 f

(For the definition of the symbols, see Ref. 30)

Table II

Optical Model Parameters for a Dueteron Transfer at $E_{^3He}$ = 1.55 MeV.

Quantity	Transferred Particle	Initial State	Final State
R_o	1.05 f	2.25 f	2.1 f
a	0.62 f	0.5 f	0.5 f
V_o	-83.6 MeV	-99.0 MeV	-95.0 MeV
R_o'	1.05 f	0.0 f	0.0 f
a'	0.0 f	0.0 f	0.0 f
W'	0.43 MeV	0.0 MeV	0.0 MeV
R_o''	0.0 f	1.23 f	1.23 f
a''	0.0 f	0.76 f	0.76 f
W''	0.0 MeV	-10.0 MeV	-10.0 MeV
R_o'''	0.0 f	0.0 f	0.0 f
a'''	0.0 f	0.0 f	0.0 f
V_{so}	-8.0 MeV	0.0 MeV	0.0 MeV
W_{so}	0.0 f	0.0 f	0.0 f
R_c	1.3 f	0.0 f	0.0 f

(For the definition of the symbols, see Ref. 30)

Table III

Proton-Asymmetry Ratios

B.E.	Asymmetry Ratios before background subtraction	Asymmetry Ratios after b.g. subtraction	RMV	IT
1.47	1.67 ± .19	1.24 ± .32		
1.58	1.35 ± .17	1.53 ± .45		
1.69	1.81 ± .19	1.83 ± .74		
1.25			2.0 ± .3	
1.54				1.23 ± .2

APPENDIX A

ALGEBRA FOR A VELOCITY VECTOR DIAGRAM

Consider a sequential process described as

$1 + 2 \rightarrow 3 + (4 + 5) \rightarrow 4 + 5.$

Velocity vector diagrams can be drawn for above reaction using the velocities of various particles in the above reaction in three different reference frames. In addition to the laboratory frame, the two other frames needed are the system center of mass frame (SCM) in which the center of mass of the particles 1 and 2 is at rest, and the recoil center of mass frame, in which the recoiling nucleus (4 + 5) is at rest. Quantities in the laboratory frame will be described with no primes on them, in the SCM with a single prime, and in the RCM with double primes. Expressions for various velocities required in drawing a velocity vector diagram for a sequential reaction are given as follows:

$$V_{CM} = \frac{M_1}{M_1 + M_2} \left(\frac{2 E_1}{M_1}\right)^{\frac{1}{2}} \qquad (25)$$

$$V_3' = \left(\frac{2M}{M_3(M_3 + M)} \left(\frac{M_2}{M_1 + M_2} E_1 + Q^n \right) \right)^{\frac{1}{2}} \qquad (26)$$

$$V' = \left(\frac{2M}{M(M_3 + M)} \left(\frac{M_2}{M_1 + M_2} E_1 + Q^n \right) \right)^{\frac{1}{2}} = \frac{M_3}{M} V_3' \quad (27)$$

$$V_4'' = \left(\frac{2 M_5}{M_4 M} \left(Q^m - Q^n \right) \right)^{\frac{1}{2}} \quad (28)$$

$$V_5'' = \left(\frac{2 M_5}{M_4 M} \left(Q^m - Q^n \right) \right)^{\frac{1}{2}} = \frac{M_4}{M_5} V_4'' \quad (29)$$

where

$$Q^n = (M_1 + M_2 - M_3 - M) c^2$$

$$Q^m = (M_1 + M_2 - M_3 - M_4 - M_5) c^2$$

Variables without subscripts refer to the initial recoiling system, (4 + 5), M's are the masses of subscripted particles, V's are the velocities of the subscripted particles, and E_1 is the laboratory incident bombarding energy of the particle 1.

where θ_1 is measured with respect to the recoil direction of the ^{5}Li nucleus, and V_R is the recoil velocity of the ^{5}Li nucleus in the laboratory frame.

APPENDIX B

COORDINATE SYSTEM FOR ANGULAR CORRELATIONS

For the study of angular correlations of heavy particles resulting from sequential decay following bombardment, all three coordinate systems described earlier in Appendix A need to be considered. Of a particular significance is the RCM, in which the angular correlation function is ultimately described.

Hency if the laboratory, center of mass, and recoil frames are denoted by no primes, single primes, and double primes respectively, the theoretical correlation function is related to the yield in the laboratory by

$$W(\theta'') \propto \left(\frac{d^2\sigma}{d\Omega_1 \, d\Omega_2} \Delta\Omega_1 \Delta\Omega_2 \right) \frac{d\Omega_1 \; d\Omega_2}{d\Omega_1'' \; d\Omega_2''} \qquad (30)$$

where $\Delta\Omega_1$, and $\Delta\Omega_2$ are the solid angles subtended by the two detectors in the lab. The angle θ'' is measured between two detectors in the recoil coordinate system. The solid angle trandformation between the laboratory frame and the RCM frame, $d\Omega_1 / d\Omega_1''$ is given by

$$\frac{d\Omega_1}{d\Omega_1''} = \frac{V_1''}{V_1} \left(1 - \frac{V_R}{V_1} \cos\theta_1 \right) \qquad (31)$$

LIST OF REFERENCES

1. F.C. Young, K.S. Jayraman, J.E. Etter, H.D. Holmgren, M.A. Waggoner, Rev. of Mod. Phys., 37, 362, (1965).

2. M.A. Reimann, P.W. Martin, E.W. Vogt, Phys. Rev. Lett., 18, 246, (1967).

3. D.T. Thompson, G.E. Tripard, Phys. Rev. C6, 452, (1972).

4. D.L. Livesey, C.J. Piluso, Can. J. of Phys., 52, 1167, (1974).

5. M.P. Baker, J.M. Cameron, N.S. Chant, and N.F. Mangelson, Nucl. Phys., A184, 97, (1972).

6. Vignon, Cavaignac, and Longequeue, J. Physique, 30, 913, (1969).

7. J.C.P. Heggie, and P.W. Martin, Phys. Lett., 43B, 289, (1973).

8. N. Austern, Direct Nuclear Reaction Theories, (John Wiley & Sons, Inc.), p. 332 - 336.

9. C. Moazed, and H.D. Holmgren, Phys. Rev. 166, 977, (1968).

10. G.R. Satchler, and W. Tobocman, Phys. Rev. 118, 1566, (1960).

11. A. Bohr, Nucl. Phys., 10, 486, (1959).

12. P.A. Deutchman, Lett. Nuo. Cim., 4, 61, (1970).

13. J.B. Marion, F.C. Young, Nuclear Reaction Analysis, Graphs and Tables, North Holland Publishing Co., Amsterdam, (1968), page 145.

14. Nuclear Data Tables, Sec. A, Vol. 7, No. 3 - 4, (1970).

15. E.H. Geer, F.B. Nelson, and E.A. Wolicki, Phys. Rev. 100, 215, (1955).

16. A.F. Kuckes, R. Wilson, and P.F. Cooper, Jr., Ann. Phys. (N.Y.), 15, 193, (1961).

17. L.M. Delves, Nucl. Phys., 20, 275, (1960).

18. F. Ajzenberg-Selove, T. Lauritsen, Nucl. Phys., A227, 1, (1974).

19. J.M. Blatt, and L.C. Biedenharn, Rev. of Mod. Phys., 24, 258, (1952).

20. G. Racah, Phys. Rev., 61, 186, (1942).

21. P.E. Hodgson, Nuclear Reaction Nuclear Structure, Clarendon Press, Oxford Press, (1971), pages 434 - 519.

22. N. Austern, Direct Nuclear Reaction Theories, John Wiley & Sons, (1970), pages 99 - 192.

23. N.K. Glendenning, Phys. Rev., 137, B102, (1965).

24. N.K. Glendenning, Ann. Rev. of Nucl. Science, 13, 191, (1963).

25. L.C. Biedenharn, and M.E. Rose, Rev. of Mod. Phys., 25, 729, (1953).

26. G.R. Satchler, Proc. Phys. Soc., A66, 1081, (1953).

27. J.C. Gunn, and J. Irving, Phil. Mag., 42, 1353, (1951).

28. R.H. Bassel, Phys. Rev., C149, 791, (1966).

29. DWUCK3, Distorted Wave Born Approximation Program, written by P.D. Kunz at the University of Colorado, (1972).

30. N. Austern, Direct Nuclear Reaction Theories, John Wiley and Sons, Inc.), (1970), page 106.